VYSOKÉ UČENÍ TECHNICKÉ V BRNĚ
BRNO UNIVERSITY OF TECHNOLOGY

FAKULTA CHEMICKÁ
ÚSTAV CHEMIE MATERIÁLŮ

FACULTY OF CHEMISTRY
INSTITUTE OF MATERIALS CHEMISTRY

PLASMA-ENHANCED CHEMICAL VAPOR DEPOSITION USING TVS/AR A TVS/O2 MIXTURES

TITLE

MASTER'STHESIS

DIPLOMOVÁ PRÁCE

AUTHOR
AUTOR
Bc. JAKUB SADÍLEK

SUPERVISOR
VEDOUCÍ PRÁCE
PROF. RNDR. VLADÍMÍR ČECH PHD.

BRNO 2013

ABSTRACT

This study is aimed at basic research on a-SiC:H and a-SiOC:H alloys prepared in a form of thin films using plasma-enhanced chemical vapor deposition. These alloys were deposited from tetravinylsilane monomer and its mixtures with argon or oxygen gas at different effective powers under pulsed plasma. Deposited films were investigated by X-ray photoelectron spectroscopy, Fourier transform infrared spectroscopy, spectroscopic ellipsometry, and nanoindentation to observe their chemical, optical, and mechanical properties as a function of deposition conditions.

ABSTRAKT

Tato studie je zaměřena na základní výzkum přípravy a-SiC:H a a-SiCO:H slitin plazmových polymerů pomocí metody plazmochemické depozice z plynné fáze (PE-CVD). Tyto slitiny byly připravovány depozicí z monomeru tetravinylsilanu (TVS) a jeho směsí s kyslíkem a argonem při různých efektivních výkonech pulzního plazmatu. Připravené tenké vrstvy byly za účelem získání závislostí optických, mechanických a chemických vlastností na depozičních podmínkách zkoumány pomocí metod spektroskopické elipsometrie (ELL), nanoindentace (NI), fotoelektronové spektrometrie (XPS) a Fourierovy transformované infračervené spektrometrie

KEYWORDS

a-SiC:H, a-SiCO:H, Tetravinylsilane (TVS), Plasma enhanced chemical vapor deposition (PECVD), thin films, ellipsometry, Fourier transformed infrared spectrometry (FTIR)

KLÍČOVÁ SLOVA

a-SiC:H, a-SiCO:H, Tetravinylsilane (TVS), plazmochemická depozice z plyné fáze (PECVD), tenké vrstvy, elipsometrie, Fourierovsky transformovaná infračervená spektrometrie (FTIR)

SADÍLEK, J.. Brno: *Plasma-enhanced chemical vapor deposition using TVS/Ar and TVS/O_2 mixtures*. Brno university of technology, Faculty of chemistry. Institute of material research, 2013. 123 s.. Master's thesis. Supervisor: Prof. RNDr. Vladimír Čech, PhD.

SADÍLEK, J. *Plazmochemická depozice vrstev z plynné fáze s využitím směsí TVS/Ar a TVS/O2.* Brno: Vysoké učení technické v Brně, Fakulta chemická, 2013. 123 s. Vedoucí diplomové práce prof. RNDr. Vladimír Čech, Ph.D..

DECLARATION

I declare, that the diploma thesis has been worked out by myself, under leadership of my supervisor and then all the quotations from the used literary sources are accurate and complete. The content of the diploma thesis is the property of the Faculty of Chemistry of Brno University of Technology and all commercial uses are allowed only if approved by both the supervisor and the dean of the Faculty of Chemistry, BUT.

In Brno............................. ....

(podpis authora)

PROHLÁŠENÍ

Prohlašuji, že jsem diplomovou práci vypracoval samostatně a že všechny použité literární zdroje jsem správně a úplně citoval. Diplomová práce je z hlediska obsahu majetkem Fakulty chemické VUT v Brně a může být využita ke komerčním účelům jen se souhlasem vedoucího diplomové práce a děkana FCH VUT.

V Brně dne ....

(Signature autor)

ACKNOWLEDGEMENT

I would like to thank supervisor prof. RNDr. Vladimir Čech, Ph.D. for technical leadership during thesis solution, for provided consultations and literature and for opportunity to increase horizon of knowledge for thin films preparation techniques. Important thanks belong to Mgr. Radek Přikryl, Ph.D. for significant help with technological problems, friendly approach and for motivation to complete the work. I would also like to thank RNDr. Josef Zemek, CSc (XPS), Mgr. Jan Mistrik, Ph.D (ELL), Ing.Veronika Schmiedová (ELL) and Ing. Erick Pálesh (AFM/nanoindentation) for measurements and analyses. Considerable thanks belong to my colleagues Bc. Jan Kucharčík and Tomáš Plichta for assistance with measurements and depositions and also for good atmosphere in laboratory. Important thanks also belong to Ing. Přemysl Menčík for technical assistance and support with designing apparatuses components and solving technical problems. Thanks also belongs to doc. RNDr. František Krčma PhD. and doc. Ing. Ota Salyk CSc. for many expertise consultations.

Special thanks belong to my girlfriend Bc. Iveta Kostovová and my family for patience and psychological and financial support.

This thesis was supported by grant project P106/11/0738 (GAČR) s named „Plazmochemické zpracování vláknových výztuží pro polymerníkompozity s vysokými užitnými vlastnostmi“.

In Brno ....

(Signature of autor)

CONTENTS

Contents 6

1 Introduction 8

2 Theoretical part 9

2.1 Thin film ... 9

2.2 Thin film deposition ... 10

2.2.1 Physical vapor deposition ... 10

2.2.2 Chemical vapor deposition ... 11

2.2.3 Plasma enhanced chemical vapor deposition ... 14

2.3 Thin film analysis ... 21

2.3.1 Spectroscopic analysis ... 21

2.3.2 Microscopic analysis ... 28

2.3.3 Others analysis techniques ... 30

2.4 PECVD films applications ... 32

3 Objective 34

4 Experimental part 35

4.1 Materials and its properties ... 35

4.1.1 Monomer and auxiliary gases ... 35

4.1.2 Substrates ... 35

4.2 Instrumentation ... 36

4.2.1 Pumping system and pressure settings ... 37

4.2.2 Vacuum measurement ... 40

4.2.3 Reactive gas mixing ... 41

4.2.4 Plasma generation ... 42

4.2.5 Deposition control system ... 43

4.2.6 Attached analytical equipment ... 45

4.3 Deposition of PP thin films ... 48

4.3.1 Deposition conditions ... 48
4.3.2 Deposition process way ... 51
4.3.3 Cleaning process ... 52
4.4 Analysis of plasma discharge ... 54
4.4.1 Plasma discharge stability measurement ... 54
4.4.2 Mass spectroscopy analysis of plasma discharge species ... 55
4.5 Analysis of prepared PP thin films ... 55
4.5.1 Chemical composition (FTIR) ... 55
4.5.2 Optical properties and thickness (ELL) ... 56
4.5.3 Elementary composition of surface (XPS) ... 57
4.5.4 Mechanical properties (Nanoindentation) ... 57

5 Results and discusion 58

5.1 Analysis of plasma discharge ... 58
5.1.1 Discharge stability measurement ... 58
5.1.2 Mass spectroscopy of plasma species ... 60
5.2 Deposition conditions ... 75
5.2.1 Pressure and self-bias ... 75
5.2.2 Deposition rates (ELL) ... 78
5.3 Analysis of prepared thin films ... 81
5.3.1 Optical properties (ELL) ... 81
5.3.2 Chemical structure (FTIR) ... 93
5.3.3 Elemental surface composition (XPS) ... 104
5.3.4 Mechanical properties (Nanoindentation) ... 106

6 Conclusion 109

References 111

List of used abbreviations 120

List of attachments 122

1 INTRODUCTION

Plasma polymerization is well recognized as the important part of material science. The first mentions about material known today as plasma polymers appeared to the middle of 19th century like the waste material with presence in areas of glow discharges. Further investigation specializes to study properties of these materials starts after next hundred years in year 1930 . From this time, materials based on plasma polymers are intensively studied [1] for exactly large amount of very different applications. Researches, which studied plasma polymer films structure observes that the plasma polymers have very different structure to compare with conventional polymers. This observation induces larger and higher sophisticated development in this scope in industrial areas such as barrier coatings for the corrosion protection of metals [2], [3], barrier coatings protecting against gas transmission trough packing (oxygen, water, CO_2 barriers) [4], [5], hard films [6], [7] , low and friction films [8], thin layers with low dielectric constant [9] and many others, until today.

Plasma polymers give sets of properties, which would not be obtained from conventional polymerization, such se foils with thickness in nanometers scale (20 nm) with structure and mechanical properties not so depending at the monomer chemical reactivity and monomer structure. Because the plasma polymerization is chemical process stimulated by physical effects, the monomers used for polymerization does not need reaction centers (like double bonds) and reactive groups, if they are not wanted in the material structure. Because of that plasma polymerization is able to produce “tailored” materials with strictly defined properties.

This diploma thesis is focused to preparation of highly defined properties thin films using plasma enhanced chemical vapor deposition. By changing deposition conditions during deposition process would be made thin films with very different values of optical, mechanical, electrical and chemical properties. For this diploma thesis the monomer from group of organosilanoles – tetravinylsilane was used and deposition conditions were regulated by flow rate, composition of reactive gas and power supplied to the reactor chamber. Properties of plasmas were monitored primary by MS and final films properties were monitored by FTIR, ELL, XPS and Nanoindentation.

2 THEORETICAL PART

2.1 Thin film

What is the thin film? At first is consequently important to define, what film is. Film is defined as layer type body. Layer is body, which has one of its dimensions significantly smaller than remaining two (Fig. 1). Easily it can be defined also by surface (S) to volume ratio (V), because the layers have $S/V >> 6$. Secondary what is thin? This question is causing semantic problems for whole science community. One of the most often used attitudes is that the thin film (layer) is so thin as the characteristic psychical property has consequently changed from the bulk material property. A change of the characteristic psychical value is caused because surfaces are so near to themselves. A typical psychical property that changes with approaching surfaces is electrical conductivity and resistance (mean free length), melting point, optical properties (like refraction angle, coherence length). Thin film can be formatted from inorganic, organic and hybrid (organometallics, organosiloxanes etc.) with amorphous, crystalline and semicrystaline structure. Typical thickness of thin layer is from 1 nm (monolayer of atoms) up to 10 μm (as the maximum thickness, where the characteristic property change is detectable) [10], [11].

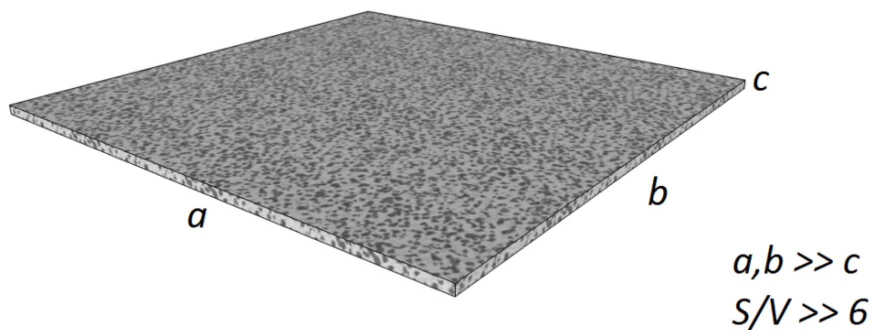

Fig. 1: Model of layer type body

2.2 Thin film deposition

Thin film deposition methods are typically divided into two separate groups by their principle. First is based on psychical processes like vaporization or kinetic energy transfer (impact) and it is named as Psychical Vapor Deposition (PVD). Second group is based on chemical reactions and it is named Chemical Vapor Deposition (CVD). This division is not so precise, because some specific methods, sometimes named as "Reactive PVD processes" (like as Reactive Sputtering), are using both principles [10], [11], [12].

Often are PVD and CVD processes distinguished by following four rules, which must PVD process accomplish [11]:

1. Psychical mechanisms by which atoms enter the gas phase (like as evaporation or impact)
2. Addiction on solid or molten sources, as opposed to generally gaseous precursors in CVD methods
3. General absence of chemical reactions (with some explanations like as reactive PVDs).
4. Higher demands on vacuum environment through which gaseous atoms are transported

Currently the decision of using specific technology for specific thin film preparation is not always obvious, because actual trends are in using hybrid technologies that have combined advantages of more methods as like as using methods, which combine PVD and CVD process [11].

2.2.1 Physical vapor deposition

2.2.1.1 Evaporation

The objective of this method for thin film deposition is to controlled transfer of evaporated atoms from heated source to substrate with lower temperature, where film formation and grow proceed atomistically by condensation. For this process is required vacuum at level at least $< 10^{-3}$ Pa [11], [13]. .

2.2.1.2 Sputtering

Sputtering is method of PVD based on impact of high energy ions or particles, generated by low pressure electrical discharge, accelerated by electrical field (DC, AC or RF)from working gas (typically Ar) to conductive cathode – target (or material on it, which may not be conductive), which cause ejection of atoms to evacuated area. Ejected atoms are transported to substrates, which are facing target, where film formation occurs [10], [11], [12], [14], [15].

Special type of sputtering is Reactive sputtering (hybrid CVD/PVD method), which is using chemical reactive gas in working gas mixture. Reactive gas reacts with erupted species of cathode material and forms new chemical substances. Typical example can be oxide formation, which is realized by using oxygen as reactive compound of working gas [10], [11]. Another types of sputtering are using additive forces to improve density of plasma discharge near to the target (cathode) and improve deposition rates, like as magnetic force in magnetron sputtering [15].

2.2.1.3 Pulsed Laser Deposition (PLD)

The applicability of pulsed laser deposition in thin-films rests largely in its simplicity in implementation. Pulsed laser deposition is PVD process, carried out in vacuum system that shares some process characteristics common with molecular epitaxy and some with sputtering. In PLD process a pulsed laser is focused onto a target of material to be deposited. For sufficiently high energy density, each laser pulse vaporizes or ablates a small amount of material, which creates a plasma "plume". The ablated material is ejected from the target in highly forward-directed plasma plume against substrate. The plasma plume provides material flow for film formation. PLD has some important advantages. For example it can directly ablate non-conductive materials, such as polymers, organic and inorganic compounds with conserve of its chemise and stoichiometry [16].

2.2.2 Chemical vapor deposition

Chemical vapor deposition is group of processes, which are specified by chemical reaction of volatile compound of a material to be deposited, with optional other gases, to produce non-volatile products of thin-film on substrates and waste gaseous products, which must be removed. Because CVD processes usually do not require high levels of vacuum or unusual consume of electric power, they are usually preferred before energy and economically demanding PVD processes. CVD processes are widely used for thin film production, but it can be also used for preparation of high purity powders and bulks. CVD processes have some large advantages in contrast to PVD processes. At first, CVD process can grow thin film in all surface of product include holes, cavities and averted sides in contrast to for example evaporation or sputtering, where substrates must be faced in front of evaporator or sputtering target. Secondary CVD processes deals higher quality of film, better uniformity and higher throughput [11], [17], [18].

CVD processes are large group, because specific technologies are using specific conditions for CVD. Reactors for CVD can be atmospheric to 10^0 Pa working pressure rated, reactors can be hot-wall or cold-wall and many other parameter can be set, which can allow them usage in large amount of very different types of industries. For example CVD processes are used very often in semiconductor industry (as example at Fig. 2 schematic of metal-oxide transistor), but also as the final coating of machinating tools (drills, milling tips) in mechanical engineering industry [11], [18].

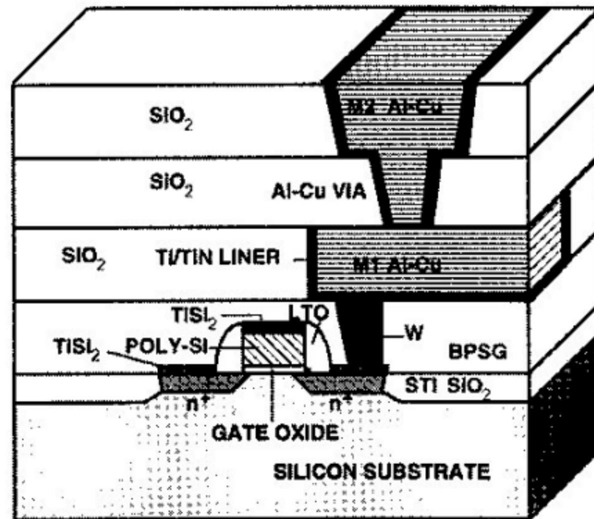

Fig. 2:Schematic cross-sectional view of typical MOS transistor. Almost everything was made by CVD technology [11].

2.2.2.1 Reaction schema of CVD processes

The fundamental reaction schema of almost every CVD process is described by following picture Fig. 3.

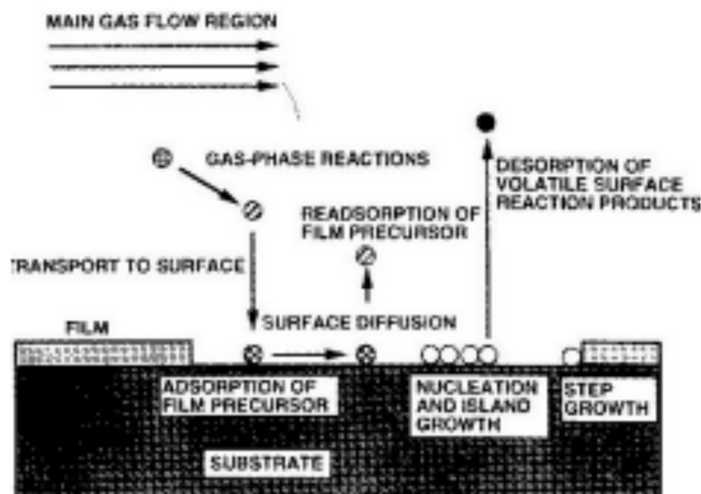

Fig. 3: Sequence of gas transport and reaction processes contributing to CVD film growth [11].

Picture Fig.3 provides information that integrates following steps [11]:

1. Convective and diffusion transport of reactants from the gas inlets to the reaction
2. Chemical reactions in the gas phase to produce new reactive species and by-products.
3. Transport of the initial reactants and their products to the substrate surface
4. Adsorption (Chemical and also Psychical) and diffusion of these species on the substrate surface.
5. Heterogeneous reaction catalyzed by the surface leading to film formation.
6. Desorption of volatile side-products of surface reaction
7. Convective and diffusion transport of the reaction by-products away from the reaction zone.

2.2.2.2 CVD reaction types

To view the scope of CVD processes, it is useful to briefly categorize types of chemical reactions that have been used to CVD thin film deposition. Usually is this chemical reactions gas-phase or gas-to-solid reactions [11].

Pyrolisis is thermal decomposition of such gaseous species like as hydrides on hot surfaces (often substrate). Following formula {1} is an example of usage of high-temperature pyrolysis of silane to produce of polycrystalline or amorfous silicon films.

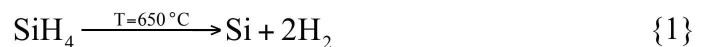

$$SiH_4 \xrightarrow{T=650\,°C} Si + 2H_2 \qquad \{1\}$$

Reduction reactions commonly employ hydrogen gas to effect the reduction of gaseous species as halides, oxyhalides or carbonyl halides. Well known is reaction example of epitaxial Silicon formation formula {2}.

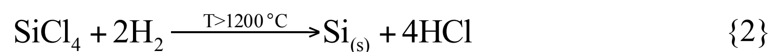

$$SiCl_4 + 2H_2 \xrightarrow{T>1200\,°C} Si_{(s)} + 4HCl \qquad \{2\}$$

Oxidation is commonly used CVD process reaction as process of silicon oxide formation for electro-technical and optical usage and alumina oxides for hard-coatingformation formula {3}.

.

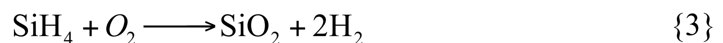

$$SiH_4 + O_2 \longrightarrow SiO_2 + 2H_2 \qquad \{3\}$$

Compound formation like as nitride, boride, carbide etc., is group of CVD processes, which require the reactive components in gas phase or in volatile form. Thin films are formatted typically on hot surfaces of products, which want to be coated - formula {4}.

$$SiCl_4 + CH_4 \longrightarrow SiC_{(s)} + 4HCl \qquad \{4\}$$

Disproportionation reactions are possible when a nonvolatile metal can form volatile compound having different degree of stability depends on temperature. Exemplar can be system $GeI_2 - GeI_4$ showed at following formula {5}.

$$2GeI_{2(g)} \underset{600\,°C}{\overset{300\,°C}{\rightleftarrows}} Ge_{(s)} + GeI_{4(g)} \quad \{5\}$$

Reversible transfer reactions are characterized by a reversal in equilibrium reaction at source and deposition region maintained at different temperatures within one reactor. Very important example is the deposition of epitaxial GaAs films by the chloride process – formula following as formula {6}.

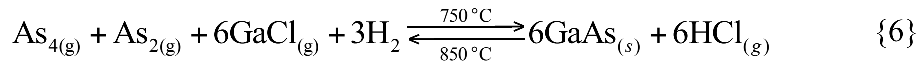

$$As_{4(g)} + As_{2(g)} + 6GaCl_{(g)} + 3H_2 \underset{850\,°C}{\overset{750\,°C}{\rightleftarrows}} 6GaAs_{(s)} + 6HCl_{(g)} \quad \{6\}$$

2.2.2.3 CVD processes division

Usually are CVD processes divided into Thermal processes of CVD and Enhanced processes of CVD.

Thermal processes of CVD are using heated substrates, where the reaction and film formation occurs. In this group was usually classed Atmospheric pressure CVD (APCVD), Low pressure CVD (LPCVD), Metal-organic CVD (MOCVD) and also some publications [[17], [11]] include in this group Molecular epitaxy methods (like as Organometallic vapor phase epitaxy (OMVPE) and Metalorganic vapor phase epitaxy (MOVPE).

Enhanced methods of CVD are using additional sources of energy that involves chemical reaction. These sources of energy are for example lasers in Laser enhanced CVD (LECVD) and very often plasmas in Plasma enhanced CVD (PECVD) [[17], [11]]. PECVD, because it is one of main themes of this work, is in higher detail described in capture 2.2.3.

2.2.3 Plasma enhanced chemical vapor deposition

In plasma enhanced chemical vapor deposition (PECVD) processes, glow discharges are sustained within chambers, where simultaneous vapor-phase chemical reaction and film deposition occur. PECVD like as many other processes of thin film deposition was accelerated mainly, because semiconductor industry needs quality films in relatively low temperatures (ideal below 300 °C), which can be by PECVD methods prepared [11], [17]. Because typical PECVD processes are at lower pressure and temperature it has also higher deposition rates than the thermal CVD methods.

2.2.3.1 Plasma

Principles of PECVD are based on plasma state; therefore some briefly specification of plasma follows.

Plasma of atoms or molecules is four state of matter, which can be specified as electro-neutral (or better quasi-neutral) mixture of electrons, negatively and positively charged species and neutral atoms and molecules. To make plasma state, electron must be separated from atoms (or molecules) to the gas state or atoms must be ionized. In cosmic scale researches assumes that the 99 % of space mass is in high-temperature and high-ionized plasma state [19] [20].

A plasma can be produced by substance temperature rising until a reasonably high fractional ionization is obtained. Under thermodynamic equilibrium conditions the Saha equation (formula {7}) defines the degree of ionization. Plasmas in thermodynamic equilibrium are very common in nature (especially in space) but non-common in the laboratories [20] [19].

$$\frac{n_i}{1-n_i} = CT^{\frac{3}{2}} \frac{1}{n_i} \exp\left(-\frac{U_i}{kT}\right) \quad \text{(eV)} \qquad \{7\}$$

n_i is number density of electrons with ionization energy, C is quantum mechanical constant contributing with weight of electron and Planck's constant (typical about $2.405 \cdot 10^{21}$), U_i is ionization energy, k is Boltzmann constant and T is temperature (°C).

Plasma can be generated by processes, which rises the degree of ionization much above the thermodynamic equilibrium. These processes can be *photoionization* or *electrical gas discharge* (also some other processes exist like collision with high energetic ion or by surface ionization) [20].

In *photoionization* principle of plasma generation photon with energy the same or higher than ionization energy must be absorbed. This process can be very complicated because for example ionization energy of oxygen 13.6eV is identical to light with wavelength 91nm. For many atoms must be used x-ray or gamma rays [20].

In *gas discharge* an electrical field is applied across the ionized gas, which accelerates free electrons to energies sufficiently high to ionize other atoms by collisions. Characteristically to this process is that the energy from electrodes is much better transferred to the light electrons than to the heavy ions, therefore temperature of electrons in gas discharge is much higher than the temperature of ions [20].

For physical specification of plasma is very often used description by *Debye length* parameter, which provides a measure of the distance over which the influence of the electric field of an individual charged particle (or some nonzero potential surface) is felt by the other charged particles inside the plasma. The charged particle arrange themselves in such a way as to effectively shield any electrostatic field within a distance of Debye length. Shielding of electric fields is consequence of the collective effects of the plasma particles. Debye length (λ_D) is defined by following equation {8}. Equation

shows that the Debye length is directly proportional to the square root of the temperature (T) and inversely proportional to square root of the electron number density (n_e) [20] [19].

$$\lambda_D = \sqrt{\frac{\varepsilon_0 kT}{n_e \cdot e^2}} \qquad \{8\}$$

ε_0 is permitivity of free space and e is ion charge.

Also is very convenient to define *Debye sphere* as a sphere inside of plasma with radius of Debye length. Any electrostatic field is originated outside of the Debye sphere is effectively shielded by the charged particles and not contribute to significantly to the electric field existing in center. Consequently every charge interacts only with particles inside of Debye sphere (N_D) [19] [20].

$$N_D = \frac{4}{3}\pi\lambda_D^3 n_e \qquad \{9\}$$

One of main consequences of this effect is that the plasma using reactors must be much larger (main size parameter L) than the Debye length. This concequence is also *first criterion* of plasma [20].

$$L >> \lambda_D \qquad \{10\}$$

Since the shielding effect of plasma is the result of the collective particle behaviour inside a Debye sphere it is also necessary that the number of electrons inside of Debye sphere be very large. A second criterion of plasma is therefore

$$n_e \lambda_D^3 >> 1 \qquad \{11\}$$

This equation means is that average distance between electrons must be very small compared to Debye length [20].

Third criterion of plasma is criterion of macroscopic charge neutrality [20].

$$n_e = \sum_i n_i \qquad \{12\}$$

2.2.3.2 Technological equipment

Plasma enhanced CVD processes are distinguished by excitation source to for example RF or microwave and also by type of coupling to capacitive or inductive. Take into consideration this construction of reactors (and apparatuses completely) varies [11], [17].

Reactor of direct system is always evacuate-able chamber from conductive or non-conductive material. Easiest type is tube or cell (tunnel type) of non-conductive material, such as glass, with coil over it (inductively coupled type) or rings or plates (capacitive coupled type) for ionization energy transfer from the source. Inductive coupling is used to apply the radio-frequency voltage leading to higher plasma density and monomer fragmentation [21] .Most often used reactor type is cylindrical with parallels plates as electrodes inside (conductive materials are used for body material of reactor) or outside (non-conductive materials are used). Typical example of cylindrical reactor is his-

torical Reinberg type, which is shown by Fig. 4. Main advantages of this type of reactors are radial uniformity of discharge between electrodes, which enables reasonably uniform and controllable grow of thin film and good distribution of reactive gas [11]. Several modification of this type of reactor exist to, e.g. add a substrate bias voltage or use non-even formed electrodes to vary ion bombardment on substrate surface.

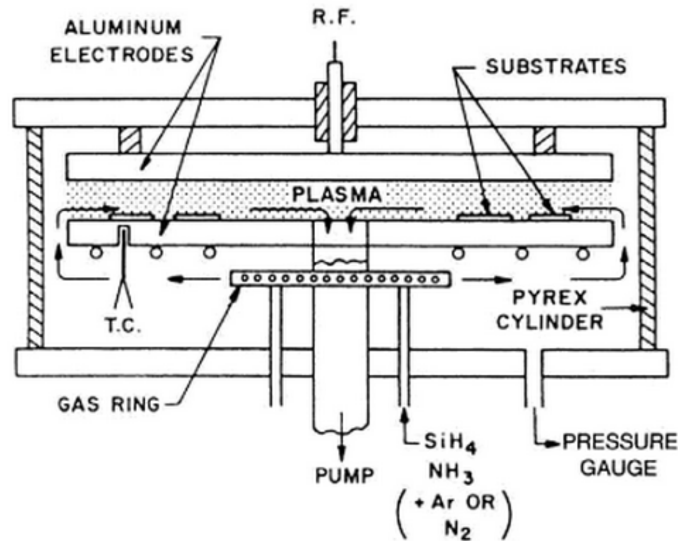

Fig. 4: Histororical reactor for PECVD process constructed by Reinberg 1971 [11]

In some special application, which needs lowered concentration of radicals and other plasma-activated species and by-products on substrates, the *Remote type of reactor* (also known as indirect) can be used. This type of reactors has distinguished zone of plasma discharge and zone of thin-film formation [11], [22].

Source of energy for PECVD reactors is typically alternating current sources, especially Radiofrequency (RF) current source with frequency between 100 kHz to 40 MHz or Microwave current source (MW) with frequency in 1–5 GHz (typically 2,45GHz) with or without magnetic enhancement (ECR). Sometimes also medium frequency plasma sources such as dual-magnetron systems (50kHz) are used. DC charges aren't used commonly because thin-films generated by PECVD is most commonly dielectric [22], [11], [17]. All of this type of sources must be matched to the impedance of the system [22]. Most often, this is realized by matching networks composed from the variable induction coil, in series to load, and variable capacitor parallel to load or by composition of non-variable induction coil and two variable capacitors – one in series with load, second in parallel, but many other solutions are possible [23].

Most frequently are PECVD systems evacuated, for these applications are used *vacuum pumps* with suitable pressure and gas flow rating accommodating selected type of technology. Commonly as fore vacuum pumps, the rotary vane pumps or for more sensitive application dry pumps like Scroll type are used. Because many PECVD technologies use pressures from 5–100Pa [22], fore-vacuum pumps may be suitable as only one

vacuum source, but in some more sensitive technologies (like in semiconductor industry) higher purity of the reactor area is needed. Purity is most commonly realized by pumping up to high-vacuum levels, therefore turbomolecular pumps or diffusion oil pumps are used (Fig. 5) [11], [24].

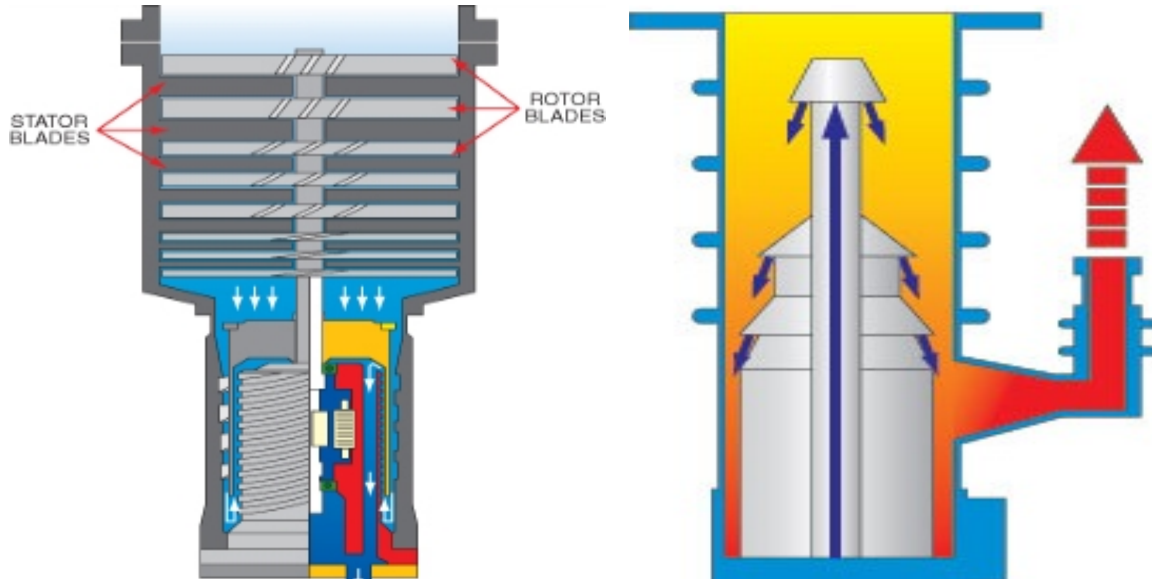

Fig. 5: Function illustration of Turbomolecularpump and Diffusion oil pump [117]

Reactivity gases flow must be accurate controlled primary for the reaction conditions stability and also for the typical high economical consumptive. For this control usually mass-flow controllers are used [25].

2.2.3.3 Mechanism of PECVD process

PECVD is method that uses low-molecular mass, volatile or vaporized species (monomers) with assistance of plasma energy to form high-molecular mass compounds – plasma-polymers (pp) in process called plasma polymerization. Plasma polymerization is process that can be specified as thin-film formatting process, where thin-films are deposit directly on substrates without any previous fabrication, than direct plasma treatment. In chemical meaning is plasma polymerization very different from any other type of polymerization. Plasma polymerization use the plasma energy to fragmentation of monomer species to radicals and ions, which means that the polymerization doesn't occurs at the end of chain as in conventional radical or ionic polymerization, but it is atomic polymerization principle (refer to schema on Fig. 6) .

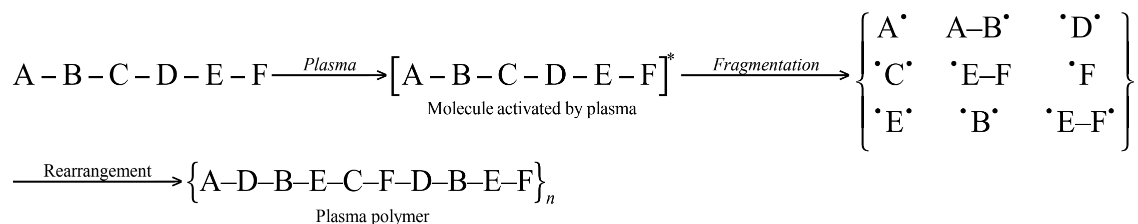

Fig. 6: Schematic presentation of plasma polymerization [11]

That means, excluding other facts, for example that the plasma polymerization can retain unsaturated bonds in its final products. Following Fig. 7 represents overall plasma polymerization principle.

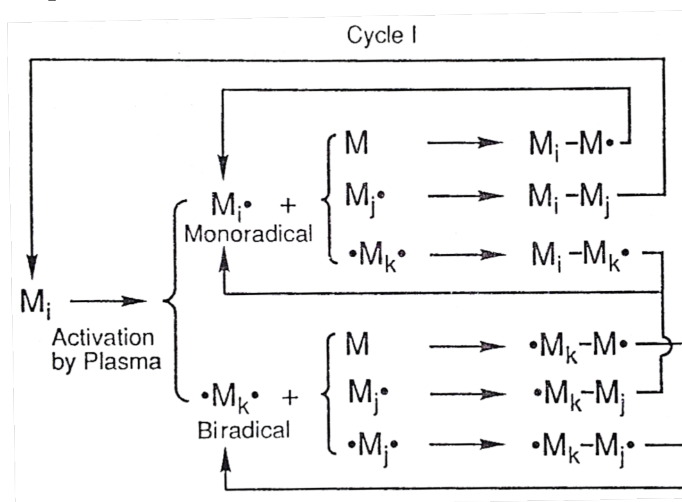

Fig. 7:Overall plasma polymerization principle [26]

Fig. 7 shows essential plasma-polymerization principle, which was proposed by Yasuda. In first step, the hydrogen atoms, was eliminated by plasma electrons and monoradicals $M_i^{\bullet}$ and biradicals (bifunctional particals as radical-ions) $^{\bullet}M_k^{\bullet}$ forms. At next step radicals (or biradicals), which was produced by plasma-electron collisions, reacts with "new" molecule of monomer or with other radical (or biradical) by recombination process to form new radical or neutral products. Also neutral molecule, which is product from previously acted reaction can be activated by plasma again and react. Cycling of this process plasma-polymers forms [26] [11].

2.2.3.4 Monomers for PECVD processes

PECVD technologies are able to produce various types of products like as e.g. mixed oxides, nitrides, carbides, hydrides, various types of plasma polymers and many others, depending only on monomers, which are used [11], [24], [22].

Monomers for PECVD may be selected for its chemical composition, which can independently ensure required thin-film composition (fluorocarbons, hydrocarbons etc.), or they are selected as particular source of final structure, which has to be supplemented by other monomer or reactive gas (nitrogen, oxygen …). By the range of the application of PECVD, really large amount of monomers can be used. In following paragraph only some examples was selected.

Significant share of PECVD industry (and research also) is focused on barrier films and low-k films, which are using organosilicon gases as monomers, to form alloys a-SiCO:H, a-SiC:H, or compounds like SiO_x or SiN_x. Typical examples of this monomers are e.g. trimethylsilane $(CH_3)_3SiH$ [27], [28], [29], [30], tetramethylsilane $(CH_3)_4Si$ [31], [32], [33], hexamethyldisiloxane $(CH_3)_6Si_2$ [34], [35], [36], tetraethylorthosilicate $(CH_3–CH_2–O)_4Si$ [37], [38], [39], tetramethyl-cyclotetrasiloxane [40], [41], hexamethylendisilazane $(CH_3)_3–Si–NH–Si–(CH_3)_3$ [22] and silane SiH_4 [42], [43], [44].

Other share of PECVD research is concentrated at diamond like carbon layers (DLC). For produce of DLC most often are used hydrocarbons like methane [45], [46], ethyne [47], [48] or mixtures of hydrocarbons and organosiloxane [49] are used.

2.2.3.5 Deposition conditions

PECVD processes needs for their successful activity sufficient amount of molecules of reactive gas, opposite the plasma treatment processes which needs only small amount of them. That is the reason, why pressures in PECVD processes are usually between 1–1400 Pa absolute pressures [11] [21]. More precisely than pressure, the flow of media in reactor must be secured. Exact flow rates depend on reactor sizes.

PECVD is used for production very different types of products, but one of its most known advantages, opposite the thermal CVD is lower temperature of process. Typical process temperatures in semiconductor industry do not exceed 450 °C [50] [21]. Very often also ambient temperatures are used, or samples are cooled to ambient or lower temperatures (e.g. because of its thermal instability) [21].

Most important parameter of PECVD processes is electric power, and its type, provided to the reactor. Frequently is RF or MW sources used with large range of power (actually power must be selected, by supposed size of plasma zone) and current densities.

A deposition rate varies with other deposition parameters, frequently from $10^{-1} - 10^{2}$ nm per second [21].

2.3 Thin film analysis

For this thesis two main tasks were entered. First task concerned preparation of thin films and second its analysis. Because of that following chapter theoretically describes basics of methods witch would be possibly used to prepared film analysis.

2.3.1 Spectroscopic analysis

Spectroscopy is the study of interaction of sample (matter) and radiated energy. Spectroscopic methods are using very long range of frequencies (wavelengths), which obviously defines it usage. For spectroscopic methods is typical, their output, which is graph of signal dependence on energy of radiation – it is called “spectrum”.

2.3.1.1 Fourier Transformed Infrared Spectroscopy (FTIR)

Infrared spectroscopy is one of most important analytical methods for characterization of chemical structure of organic and also inorganic molecules. Infrared spectroscopy offers important advantages in that the measurements can be carried out for nanolayers located not only on a solid substrate but also on solid-gaseous, solid-liquid, liquid-liquid interfaces, with no destruction on either medium [51].

Principle is infrared spectroscopy based on adsorption of characteristic infrared beam (780nm – 1mm wavelength) by molecules of analyzed sample, which involves in molecules changes of its vibrational and rotational states.

Fourier transformed infrared spectrometer is composed from following basic parts [52]:

1. IR emitter (source – usually electrical heated ceramic body)
2. Beam splitter (device splitting beam from source into mirrors of interferometer and sample)
3. Michelson interferometer (based on fixed and moving (scanner) mirror)
4. Detector

Typical schema of FTIR spectrometer is shown at picture Fig. 8.

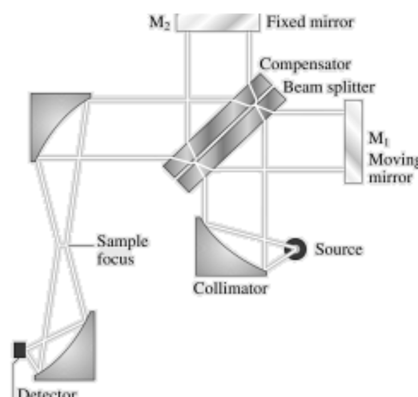

Fig. 8: Basic principle of FTIR spectrometer [52]

For usage infrared spectroscopy (witch some exceptions only Fourier transformed IR is used) for analysis of thin films typical methods have to be adapted to measure spectra with very small amount of substance. For example thin film on substrate, which is IR transparent, is offending, because very thin layer deals only very low signal. For this application Multiple Internal Reflection (MIR) technique was developed. Many other techniques are developed or modified from bulk material analysis e.g. Diffuse Reflectance Infrared Fourier Transform Spectroscopy (DRIFTS), Infrared Reflection Absorption Spectroscopy (IRRAS), Attuned total reflectance (ATR) etc. Techniques used for analysis in IR spectra commonly uses polarization of incidence light [51].

Fourier transformed infrared spectroscopy is very often used for analysis of thin films prepared by PECVD processes. Frequently is FTIR used for determination of structure of a-Si:H layers [53], [54], a-SiCO:H [55], [56] as like determination density of significant bonds in structure [57] and also in special cases also for quantitative (and semi-quantitative) analysis [57].

2.3.1.2 Spectroscopic ellipsometry

Ellipsometry is a spectroscopic optical measurement technique that characterizes light reflection or transmission from sample. The key feature of ellipsometry is that it measures the change in polarized light upon light reflection on a sample (or light transmission by a sample). Name “Ellipsometry” originate in elliptical polarization of light, which is used for ellipsometry measurement [58], [59].

Measurement of ellipsometric spectra consist of data phase difference (Δ) and amplitude ratio (ψ), between *p*-polarized and *s*-polarized light, depending on wavelength of light. In general, the spectroscopic ellipsometry measurement is carried out in the ultraviolet-visible (UV-VIS) region, butmeasurement in the infrared region has also been performed widely [58], [59].

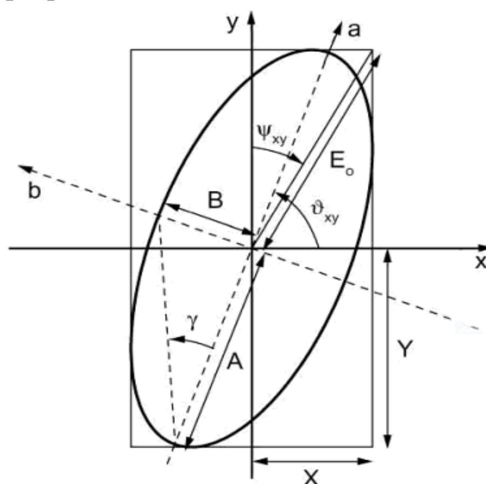

Fig. 9: Elliptical polarization of light

Usage of spectroscopic ellipsometry (ELL) is really wide. Frequently is ELL used for determination of optical constants as like complex reflective index [60] [61], absorption coefficient [60] [61], complex dielectric constant [61], thin-film thicknesses [61], Bandgap [62], Surface temperature, Phase structure and also some concentration and mobility measurements [63]. Very often is ELL also used in in-situ modification, which allows ELL to make real-time measurements, like kinetic studies or as real-time control of CVD and molecular beam epitaxy (MBE) processes [58], [59].

ELL is able to measure films with thickness between $0.1\,\mathrm{nm}$ to $100\,\mu\mathrm{m}$ with number of interlayers limited only by optical constants. Only two limitations exist; Surface of the sample must be sufficiently reflective and Surface must have sufficiently small roughness [59].

Ellipsometers have usually construction type: Light source, polarizer, sample, polarizer detector. Advanced configurations include phase shift device (retarder) before or after sample. By construction of retarder various types of ellipsometers exists, but most often are rotating element and polarization modulation types exploited. Rotating element ellipsometers are using continuously rotating element $(10-40\,\mathrm{Hz})$ and polarization modulation types are using photoelastic modulators (PEM) [58], [59].

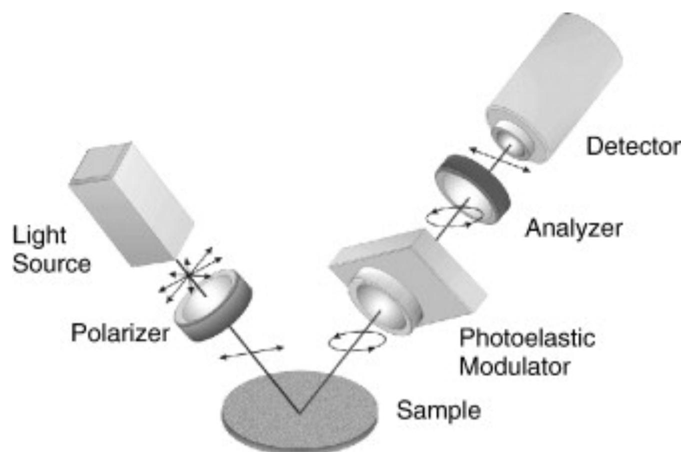

Fig. 10: Schema of spectroscopic ellipsometer with PEM modulator [64]

As detectors are frequently used photomultiplier tubes or photodiodes (monochromator distincted). For detection whole spectra at ones (RT-applications) photodiode arrays (PDA) or charge coupled detector (CCD) detectors are used [58].

2.3.1.3 X-Ray Photoelectron Spectroscopy (XPS)

X-ray photoelectron spectroscopy (XPS) is currently one of most widely used surface analytical technique [65], [66], [67]. Sometimes is this method by industrial laboratories named ESCA – Electron spectroscopy for chemical analysis, but this term is to general, because many other surface-electron spectroscopies techniques exist [68], [69].

XPS utilizes X-ray photons to ionize atoms and analyzes the kinetic energies of ejected photoelectrons. Atoms core electrons binding energies of the elements are distinctive; therefore XPS can be very valuable method to determining of material composition. Because the binding energy of atom electrons is influenced by chemical valence, also chemical valence takes effect on kinetic energy of ejected core electrons, which allows XPS to observe chemical binding information [68], [69].

In principle, the surface to be analyzed is irradiated with soft X-ray photons. When a photon of energy *hv* interacts with an core electron in a level of energy *X* and binding energy E_B, the entire photon energy is transferred into the electron, which results that the core electron is ejected with kinetic energy E_{KIN}, which is defined by following equation {13}.

$$E_{KIN} = h\nu - E_B - \phi_S , \qquad \{13\}$$

where ϕ_S is small, almost constant work function term.

Obviously X-ray photon energy *hv* must be greater than binding energy of atom. After the photoelectron has been ejected, the atom is left with vacancy in core level. An electron from higher energy level generally occupies this, and subsequent de-excitation of the atom energy may occur by emission of Auger electron or X-ray fluorescence. Thus this in all spectra of XPS features appears as result of both - Photoemission and Auger emission (Fig. 11).

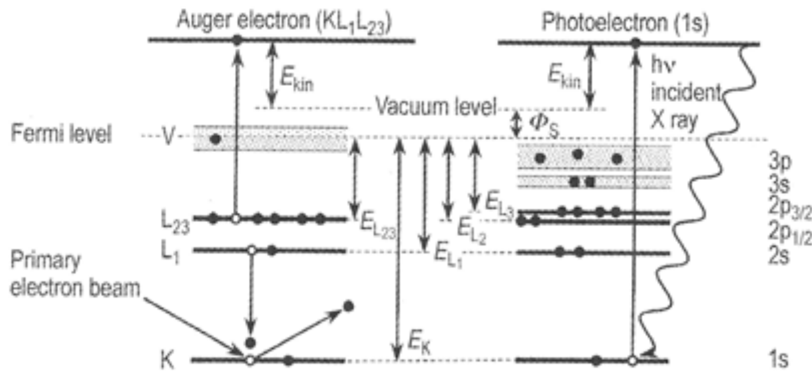

Fig. 11: Principle of photoelectron and Auger emission

For the principle of the work, XPS systems must be evacuated to ultra-high vacuum (UHV) with level at least up to $1 \cdot 10^{-7}$ Pa and all of purity criteria for UHV must be satisfied. As the typical primary X-Ray beam sources, Mg and Al (K_α) X-ray tubes are used. For perfectly adequate and more precise measurement "tunable source" Synchrotron beamlines may be used. For the analysis of ejected electron energies the concentric hemisoheral analysers (CHA) are applied and photomultiplier tubes realize detection.

2.3.1.4 Rutherford Backscattering Spectroscopy (RBS)

Rutherford backscattering spectroscopy is one of most often used analytical techniques for quantitative analysis of composition, thickness and depth profiles of thin solid and bulk solids surfaces. Because of its quantitative feature, RBS often serves as standard for other techniques (e.g. calibration of quantitative interpretation of FTIR [57]).

In RBS, a beam of mono-energetic ions, usually He^+ of typical energy from range $0.5-2.5\ \mathrm{MeV}$ is directed at the target, and the energies of the ions, which are scattered backwards is analyzed. In the backscattering collision, energy is transferred from the projectile ion to the target atom. Energy ratio between energy of projectile ion E_1 after collision and energy before collision E_0 is called the kinematic factor *K (*figure {14}) [68] [70] [71].

$$K = \frac{E_1}{E_2} = \left(\frac{\sqrt{M_2^2 - M_1^2 \sin\theta} + M_1 \cos\theta}{M_2 + M_1} \right)^2 \qquad \{14\}$$

Kinematic factor K shows that the energy after scattering depends only at mass of the projectile (M_1), mass of the sample atom (M_2) and angle of incidence (θ). Typically M_1, E_0 and θ are known, which allows to determine M_2 and identify the sample atom. For sufficient scattering mass of sample atom M_2 must be higher than projectile ion mass M_1 [68] [70] [71].

Main advantage of ion methods is that they are not acting only at surface but also in volume of material. Equation 15 is valid only for atom scattered on surface of sample. In fact, the ion penetrates the target and an ion might be scattered by any sample atom trough the beam path. Energies of projectile ions which are used in RBS provide straight line trajectory trough the sample. When the projectile ion passes through the sample, his energy is decreased by excitation and ionization of sample atoms (electronic energy loss). The energy loss per unit of path length (depth in sample) is called as stopping power, which acts on RBS spectrum by widening of sample atom peak [68] [71].

RBS is psychical method of analyze sample, because of its principle, it cannot deal any sample chemical information [71]].

Ion beams suitable for RBS are typically produced by particle accelerators, most widely by Van den Graaff type. One type of ions is selected by analyzing magnet. The beam spot is most often selected as $1\ \mathrm{mm}^2$ and for more precisely mapping spot reducing electromagnetic lens are used. Whole volume of RBS aperture is usually evacuated to UHV vacuum (but at least to 10^{-4} Pa). For general analysis technique, sample is mounted on holder with selected angle of incidence. When the structure is also demanded, sample is mounted on multiple axis manipulator. Best angle of incidence is $180°$ but for practical reasons $\approx 170°$ is used. As detector solid state detector (SSD), surface barrier detector (SBD) or passivated implanted planar silicon (PIPS) may be used [68] [70] [71].

Because RBS is a major technique for the analysis of thin solid films and surfaces of bulk material, it has very large spectrum of usage. Most RBS uses are field tor analysis of semiconductors and other support material in semiconductors technology.

For study of PECVD silicon and organosilicon films was RBS used in [Chang] for study Si/O_2 ratio in nanocrystals, for study of SiC content [72] and for study multilayers [73].

2.3.1.5 Elastic Recoil Detection Analysis (ERDA)

Elastic Recoil Detectionis an Ion Beam Analysis technique in materials science to obtain elemental concentration depth profiles in thin films. In ERDA target atoms, which are recoiled in the forward direction by projectiles with energies in MeV range, are analyzed, but not the scattered projectiles (RBS technique). Because the sensitivity of ERDA is almost the same for all types of atoms, method is most commonly used for analysis of light elements, which are very hard to analyze by RBS.

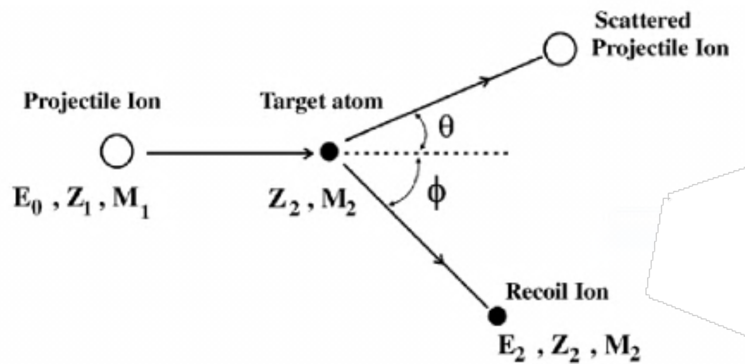

Fig. 12: Principle of projectile ion action in ERDA and RBS technique

The ERDA provides depth as well as mass information regarding the target particle location and therefore allows simultaneous profiling of all elements within the substrate.

In ERDA the particle yield is measured in forward scattering geometry – at angles of detection lower than 90° relatively to the beam. As the projectile ion are most commonly used light projectiles like He or C ions with energies between 2-10 MeV for analysis of very light elements (e.g. hydrogen). Moreover medium heavy (e.g. Cl) or Heavy (e.g. Au) with energies about 30MeV respectively 100MeV are used for the analysis of light and intermediate elements. Projectile ions are produced by ion accelerators (mainly by tandem Van den Graff type).

Particle identification can be achieved by Energy loss measurement or by velocity measurement (TOF method). Energy loss method is using thin solid foil or gas layer in front of detector to identify particles of the same energy (in most cases Milar foil or Al foil is used). In TOF systems, particle energies are usually determined by time of flight measurement between two thin foils (most often Carbon). First foil delivers start signal and second stop signal.

Detection of recoiled ions is realized by solid-state or surface barrier detector (SDSs) detector.

In thin film analysis is ERDA mainly used for study of light elements profile like oxygen [74], carbon [75] and mainly hydrogen [75], [76], [74].

2.3.1.6 Mass spectrometry (MS)

Mass spectrometry is for application to study of thin-films used in two very different ways. First usage is for *in-situ* monitoring of reactive gas during deposition and monitoring of residual gas. Second application is uses for analysis of prepared films by Matrix-assisted laser desorption/ionization with (frequently) time of flight analyzer (MALDI-TOF) technique.

Mass spectrometry is simply analytical technique, which offers division of charged particles by their mass, respectively mass to charge ratio *m/z* [77].

Every mass spectrometer consists of three major parts: the ion source, the mass analyzer and the detector. Since the mass analyzer and the detector require low pressure for operation, the instruments needs to have a sufficiently powerful HV pumping system [77] [78].

Role of the ion source is to create gas phase ions. Because, this thesis is focused on thin layers and its technology of preparation, next information has contribution with that. For reactive (plasma) gas analysis only Electron ionization type of ion source makes sense, because it is only one, which results (with optimal settings) can be compared with databases. Other types of ion sources are unspecific. For analysis of prepared film MALDI would be used as ion source, but this method cannot be compared with databases spectra [77] [78].

Analyzer for plasma monitoring is frequently quadrupole or in tandem ranked tree quadrupoles. Quadrupole consist of four cylindrical rods, set parallel to each other, when always pair has same potencial with submitted RF current. RF current causes the electrical field, which is passable only for selected m/z ratio particles on the way to detector. All other particles collide with rods. For MALDI ionization technique frequently TOF is used. TOF is simply long glass tube with accelerator at start (gives start signal) and detector at the end (term signal). Division is realized by difference of speed of particles with different *m/z* ratio. Other methods like magnetic or electrostatic analysers may be also used, but they are not so common for their space requirements or like “Orbitrap” or FT Ion cyclotrone resonance for them economic aspects [77], [78].

Detection is most commonly realized by two types of detectors Faraday cup and electron multiplayer (SEM) which only noteworthy differencesare range of use and sensitivity [78]. Because of that in some systems both are installed.

For process gas analysis the mass spectroscopy were used for deposition plasma in various types of modification [79], [80], [81].

2.3.2 Microscopic analysis

Microscopic analysis of prepared thin layers is one of most important analytical methods, because it may deal (especially in nanoscale) information about quality of prepared layer, its topography same as important parameters of it mechanical, electrical and magnetic properties.

2.3.2.1 Atomic Force Microscopy (AFM)

Atomic Force microscopy (AFM) belongs to the group of scanning force microscopies (SFM) techniques. AFM is the method to see the surface in three-dimensional detail down to the nanoscale. AFM can image surface of every almost every material (hard, soft, …), syntactical or natural (including biological) irrespectively of its opaqueness or conductivity. The morphology is perceived by measuring height of the sample in each pixel of the photo. Principally is AFM "blind" microscopy because it is using "touching" of measurement very sharp tip on soft cantilever to the sample to achieve local height, unlike light or electron microscopies. Physically, AFM is based on atomic repulsive force between atoms of sharp tip and atoms of sample [68], [82].

AFM measurement is almost contact technique, but simultaneously the contact force is set to its minimum by pulling the probe tip over the attractive force out. The pull-out force may be reduced by using liquid environment to reduce capillary forces. One other option to imagine surfaces more gently is *Tapping mode*, which is characteristic by driving the cantilever (and tip on it) near its resonance frequency by piezo-oscillator. Thus this, only internment contact of tip with sample occurs [68], [82].

AFM can be operated in two different modes, the *constant force mode* and the *constant height mode.* In constant force mode, the cantilever deflection is kept constant by changing vertical position tip-sample. Main advantage of this method is that relatively large areas can be scanned without destroying the tips. Constant height mode is mode when the vertical position of sample is constant and cantilever deflection is varying. This mode is faster and it is eliminating temperature drifts, but tip crash are possible.

Every AFM system must have following basic components [68], [82]:

1. Sharp tip on a soft cantilever
2. Detection system for measuring cantilever deformation
3. Piezoelectric translator to move probe relative to the sample (x,y,z)
4. Feedback system to keep constant by height adjustment
5. Imagine system to convert data points to image

The tips are almost every time silicon or silicon nitride with radius ofcurvature in nanometers order. The cantilever must be sufficiently soft, than no damage on sample arises. Position of probe is measured by incidence of laser beam to the cantilever and measurement its angle of reflection by two photodiodes in defined spacing between them [68], [82].

In additional to topography, some other techniques of AFM are used. *Friction force microscopy* and *Lateral force microscopy* measures the friction between tip and sample surface. *Young modulus microscopy* is using measure of the response of the tip on verti-

cal modulation of sample while tip is in contact to achieve differences of surface elasticity. Also other than mechanical forces microscopy can be used. Using electrical conductive tip electrostatic forces can be achived by *Electric force microscopy*. Also if tip has magnetic domain inside, magnetic properties can be analyzed be *Magnetic force microscopy* [68], [82].

2.3.2.2 Scanning electron microscopy (SEM)

Scanning electron microscopy is one of the most famous and widely used microscopic methods, with the only possible exception of optical microscopy.

Principally imaging part of typical SEM is based on measuring signal given by detector of secondary electrons, which are spurted from the sample by primary electron beam. Primary electron beam is most commonly produced by thermoionization process on electrically heated tungsten cathode or at systems with higher requirements to resolution is Shottky cathode. Electron beam is focused by set of electronic condenser lenses to the sample. Secondary electrons (SE) are detected by detector of SE, which is orientated almost perpendicular to the primary electron beam. Electrical signal detected on SE detector gives information about topological contrast [83] [84].

Primary electron beam incidence to the sample causes exclusion of previously mentioned secondary electron spurt also backscattered electrons (BSE), primary X-rays, X-ray fluorescence (secondary), UV and visible light (cathodoluminiscence) and Auger electron emission. All of these emissions are used for chemical and phase analysis by additional detectors. Most commonly are at SEM microscopes installed X-ray detectors (mainly energy-dispersive (EDX) but also wavelengthdispersive), which offers characteristic elemental chemical analysis. BSE electrons are electrons reflected from sample and they energy is strongly related to atomic number. That allows to make mapping of elemental composition of sample [83], [84].

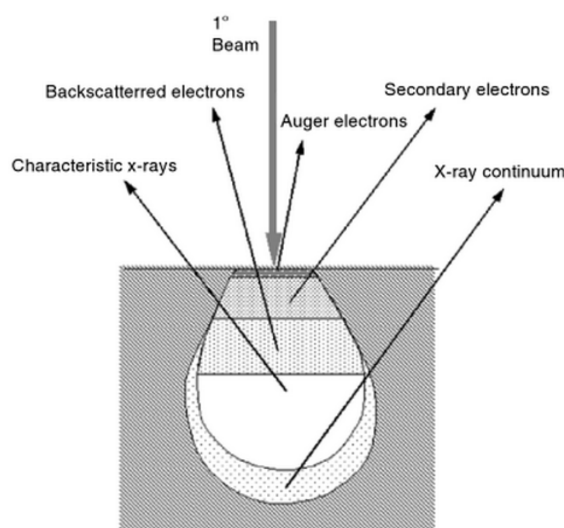

Fig. 13: Illustration of signals generated by incidence of electron-beam in SEM

Only one, but very important disadvantage of SEM is requirement of conductivity of sample. That does not mean, that nonconductive samples cannot be imaged (or measured), but surface of the sample must be overcoated by conductive layer [84].

SEM imaging is very often used to determine surface quality and thin film properties measurements [85]. For verification of PECVD film morphology and topography was SEM used [86] [87] [88]. Also SEM can be used as method for thickness monitoring (image analysis of cross section) [89].

2.3.3 Others analysis techniques

2.3.3.1 Nanointendation

The fundamental difference between nanoindentation and AFM is that during nanoindentation experiment an external load is applied to intender tip. This load enables the tip to be pushed into the sample, creating a nanoscale impression on the surface, otherwise referred as a nanoindent.

When indentations are performed on the nanoscale there is a basic problem in measuring the size of the indents. Standard optical microscope cannot be used to image anything smaller than $1\,\mu\text{m}$, while electron microscopy is simply impractical to use (vacuum, metallization of sample etc.). To overcome this problem, nanoindentation methods was developed that continuously record the load, displacement, time and contact stiffness throughout the indentation process (that's the reason, why it can be also classified to microscopy group).

In general, nanoindentation instruments include a loading system that may be electrostatic, electromagnetic or mechanical, along with a displacement measuring system that may be capacitive or mechanical with optical feedback.

Nano indentation is able to measure plastic same as elastic properties of the sample material. The elastic modulus is obtained by from the contact stiffness (S) calculated by following formula {15},

$$S = \frac{2}{\sqrt{\pi}} E_r \cdot \sqrt{A}, \qquad \{15\}$$

where A is contact area tip surface and E_r is reduced modulus of the tip. And final modulus of elasticity is calculated by equation $\{16\}$.

$$E = \frac{E_\text{i} E_\text{r} \left(1-\nu^2\right)}{E_\text{i} - E_\text{r}\left(1-\nu_\text{i}^2\right)}, \qquad \{16\}$$

where E is modulus of film elasticity, ν is Poissons ratio of the film and E_i, ν_i are constants of the tip.

In application of nanoindentation to thin films is really important to assume, how large a plastic zone before the indenter is. The depth of tip penetration must be selected such way to prevent effect of underlying substrate or interlayer (most commonly around 10% of film thickness)

Nanointendation was used for study of materials prepared by PECVD for study e.g. Young's modulus [90], [91], [92], depth profile stiffness and hardness [93] [94], time-dependent plastic properties [94], phase transformation etc.

2.3.3.2 Contact angle (Wetting) and free surface energy

Wetting is the ability of a liquid to maintain contact with a solid surface, resulting from intermolecular interactions when the two of surfaces are brought together. Adhesive forces between liquid and solid causes that a liquid drop spreads across the surface. Cohesive forces within the liquid cause the drop to ball up and cause contact with the surface. The result of adhesive and cohesive forces is formation of "contact angle" between the interfaces.

If drop of liquid is dropped onto solid surface, there are to possibilities: the liquid spreads the surface completely (super-wetting, contact angle $\theta = 0°$) or finite contact angle is established. In the second case a three-phase contact line (wetting line) is formed. At this interface three-phases are in contact: the solid, the liquid and the vapor (or in some cases other liquid). Young's equation relates the contact angle to interfacial tensions γ_S, γ_L and γ_{SL}.

$$\gamma_S - \gamma_{SL} = \gamma_L \cdot \cos\theta \qquad \{17\}$$

If the interfacial tension of bare solid surface γ_S is higher than the solid liquid interface γ_{SL}, the left side of the equation 17 will be positive. Contact angle has to be positive and smaller than $\cos\theta < 90°$; liquid wets solid. Other way, if $\cos\theta > 90°$ the liquid is not wetting solid completely. [[95]]

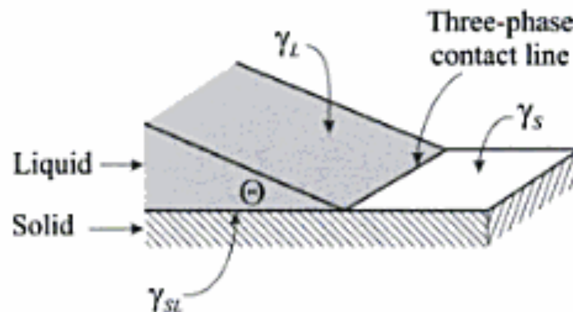

Fig. 14: Illustration of three-phase contact of liquid drop at solid [95]

Determination of contact angle is most commonly realized by observing a sessile drop with telescope or microscope. The light source is placed behind the drop, which then appears dark. The contact angle is determinate directly with goniometer or by the image processing in computer fitting to Laplace equation. For small drops are hydrostatic effects negligible and contact angle can be determinate directly by measurement of drop height (h) and contact area radius (a).

Contact angle is calculated by equation {16}.

$$\tan\left(\frac{\theta}{2}\right) = \frac{h}{a} \qquad \{18\}$$

Also some other methods like Wilhemy plate method or Capillary raise method may be used [95].

In thin film preparation techniques are this method of analysis used primary for determination quality of preparation processes (cleaning) of substrates [24] or for study of prepared films with controlled wetting like superwetting films e.g. by PECVD films from fluorocarbons [96] increasing wetting by DLC [97] or preparation of TiO_2 films with photocatalitic and superhydrophilic acting [98].

2.4 PECVD films applications

As previously mentioned PECVD processes are one of most widely used processes of thin film processing all over the world. Main development in this area is oriented to production of functional parts in semiconductor industry (MEMS devices, barriers and solar cells), but also some other very applicable areas of usage was developed such as gas barrier coatings, corrosion and abrasion protection and specific interlayers in polymer composites.

In semiconductor industry main development is situated in area of preparation low dielectric films (low-k) or ultra-low dielectric films for usage as non-conductive barrier in shrinking transistors arrays (e.g. computer processors) and other electronic components, which needs electrical barriers with constant of conductivity $k < 3$. This parameter can be achieved e.g. by PECVD process with organosiloxanes as precursors. For example Cho et. al. achieved that dielectric constant of multilayer thin films prepared from TEOS and Toluene as precursors by PECVD process are very dependent on ratio of amount inorganic/organic layers [39]. Some investigation of specific "tailoring" of precursors was also done by François Doniat et. al., which studied dielectric films from $R_1R_2R_3$–Si–C_xH_{2x}–Si–$R_4R_5R_6$ with x = 1, 2 and R = H, Me, OEt precursors assuming low-k films with $k = 2.5$ [99]. Also using mixture of MTMS ($C_4H_{12}O_3Si$) and oxygen gases as precursors in a PECVD system at room temperature R. Navamathavan et. al. studied dependence of effective RF power to dielectric constant of prepared film and concluded, that dielectric constant is in range 600-900W decreasing with increasing RF power (3.4 for 600W to 2.2 for 900W) [55]. Commonly is also PECVD technology used for preparation of a-Si:H (amorphous silicon) films in the production of solar cells [100].

Food industry same as part of medicinal and military industry uses PECVD processed films as gas barrier coatings. Primary application fields on food packed in protective (almost inert) atmosphere, which is frequently packed into polyethylene (PE), polypropylene (PP) or polyethylene-terephthalate (PET) packages or bottles. This materials are inexpensive, and well workable, but has disadvantage in the gas (O_2, CO_2, H_2O) and other pollutants (favors, aromatic compounds) permeability. This permeability may be reduced by SiO_x and SiO_xN_y coating. Simone Plong et. al. studied effect of layer thickness and O_2:HMDSN (x:1) gas mixture ratio on the water vapor transmission rate and oxygen permeation, while obtained the reduction of the O_2 permeation by more than two orders of magnitude with only 100nm thick film [101]. Recently also DLC layers are studied for application as gas barriers [102].

Other application of gas barriers e.g. is in liquid crystal display manufacturing, where the water vapor transmission rate (WVTR) is very important parameter. WU Cheng-Yang et. al. investigated SiO_x films from TMS precursor with the MOCON detection limit ($<1 \times 10^{-2}$ g/m^2/day), which allows to use this films for flexible and thin optoelectronic devices [103].

In recent decades investigation of a-SiC:H and a-SiCO:H alloys for application as surface corrosion or abrasion protection was started. S. Guruvenket et. al. studied the corrosion resistance of a-SiC:H layer, prepared from mixture of silane and methane obtaining that with increasing carbon content enhanced mechanical performance obtain, but also when Si/C ratio is about 1 layer delaminates from steal and titan substrates easily [104].

Intensive development on interlayers in polymer composites is currently being at Faculty of chemistry, Brno university of technology under leadership of Prof. RNDr. Vladimír Čech PhD. Simplified the research leads to development of composite “without” sharp interface between glass fibers and polymer matrix. That can be assumed by preparation of multilayer interface with glass-like properties at one side and polymer-like properties at second side [105], [106], [107].

3 OBJECTIVE

This diploma thesis has the task to monitor contemporary research in the field of plasma enhanced chemical vapor deposition (PECVD) processed plasma polymer thin films. In experimental part of this thesis will be prepared a-SiC:H and a-SiOC:H alloys samples produced by PECVD process from tetravinylsilane monomer and its mixtures with argon and oxygen gas at different effective powers under pulsed plasma. Deposited films were investigated by X-ray photoelectron spectroscopy, Fourier transform infrared spectroscopy, spectroscopic ellipsometry, and nanoindentation to observe their chemical, optical and mechanical properties as a function of deposition conditions. Steps with have to be accomplished are following.

1. Background research of PECVD process and analytical methods for chemical, mechanical and optical analysis of plasma polymer thin films
2. Completion of the material base and used technology
3. Deposition of thin films at planar silicon wafer substrates
4. Characterization of chemical, optical and mechanical properties of deposited thin films
5. Investigation of thin film properties as a function of deposition conditions.

4 EXPERIMENTAL PART

4.1 Materials and its properties

4.1.1 Monomer and auxiliary gases

For reactive gas mixing only one monomer was used. This monomer was Tetravinylsilane $\left(C_8H_{12}Si, \text{CAS: } 1112\text{-}55\text{-}6\right)$ with purity 97%, fabricated by SIGMA-ALDRICH Co. Main properties are described by following table Tab. 1. As auxiliary gases for reactive gas mixing Oxygen 99,995% purity (4.5) and Argon 99,999% purity (5.0) from Linde Gas a.s. was used.

Tab. 1: Characteristic properties of Tetravinylsilane monomer [108]

Characteristic property	Value
Purity (GC)	96,50%
Density	0.8 g·dm^{-3}
Index of refraaction	*n*20/D 1.461
Boiling point	130-131°C
CAS number	1112-55-6
Molecular mass	136.27

4.1.2 Substrates

As substrate was selected both side polished, Boron doped (P type), 100 orientated Silicon wafer with thickness $625 \pm 15\ \mu m$ produced by ON-SEMICONDUCTOR s.r.o. company, department Rožnov pod Radhoštěm, primary for its IR transparence.

Fig. 15: Loading silicon wafer sample to sample holder

4.2 Instrumentation

Deposition apparatus (called A3, picture Fig. 16) was designed for PECVD process with capacitive coupled plasma. Whole apparatus was constructed as High-vacuum (HV) system composed from cylindrical reactor $(\text{DN250}, h = 250\,\text{mm})$ chamber with by valve separable load-lock, connected analytical equipment, pumping system and support piping constructed almost from stainless steel. Reactor chamber and piping are equipped by CF (ConFlat) flanges sealed by Copper gaskets, KF (Klein Flansche) flanges sealed by fluoropolymer elastomer o-ring seals or ISO-K and ISO-F flanges also sealed by fluoropolymer elastomer o-ring seals.

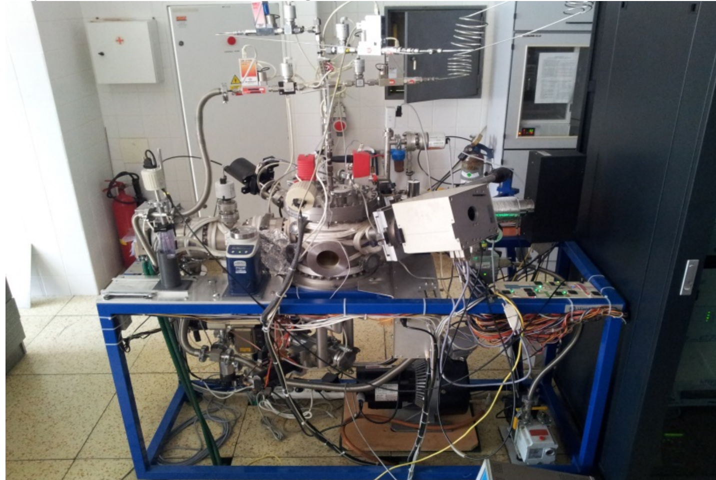

Fig. 16: Overall view to apparatus A3

The reactor is equipped inside with two plan-parallel electrodes. Bottom electrode (RF life) is made from copper OFHC (Oxygen Free High Conductivity) and have diameter 115 ± 0.5 mm. Construction of this electrode is based on T-slots equipped copper upper part (Fig. 17), which enables to insert up to 6 sample holders and secure it in very precise position, separated by aluminum oxide ceramics ring from the electrical grounded neighborhood components of reactor. Upper electrode is constructed as gas shower from stainless steel and it is electrically grounded (connected to reactor chamber). Diameter of this electrode is very same to the bottom one.

Removing or inserting samples is realized under high vacuum by magnetic linear drive manipulator from (or to respectively) the separately evacuated load-lock chamber with ability to store 12 sample holders (2 full batches).

Reactor chamber is equipped by flexible glass isolated heating cables, which allows to bakeout reactor chamber up to $120\,°\text{C}$. Bottom electrode is prepared for heating by electrically non-conductive media up to $300\,°\text{C}$ and cooling up to $-100\,°\text{C}$.

Fig. 17: Photo of electrodes during deposition (below rotational electrode with sample holders)

4.2.1 Pumping system and pressure settings

Pumping system of A3 aperture is composed from vacuum sources and piping between reactor and pumps with regulation valves.

As the vacuum sources a turbomolecular pump (TMU 261 P, Pfeiffer Vacuum, pumping speed $170\,\mathrm{dm}^3\cdot\mathrm{s}^{-1}$, rotating velocity 60,000 RPM) with a dry scroll pump (TriScroll 300, Varian, pumping speed $3.5-5\ \mathrm{dm}^3\cdot\mathrm{s}^{-1}$), serving the fore-vacuum for turbomolecular pump as the first stage, are used. For increase pumping speed and decrease water vapor content in reactor liquid nitrogen (LN_2) cooled trap may be used. Pumping system was designed to attainment vacuum level basic pressure in order to 10^{-6} Pa.

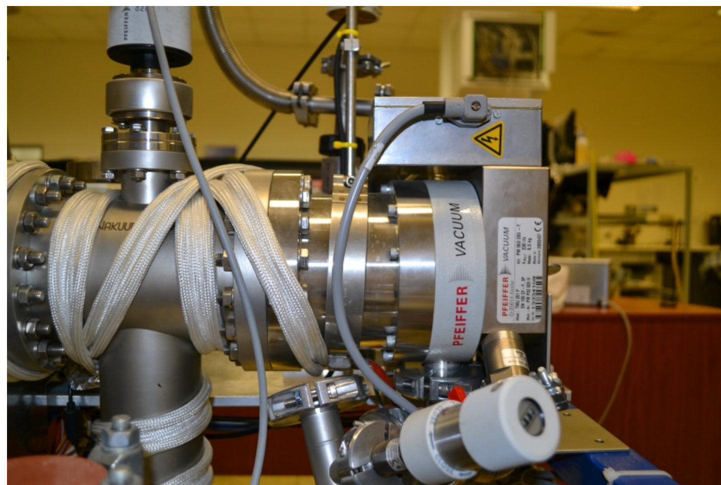

Fig. 18: Photo of Pfeiffer turbomolecular pump and T piece, where Pumping ways I and II combines.

Piping of around the reactor is mainly divided to two parallel ways (at schema attached to this document as attachment 1 marked as I and II). First is high pumping performance and pumping throughput direct pumping way (marked I), which is used for preparation aperture to basic vaccum. Second way (marked II) is designed as process pumping way, which is used for pumping of waste and process gas, when the deposition occurs, or when for other reasons, reactor have to been pressurized. In this way regulation butterfly valve (marked as valve 8) is installed, which propose settings of pumping velocity by reducing the piping cross-section. In this sections other valves are installed it function describes following numbered list (number in this list corresponds with number of valve in schema at attachment 1).

1. Valve is pneumatically actuated, normally closed, angle valve. Valve is designed for turbomolecular pump separation from primary pump.
2. Valve is pneumatically actuated, normally closed, gate valve designed for interruption of I pumping way.
3. Valve is pneumatically actuated, normally closed, gate valve designed for interruption of II pumping way at the pumps side.
4. Valve is pneumatically actuated, double operated, gate valve designed for interruption of II pumping way at the reactor side.
5. Valve is pneumatically actuated, normally closed, angle valve. Valve is used only when turbomolecular pump is stopped for direct connection of primary pump to II pumping way.
6. Valve is pneumatically actuated, normally closed, angle valve. Valve is used for connection of manipulator and load-lock section to primary pump.
7. Valve is manually operated gate valve and separates load lock chamber from the main deposition chamber. Opened is only when samples are moved from or to load-lock or when the reactor chamber is vented.
8. Valve is previously mentioned motorized butterfly valve with electronics, which allows to set its position to 100,000 different position at angle of rotation $90°$.
9. Valve is electromagnetic solenoid valve DN25, which is connected to source of dry air and which is used for venting whole reactor chamber or venting the load-lock system.
10. Valve is manually operated gate valve and separates mass spectrometer assembly from the reactor chamber. Mainly used when the vacuum chamber is vented.
11. Valve is electro-pneumatically actuated, normally closed, angle valve. Valve is used as breaker valve for hydrocarbon sensitive vacuum measurement sensors (marked as M2 and M3)
12. Valve is electro-pneumatically actuated, normally closed, angle valve. Valve is used as breaker valve for capacitance sensor valve (marked M7).
13. Valve is inline pneumatically actuated membrane valve, which is used as breaker valve for separation of vacuum system from mass flow controller of oxygen gas.

14. Valve is inline pneumatically actuated membrane valve, which is used as breaker valve for separation of vacuum system from second mass flow controller of oxygen gas.
15. Valve is inline pneumatically actuated membrane valve, which is used as breaker valve for separation of vacuum system from second mass flow controller of argon gas.
16. Valve is inline pneumatically actuated membrane valve, which is used as breaker valve for separation of vacuum system from second mass flow controller of monomer vapor.

Exact configuration of valves trough processes on aperture A3 is described later in chapter 5.3.

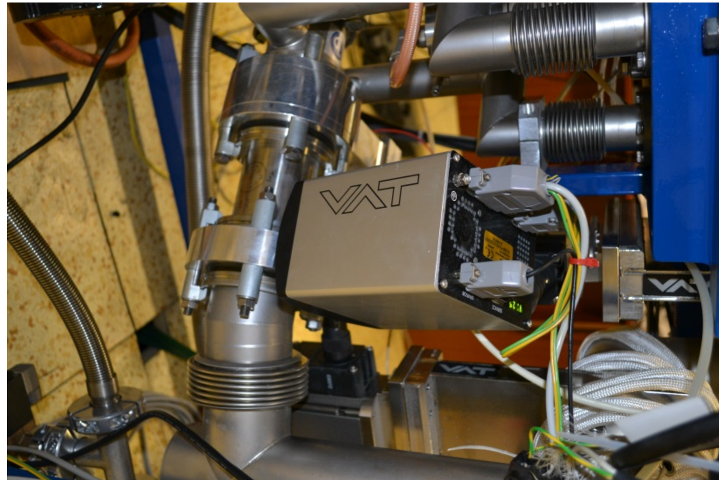

Fig. 19: Detail photo of regulation valve (number 8)

4.2.2 Vacuum measurement

For knowledge of actual conditions in reactor and main support parts the vacuum measurement sensors are installed. At the schema of vacuum components (attachment 1) are sensors marked by prefix *V*. Function and basic description of these sensors represents following number list.

1. Sensor V1 is "full-range" sensor Pfeiffer vacuum PKR 261 with measurement range $5 \cdot 10^{-7} - 10^{5}$ Pa. Internal construction is combination of Piranni and Penning type of sensor. Sensor is used for monitoring of pressure in T-shape piece (point of combination of I and II pumping way) before turbomolecularpump.
2. Sensor V2 is "full-range" sensor Pfeiffer vacuum PKR 261 with measurement range $5 \cdot 10^{-7} - 10^{5}$ Pa. Sensor is used for monitoring of pressure in the reactor.
3. Sensor V3 is "full-range" sensor Pfeiffer vacuum TPR 261 with measurement range $5 \cdot 10^{-2} - 10^{5}$ Pa. Sensor is used for monitoring of pressure in the reactor.
4. Sensor V4 is "full-range" sensor Pfeiffer vacuum PKR 261 with measurement range $5 \cdot 10^{-7} - 10^{5}$ Pa. Sensor is used for monitoring of pressure in the LN_2 cooled trap and also for monitoring of pressure in whole II pumping way.
5. Sensor V5 is "full-range" sensor Pfeiffer vacuum PKR 261 with measurement range $5 \cdot 10^{-7} - 10^{5}$ Pa. Sensor is used for monitoring of pressure in the manipulator and load-lock section.
6. Sensor is not equipped.
7. Sensor V7 is capacitance sensor Leybold Vacuum CTR 91 with aluminum oxide membrane. Measurement range is $0.01 - 10^{3}$ Pa absolute pressure. This sensor is one of most important sensor equipped on the equipment, because it is sensor by its value the reactor pressure trough the deposition is set.
8. Sensor V8 is capacitance sensor Leybold Vacuum CTR 91 with stainless steel membrane. Measurement range is $0.01 - 10^{3}$ Pa absolute pressure. This sensor is used for monitoring of monomer vapor pressure.

The Pfeiffer sensors are connected to the Pfeiffer TPG 256 A controller, which transforms the analog signal $0 - 10$ V to the digital transmissible value, which may be readout by RS232 or RS485 buses. Also the Leybold Vacuum sensors are connected to Leybold Capacitron DM22 Controller, which offers RS232 communication bus. This is important to readout the values and control it from computer (chapter 5.2.6) or other control system like industrial PLC, PXI etc.

4.2.3 Reactive gas mixing

Because the PECVD process is very sensitive to flow and pressure of the species to the plasma zone, the flow has to be precisely regulated and monitored. At the A3 equipment four of the mass flow controllers with the heat conductivity measurement are used.

For high-pressure gases (oxygen and argon) two of the F-201AV series from Bronkhorst inc. controllers, with flow setting between $2-100\,\mathrm{sccm}$ are installed. For more precisely dosing of oxygen the F-201CV series from Bronkhorst inc. controllers, with flow setting between $0.001-3.000\,\mathrm{sccm}$ is equipped.

For the monomer flow control, because of its very low overpressure to the reactor pressure, the other type of mass flow controller (MFC) has to been used. The Series F-101D from Bronkhorst inc. company was used with flow rate settings $0.01-100.00\,\mathrm{sccm}$. Because the flow controllers are not able to control flow rate of special gases by the factory default table it must be recalibrated. Most easily way how to do it is establishment of real monomer flow to the setup flow of reference gas (in our case nitrogen) calibration curve. The calibration curve may be most easily made by measuring the pressure increase in enclosure chamber with constant flow of gas. Folowing equation describes this problem for the A3 reactor chamber. Second way is calculation of MFC internal constant which deals relationship between heat capacity of gas, its pressure and flow.

$$F = \frac{6\cdot 10^7}{101325}\cdot V\left(\frac{dp}{dt}\right)_V, \qquad \{19\}$$

Where $F\left(\mathrm{sccm}\right)$ is the real monomer flow rate, $V\left(m^3\right)$ is defined as apparatus volume (in the case of the apparatus A3 it is $15.7\,dm^3$) and $\left(\frac{dp}{dt}\right)_V$ $\left(Pa\cdot s^{-1}\right)$ is the angular coefficient of pressure growth at constant volume.

All of used MFCs are digitally driven using Flowbus industrial bus based on RS485 standart. For communication with superordinate system the translation to RS232 communication is used.For increase the gas mix homogeneity the static mixer (Fig. 20) was equipped to the central gas flow way. Gas mixer is composed from CF16 full-nipple and two reducing flanges CF16 – ¼ VCR as the body. Currently as the mixing barriers the stainless steel wool is used.

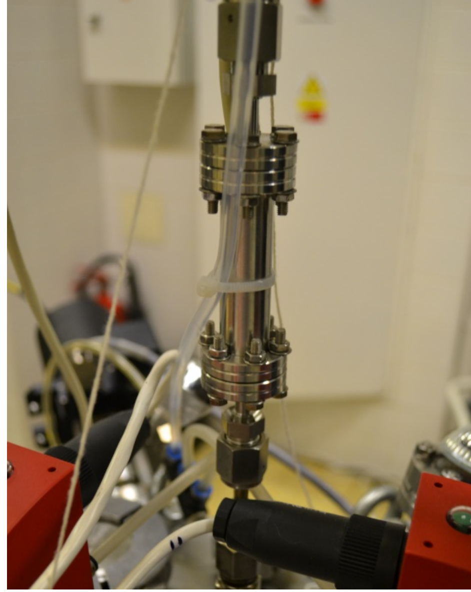

Fig. 20: Photo of compact static gas mixer

4.2.4 Plasma generation

At the A3 equipment the capacitively coupled RF plasma is used. For its generation the RF generator Ceasar 1310 from Advanced Energy Company is used. This 13.56 MHz RF generator deals the settings of forward power $1-1000\ \mathrm{W}$, maximum bias of $4000\ \mathrm{V}$ and deals internal pulsing ability by pulse width modulation (PWM). The PWM frequency can be set in range $1\mathrm{Hz}-100\mathrm{kHz}$ with duty cycle time (t_{off}) in range $1\%-99\%$ of run time (t_{on}). When the pulsing mode is used, variable, which defines power for comparison with continual mode, is Effective power. Effective power P_{eff} is defined by following equation 19.

$$P_{\mathrm{eff}} = \frac{t_{\mathrm{on}}}{t_{\mathrm{on}} + t_{\mathrm{off}}} \cdot P, \qquad \{20\}$$

where t_{on} is variable defining time when generator supplies power, t_{off} is time of duty cycle and P is nominal power.

The RF generator is not able to deal power to non-resonance system (like is radio antenna), because the reflected power (losses mostly caused by thermal losses) is too high. To secure the resonance of system, the matching network may be used. On A3 equipment the VM1000 Digital matching network from Advanced energy is used. Used matching network is essentially LC matching network (schema at Fig. 21) with presettable induction solenoid type coil and two stepping motors driven variable capacitors (one in series with coil and second in parallel). Matching network is able to set capaci-

tor values automatically (continual mode of power supply only) or manually by operator settings (when pulsing mode is used) to obtain minimal reflected power.

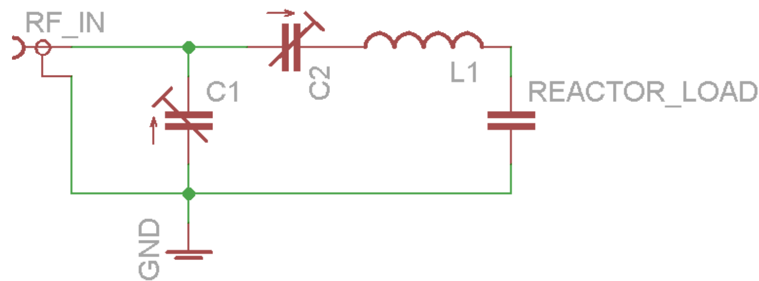

Fig. 21: Schema of LC matching network used at A3 apparatus

4.2.5 Deposition control system

The PECVD process is really sensitive to setup of conditions; therefore the scientific research in this area must take care of right measurement and settings of these conditions to earn reliable, accuracy and repeatable results. Because of that reason the apparatus A3 is almost fully controllable from operating computer. For controlling the process the bespoke software called A3_controler was made.

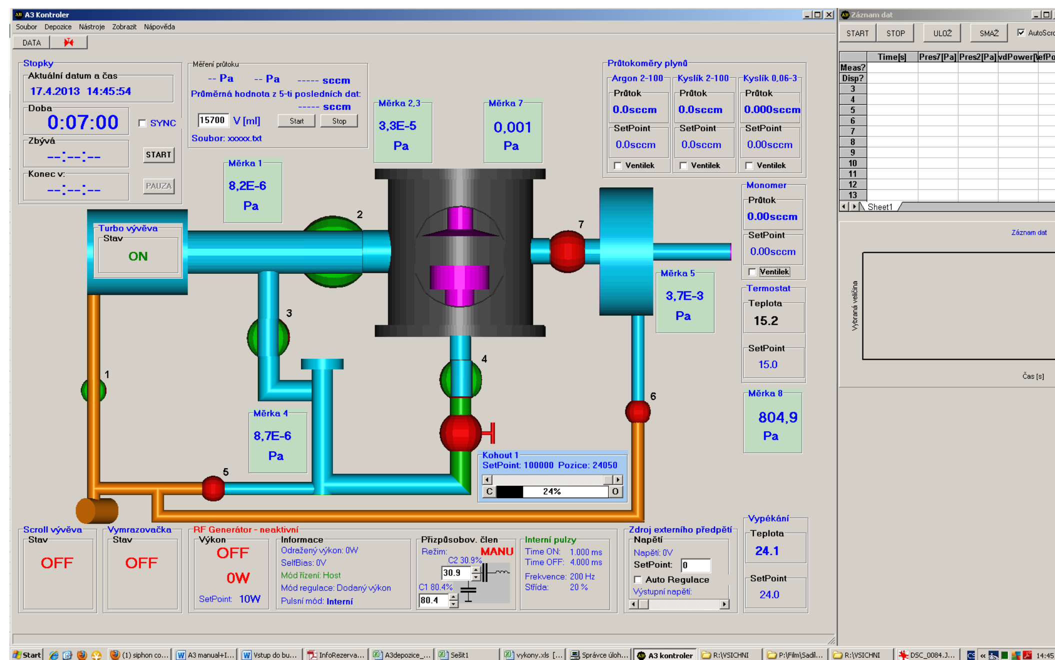

Fig. 22: Screenshot from A3 controller software during pumping of apparatus (pumping ways I and II are opened)

A3_controler software allows controlling almost every component of the apparatus using digital communications with components (e.g. RS 232) or using digital signals produced by special card. For process control the A3 controller allows to operate all pneumatically operated valves (in exclusion of valves 11 and 12, which was added freshly and have not yet been connected), by communication sets the Butterfly valve (Valve 8) positions and sets the parameters for the RF generator and Matching network. Software is also able to readout all sensors, which are actually equipped on apparatus, readout the temperature probes and set the bakeout temperatures. By special procedure the software is able to setup working pressure in reactor by setting off flow to the MFCs and by regulation of butterfly valve position. Other very commonly used feature of A3_controler is data logging of deposition pressure, RF power, reflected power and flows of gases, which may be later used for reverse analysis. Typical screen for operator during pumping deposition is shown by Fig. 22.

In emergency case, or when special condition occurs, the A3_controler may be by-passed by manually control panel placed directly on apparatus. This panel is shown on figure Fig. 23.

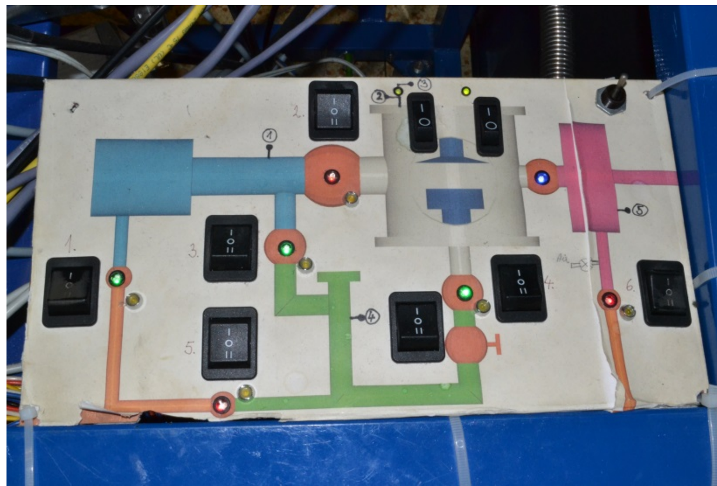

Fig. 23: User control panel of A3 apparatus used for manual control of valves

System is prepared for exchange of in present used control software by industrial standard one.

4.2.6 Attached analytical equipment

4.2.6.1 Mass spectrometer

The apparatus is also equipped with mass spectrometer HAL 511/3F from Hiden Analytical Company (figure Fig. 24). At the apparatus A3 the mass spectrometer (MS) is employed for three different applications. First application is usage the MS for analysis of background of reactor, second is analysis of deposition conditions (fragments, species) and third is usage as Helium leak detector.

Equipped mass spectrometer is designed for work with cooperation of high vacuum system. For this reason the vacuum part of this machine is designed to ability for intake of sample gas by pressure gradient. MS is evacuated by turbomolecular pump TMU 071P (Pfeiffer Vacuum Company, pumping velocity $60\,dm^3 \cdot s^{-1}$, limit pressure $1 \cdot 10^{-8}$ Pa, 90,000 RPM) with backing rotatory oil vane pump (DUO 2.5 from Pfeiffer Vacuum Company) with pumping velocity $0.78\,dm^3 \cdot s^{-1}$ and limit pressure $5 \cdot 10^{-1}$ Pa. Pressure is monitored by Penning type IKR 251 sensor from Pfeiffer Company, which is important to secure data for internal fuses and trip situations to prevent MS destruction.

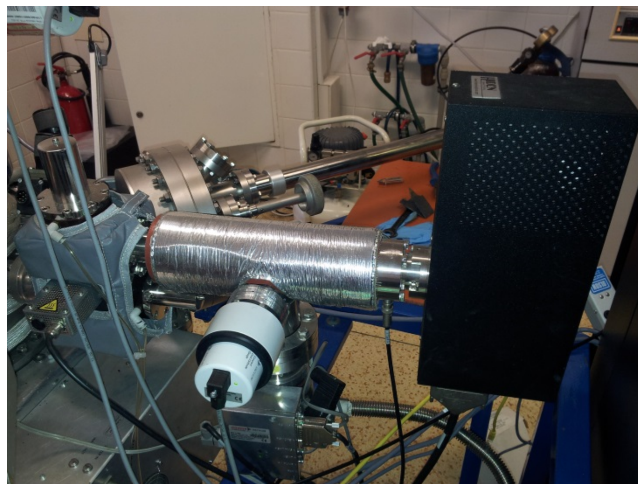

Fig. 24: Overall view to mass spectrometer equipped on apparatus A3. From left the RGA valve (HPR 30), probes section with triple quadrupole and detector electronic section (Black box)

The inlet part (factory marked as HPR 30 inlet assembly) of the spectrometer is composed by two pneumatically actuated valves and connected the sampling tube. The slit, which is located at the end of the sampling tube, ensures the pressure reduction to pressure, where the MS can operate. Using inlet valves part the MS can work in following regimes:

1. Regime "*STAND BY*" (STB). The spectrometer inlet is closed and only internal background gases are analyzed. This prevent fake signals in measurement of residual gas or sample process gas.

2. Regime "*SAMPLE PROCESS GAS*" (SPG). The spectrometer is opened to reactor using slit at the end of sample tube for pressure reduction. By selecting slit size 0.05, 0.20 and 0.75 mm, the intake pressures can be respectively max. 133.2, 6.67 and 0.67 Pa.
3. Regime "*RESIDUAL GAS*" (RGA). This regime is designed to sample gases from UHV to max. pressure $7 \cdot 10^{-3}$ Pa. This regime mainly usage is for analysis of background of the reactor (residual gases, water content) or for usage the MS as helium leakage detector.

Incoming gases from the sample tube are ionized by electron impact ionizer and electrostatically accelerated to the analyzer. Analyzer of described spectrometer is triple quadrupole type (3F). First and Third quadrupoles are used as filters with RF current only; second is analyzing using RF and DC current. This configuration provides very good resolution for heavier samples and long term stability given by first filter.

Detection of partial pressure is realized by one of two equipped detectors. First detector is Faraday cage with partial pressure range $1 \cdot 10^{-12} - 1 \cdot 10^{-3}$ Pa equipped in particle flight axe and second the Single Chanell Electron Multiplayer (SCEM, SEM) $1 \cdot 10^{-10} - 1 \cdot 10^{-2}$ Pa. Whole spectrometer is operated from PC using special software MasSoft from Hiden analytical.

Settings of parameters of MS are automatic, but user modifiable. Our equipped version is able to monitor species up to 510 amu with sensitivity 100% to 5 ppb.

4.2.6.2 Spectroscopic ellipsometer

Apparatus A3 is equipped with phase modulated spectroscopic ellipsometer UVISEL® from HORIBA Jobin-Yvon Company. The ellipsometer consist of a light source module, a analyzer module, a modulator module, two detectors modules and control computer with server application.

The analyzer and monochromator modules (figure Fig. 25) are installed directly to reactor chamber with fixed angle between them to angle of incidence $\mathrm{AOI} = 70°$. Principle of this reflection ellipsometer is based on light transmission (given by light source module) through analyzer module (using factory designation, physicaly it is just polarizer section) and its polarizing filter to the sample, where interacts with sample layers and reflects to the modulator module and from there to the one of detectors. As the light source the 75W Xe lamp is used. Connection between the analyzer and light source is realized by optical fibers. The analyzer has equipped earlier mentioned polarizing filter, which is rotated by stepping motor to user required position $\left(-45° - 90°\right)$. Same system of rotation able polarizing filter is installed in the modulator section, but between the sample and second (analyzing) polarizer is located the photo-elastic modulator (PEM), which sets the modulation angle by oscillation on selected frequency. At the optical end of the modulator section is placed the fiber switching unit, which is used for selecting used detector.

Selection of detector type depends on requirement analysis. When the sample is not changing with time and high levels of reliability, accuracy and repeatability is required the monochromator analyzer detector unit FUV 200 is used. This type of detector consist from an optical grating positioned by stepping motor, which allows to measure all wavelengths one-by-one and photomultiplier tube for detection. This measurement in basic mode takes about 20 minutes, which is really long time for kinetic and in deposition process measurement. For this type of measurements the Multi-wavelength detector module is used. This type of detection module consists from 32 photomultiplier tubes and optical grating, which splits the light to the photomultipliers. With decreased scan-scan speed, this detector module can obtain 64 signal points using change the AOI of light to the grating which changes the wavelengths measured by photomultipliers.

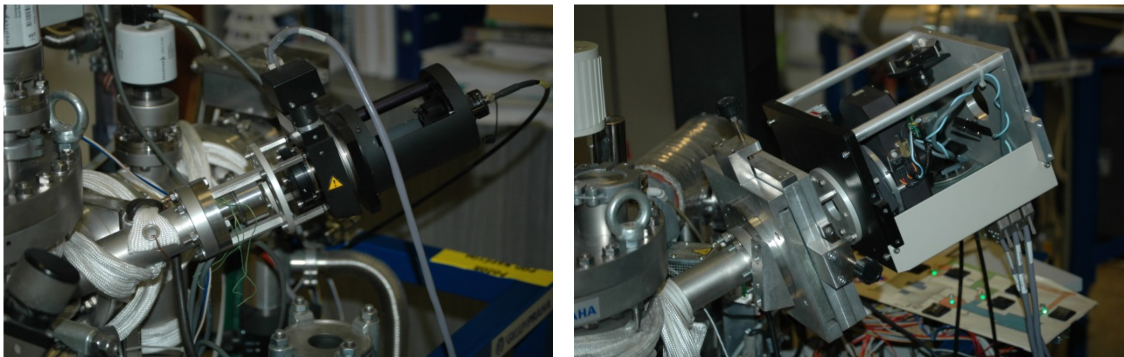

Fig. 25: Detail photo of analyzer module (left side) and modulator module (right side) of Uvisel spectroscopic ellipsometer.

Signal delivered from detector is acquired by controller computer with server application, where preprocessing of measured data occurs. Preprocessed data are sent to the client computer with DeltaPsi2 software. DeltaPsi2 software (screenshot at Fig. 26) allows to control the acquisition same as allows to evaluate the measured data. Evaluation of spectroscopic data is based on fitting mathematical model of expected material, which is almost based on real material measurements. The model may be also created, but it is really complicated matter requiring intensive knowledge in ellipsometry.

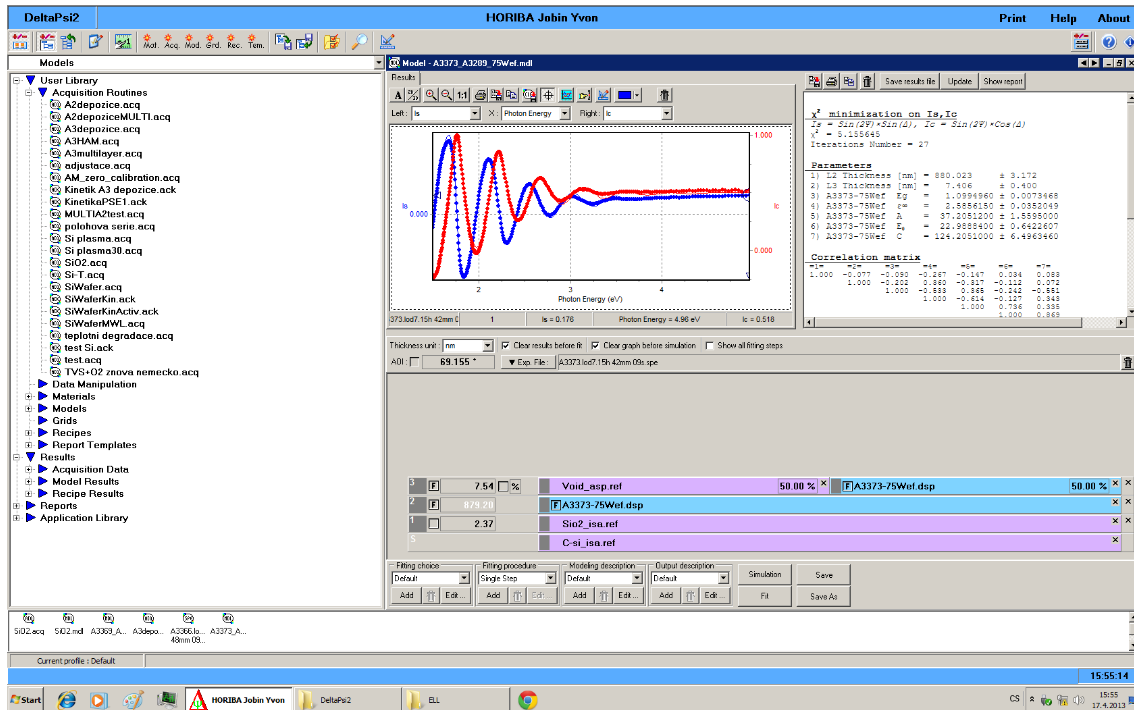

Fig. 26: Screenshot from DeltaPsi2 software showing after sample fitting results.

4.3 Deposition of PP thin films

4.3.1 Deposition conditions

4.3.1.1 Pre-deposition conditions

Deposition conditions and its substantiation, described below, were obtained by colleges previously worked at this apparatus [109], [110], [111] through its usage for thin film deposition or support analysis.

For preparation of reliable and repeatable samples the environment in aparature has to be very strictly monitored. As the upper level of critical pressure value, which is selected as the cleanness representing value, was set to $5 \cdot 10^{-5}$ Pa. It was expected, that this level of pressure is sufficiently distanced from deposition conditions and the background of the reactor does not have significant influence to deposition conditions.

If the vacuum level does not reach the absolute maximum pre-deposition pressure, the reason why was checked by mass spectroscopy analysis. If the obtained reason was water content the vacuum chamber was heated up to 110 °C for at least 8 hours, to forcibly desorption of water from reactor chamber and piping. If the higher level of pressure does not be reasoned by water content, the mass spectrometer was configured to regime of helium leakage detection and apparatus was selectively rinsed by helium. In the area of leak the helium was sucked into apparatus and mass spectrometer registered the helium peak.

If the apparatus is newly cleaned, first deposition is just for preparation the environment of reactor to prevent the influence of other materials in reactor. Typically the 25W continual deposition to 500 nm thick film of 3.8 sccm flowing TVS is used. Thickness of this probationary film was measured same as optical constants using spectroscopic ellipsometry, which gives us information if any change in technology between cleanings was made.

4.3.1.2 Selected deposition conditions

For deposition of the thin film samples commented in following chapters following settings represented by Tab. 2 – 4 was selected. First table Tab.2 shows setting for reference samples prepared from Tetravinylsilane plasma only.

Tab. 2: Table of selected configuration for preparation of reference TVS only samples

Series designation	Sample number	RF Power settings				Flows of gasses			Pressure
		P_{eff} [W]	P [W]	t_{on} [ms]	t_{off} [ms]	O2 [sccm]	Ar [sccm]	TVS [sccm]	p_7 [Pa]
TVS_only	A3342	250	500	1	1			3,87	2,7
	A3343	150	300	1	1			3,87	2,7
	A3344	75	300	1	3			3,87	2,7
	A3345	25	200	1	7			3,87	2,7
	A3346	10	50	1	4			3,87	2,7
	A3347	2	10	1	4			3,87	2,7

Table Tab. 3 shows the configuration for samples prepared with argon to TVS and oxygen to TVS mixtures. Samples with [1)] mark in table Tab. 3 are samples obtained from probationary series.

Tab. 3: Table describing selected deposition conditions for samples preparation

Series designation	Sample number	RF Power settings				Flows of gasses			Pres-sure
		P_{eff} [W]	P [W]	t_{on} [ms]	t_{off} [ms]	O2 [sccm]	Ar [sccm]	TVS [sccm]	p_7 [Pa]
TVS_13.7_Ar_2.2	A3349	250	500	1	1		2,2	1,84	2,7
	A3350	150	300	1	1		2,2	1,84	2,7
	A3351	75	300	1	3		2,2	1,84	2,7
	A3352	25	200	1	7		2,2	1,84	2,7
	A3353	10	50	1	4		2,2	1,84	2,7
	A3354	2	10	1	4		2,2	1,84	2,7
TVS_6.0_Ar_3.0	A3356	250	500	1	1		3,0	0,82	2,7
	A3357	150	300	1	1		3,0	0,82	2,7
	A3359	75	300	1	3		3,0	0,82	2,7
	A3360	25	200	1	7		3,0	0,82	2,7
	A3361	10	50	1	4		3,0	0,82	2,7
	A3362	2	10	1	4		3,0	0,82	2,7
TVS_2.2_Ar_3.5	A3328	250	500	1	1		3,5	0,32	2,7
	A3329	150	300	1	1		3,5	0,32	2,7
	A3331	75	300	1	3		3,5	0,32	2,7
	A3332	25	200	1	7		3,5	0,32	2,7
	A3333	10	50	1	4		3,5	0,32	2,7
	A3334	2	10	1	4		3,5	0,32	2,7
TVS_13.7_O2_2.2	A3314[1)]	250	500	1	1	2,2		1,84	2,7
	A3315[1)]	150	300	1	1	2,2		1,84	2,7
	A3316[1)]	75	300	1	3	2,2		1,84	2,7
	A3317[1)]	25	200	1	7	2,2		1,84	2,7
	A3318[1)]	10	50	1	4	2,2		1,84	2,7
	A3319[1)]	2	10	1	4	2,2		1,84	2,7
TVS_6.0_O2_3.0	A3363	250	500	1	1	3,0		0,82	2,7
	A3364	150	300	1	1	3,0		0,82	2,7
	A3366	75	300	1	3	3,0		0,82	2,7
	A3365	25	200	1	7	3,0		0,82	2,7
	A3368	10	50	1	4	3,0		0,82	2,7
	A3369	2	10	1	4	3,0		0,82	2,7
TVS_2.2_O2_3.5	A3326[1)]	250	500	1	1	3,5		0,32	2,7
	A3338	150	300	1	1	3,5		0,32	2,7
	A3336	75	300	1	3	3,5		0,32	2,7
	A3337	25	200	1	7	3,5		0,32	2,7
	A3339	10	50	1	4	3,5		0,32	2,7
	A3340	2	10	1	4	3,5		0,32	2,7

By [1)] symbol is marekered samples with was only from probationary series

4.3.2 Deposition process way

Following numbered list paragraph describes way how to the samples are prepared. Process way assumes that the vacuum chamber is evacuated to basic vacuum.

1. First step is *loading the cleaned silicon wafers* to cleaned sample holders (refer to chapter 5.3.3)
2. Second step is *loading prepared samples* to load lock. Load lock is during loading samples vented. To prevent very long time pumping and contamination of reactor chamber, the load lock is vented for as short time as possible using dry air. To prevent troubles caused by dust etc. the samples are using helium source rinsed. Earlier prepared samples are removed from load-lock and from their sample holders.
3. In this step *load-lock section is evacuated.* Evacuating of load lock is processed by closing the valve 1 to prevent pressurizing of primary vacuum section under turbomolecular pump, which can cause destruction of turbomolecular pump and opening of valve 6. Valves are switched back after pressure in load-lock section decreases below 5 Pa.
4. Next step is concentrated to *exchange of sample holders* with prepared samples in electrode by new one in load-lock. To balance pressures in reactor and load lock the Valve 7 is very slowly opened. After it, the sample holders may be, using magnetic linear drive manipulator, moved from or to load-lock. If these samples are too fresh (less old than 12 hours from deposition) the valve 7 is opened and basic vacuum is obtained in load-lock section too.
5. Next step is *preparation deposition*. If the valve 7 was opened it has to be closed now. Reactor chamber is evacuated to basic pressure and residual gas is controled by MS.
6. If are conditions in reactor sufficient, the *activation of sample surface* may occurs. To clean and activate the sample surface for deposition of thin films the argon plasma treatment is used. Plasma is generated to reactor filed by dosed Ar gas with flow $10\,\mathrm{sccm}$ and 5W of RF forward power in continual regime and matching network was setup to automatic mode. Pressure in the reactor was regulated before supplying power, to value $5.7\,\mathrm{Pa}$ by closing pumping way I by closing valve 2 and setting position of regulation valve 8. Argon treatment plasma is activated for 10 minutes.
7. After plasma treatment the Ar flow is stopped and *reactor is evacuated*. Valve 2 is reopened and reactor is evacuated to as high as possible vacuum in maximally 10 minutes long cycle.

8. Next step is *deposition of sample thin film*. Valve 2 is closed, Valve 11 is closed to prevent destruction of vacuum sensors and flow of gases is set to required values. Using valve 8 the pressure is set to value $5.7\ \mathrm{Pa}$, RF generator is preset to required values (usually: internal pulsing mode by setting t_{on} and t_{off} times and nominal power P) and if the internal pulsing is used, matching network is set to manual control. Deposition is started by start of supplying power from generator. Concurrently with start of supplying power from generator stopwatch is started and data logging is started. The deposition time directly control the final thickness of film. When the discharge is stable and in right configuration the MS spectrum using SPG regime is obtained.
9. After deposition time expires the RF power is stopped, same as flows of gases and valve 2 and 8 are fully opened. Reactor is evacuated for 10 minutes to as so high vacuum level as possible.
10. At the last step the *reduction of free radicals occurs*. To reduce free radicals at the surface of samples (and also everywhere in reactor) the argon flow is preset for one hour. Setting is same to step 6 but without discharge.
11. After one hour the flow of argon is stopped, valves 2 and 8 are fully opened and reactor is evacuated. After reactor reaches sufficient vacuum level it is prepared for new deposition.

4.3.3 Cleaning process

4.3.3.1 Cleaning process of samples

Silicon wafers are from fabrication very clean, but after the evacuated or inert gas filled storage box is opened, the wafers are directly exposed to laboratory atmosphere. Secondary source of contamination is achieved during the wafer cutting for sample holder by laser gouging and following breaking.

Silicon wafer species of dimensions $10\times10\times0.6\ \mathrm{mm}$ are placed to technical ethanol $95\ \%$ and let in ultrasonic bath for 30 minutes. If the cleaning process was non-sufficient, it was repeated. After the ultrasonic cleaning the wafers was removed from ethanol solution and dried by vacuum drier.

Fig. 27: Cleaning samples by ultrasonic bath and preparation of samples to drying

4.3.3.2 Cleaning process of sample holders and reactor

Thin films prepared by PECVD technology are very often very hard to remove from surfaces of the reactor and reactor accessories because their good adhesion, very bad solubility and good chemical resistance. To remove these materials, almost in every case the mechanical removal methods are used.

Maximum thin film thickness in A3 apparatus reactor is about $6\ \mu m$ because its dielectric effect. When the thickness reaches the maximum value, apparatus have to been stopped, vented and opened. After it the deposition reactor chamber and its internal accessory have to been cleaned by grinding using sandpapers. After grinding is completed the dust is removed by vacuum cleaner and residual dust is removed by cloth soaked in technical ethanol. Sample holders are cleaned by very same way, only dust is removed by compressed air.

Fig. 28: Cleaning sample holders by sandpaper

4.4 Analysis of plasma discharge

4.4.1 Plasma discharge stability measurement

To obtain reproducible and reliable samples from PECVD process, the stability of plasma discharge have to be secured. To gain information about discharge stability many systems are used (like probes measuring plasma density etc.), but easiest way how to check plasma at least a rough estimate is measuring optical-emissivity response of plasma.

To control plasma discharges in all used regimes, the phototransistor sense in wiring represented by Fig. 29 were used.

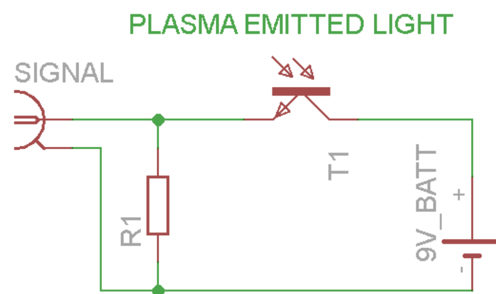

Fig. 29: Schema of phototransistor sense electrical wiring

As reference signal was used inducted current from coil attached on supply coaxial cable (Fig. 28) (signal is used for triggering time main signal waveform). Data was acquired using HAMEG HM1507-2 (Fig.30) oscilloscope and downloaded to PC by SP107E software. Exported data was post-processed by Origin software.

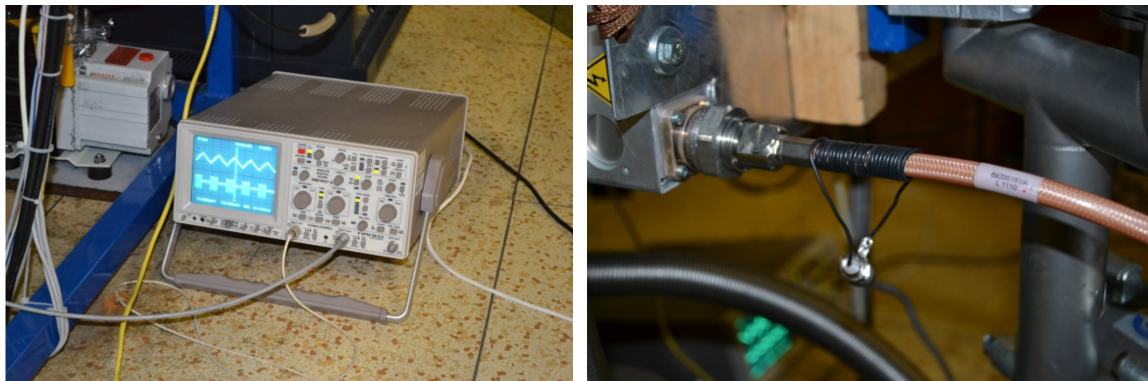

Fig. 30: Photo of HAMEG oscilloscope during measuring (left) and sensing coil used as reference (right)

4.4.2 Mass spectroscopy analysis of plasma discharge species

Mass spectrometry of plasma species was measured by previously mentioned in-situ mass spectrometer HAL 511/3F with following configuration using SPG mode of measurement.

Tab. 4: Parameters, which was setup for mass spectra measurement

Parameter	Value
Range	1-150 amu
Resolution	0.2 amu
Used detector	Faraday
Emission current	1000 μA
Ionizing energy	70 eV
Tension of ionizing source	3 V
Dwell time	Auto (100%)
Settle time	Auto (100%)

Obtained spectra was exported from MasSoft software and post-processed by Origin software.

4.5 Analysis of prepared PP thin films

4.5.1 Chemical composition (FTIR)

To obtain information about chemical composition of prepared samples, the FTIR spectrometry was used.

FTIR spectra was measured by Vertex 80v FTIR spectrometer from Bruker Corporation. This spectrometer is constructed as one beam FTIR with evacuate-able body. Vacuum in FTIR body is dealing defined environment during measurement and also removed influence of residual water vapor and carbon dioxide. To remove problem with time consumptive evacuating during every measurement the sample compartment section is vented and evacuated separately. As accessory the Transmission module, Real transmission module A480/8 (Fig. 31) and Miracle® ATR module with diamond crystal were used.

Fig. 31: Photo of Real transmission module A480/8

The spectrometer was evacuated at least 1 hour before first measurement with required accessory and, if it was used, also sample holder, inside the sample compartment. After the spectrometer reached the sufficient vacuum level (vacuum level at least 120 Pa) the background measurement was made. For background measurement the 256 scans were used. After the measurement of background was completed the sample compartment was vented and sample was loaded. Sample compartment was evacuated to at least 120 Pa and after it, the acquisition of sample was started. Sample was measured for 256 scans. Almost for every sample the resolution was set to $2\ \text{cm}^{-1}$.

For measuring of high reflectively samples as was the silicon substrates and films on them, the real transmission module was used. Real transmission module is composed from set of mirrors and edge in center of incoming signal. All reflected signal is cut off by this edge. This process removes from signal interference with incoming signal, which causes fake intensities of bands. For analyze of liquid Tetravinylsilane the ATR module was used. Standard transmission module will not be satisfactorily reliable.

4.5.2 Optical properties and thickness (ELL)

Optical properties of the sample same as their thickness was obtained by previously mentioned spectroscopic ellipsometer Uvisel from Horiba Jobin Yvon company. Ellipsometer is phase-modulated, so modulator and analyzer are fixed in the known positions.

For measuring of samples later described in this work, the configuration was set on modulator $M = 0°$, analyzer $A = +45°$, range of wavelengths to measurement at FUV monochromator detector $(250-830)\ \text{nm}$, with step $2\ \text{nm}$. Before every measurement the analyzer and modulator motor position was calibrated. Because the electrode is not absolutely uniform, and sample holders cannot secure absolutely right position of sam-

ple, the angle of incidence (AOI) has to be mathematically calculated. The real value of AOI could be $69 - 72°$.

For optical and physical constants the Tauc-Lorentz model was chosen because it is suitable for amorphous materials.

Part of samples was because of ellipsometer malfunction measured by ex-situ ellipsometers Horiba scientific Uvisel 2 at Department of Chemistry, Brno University of Technology operated by Ing. Veronika Schmiedová and by spectral ellipsometer with rotating analyzer Wollam VASE at University of Pardubice operated by Mgr. Jan Mistrík, Ph.D.

4.5.3 Elementary composition of surface (XPS)

The elementary composition (C, Si, O) of the surface region of the deposited thin films was determined by XPS on an ADES 400 (VG Scientific U.K.) photoelectron spectrometer at institute of Physics of Acedemy, Sciences of Czech republic operated by RNDr. Josef Zemek, CSc.

For the measurement, the MgKα (1253.6 eV) photon beams, normal emission angle, twin anode X-ray source with the standard Al/Mg anodes and a rotational hemispherical energy analyzer were used.

4.5.4 Mechanical properties (Nanoindentation)

Nanoindentation was used for characterization of mechanical properties of prepared thin films. The measurement was realized by Ing. Erik Pálesch from Brno University of Technology, Department of chemistry at 2D TriboScope (Hysitron) system attached to an NTegra Prima Scanning Probe Microscope (NM-MDT, Russia).

For measurement, standard transducer with maximum load force approximately 10 mN and Berkovich tip with a radius of curvature 50 nm were used. Determination of Young's modulus and Hardness was realized from depth profiles made by cyclic nanoindentation test at 5 very different locations for each sample. The mechanical properties were obtained from every depth in depth profile (in the case of samples mentioned in this work maximal depth was 120 nm) and the final value was acquired from interpolation of linear obtained data fit to zero depth.

5 RESULTS AND DISCUSION

5.1 Analysis of plasma discharge

5.1.1 Discharge stability measurement

Before the conditions for production series are definitively set, the probationary series was made. Through the deposition of this probationary series the plasma regimes was controlled. When the deposition plasma discharge was verified as stable, the regime was used for production series. Also the production series plasma was monitored and diagrams obtained from this production series, because this measurements has exact connection to samples commented later in this work, are used for following paragraph.

As the example of discharge stability measurement the figure Fig. 32 is showing typical waveform of plasma response to pulsing (PWM) mode of RF power supply.

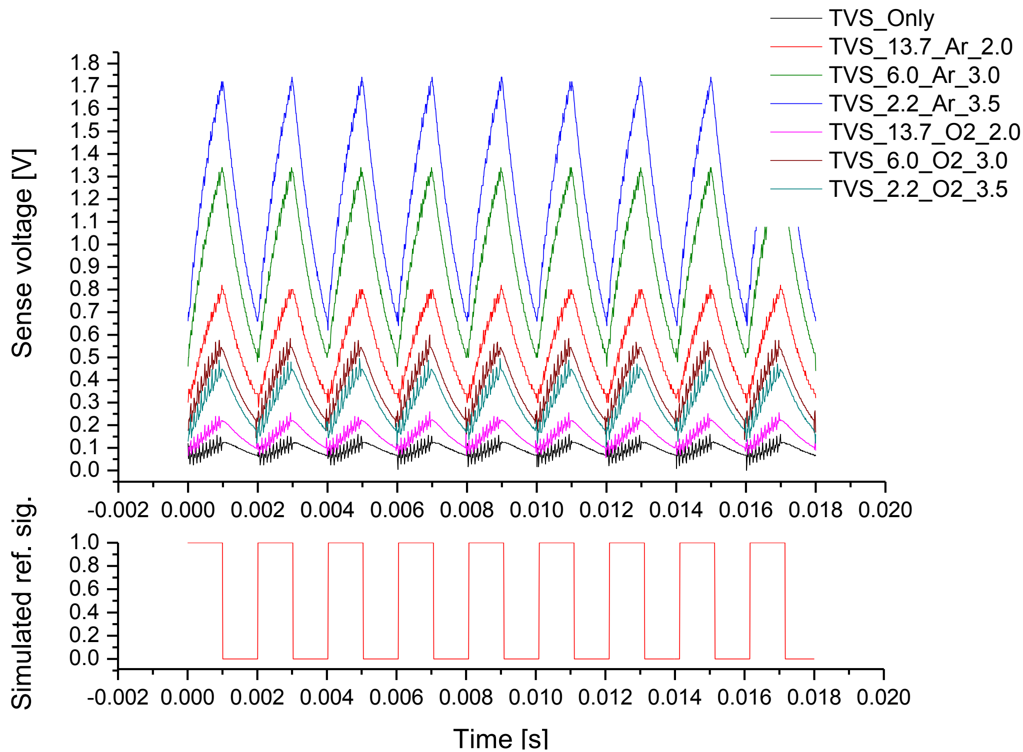

Fig. 32: Graph of time dependence of plasma total light emission (Sense voltage) response to PWM modulation (showed as simulated ref. sig.) of supplied power. For this measurement the power was set on forward power 300W and PWM frequency to 500 Hz $\left(t_{on}, t_{off} = 1\,ms\right)$ *and reactive gas mixtures described in legend.*

From the obtained data of all measurements the dependences of plasma total light emission (Sense voltage) response to effective value of power was constructed. These dependences are represented by graph on figure Fig 33.

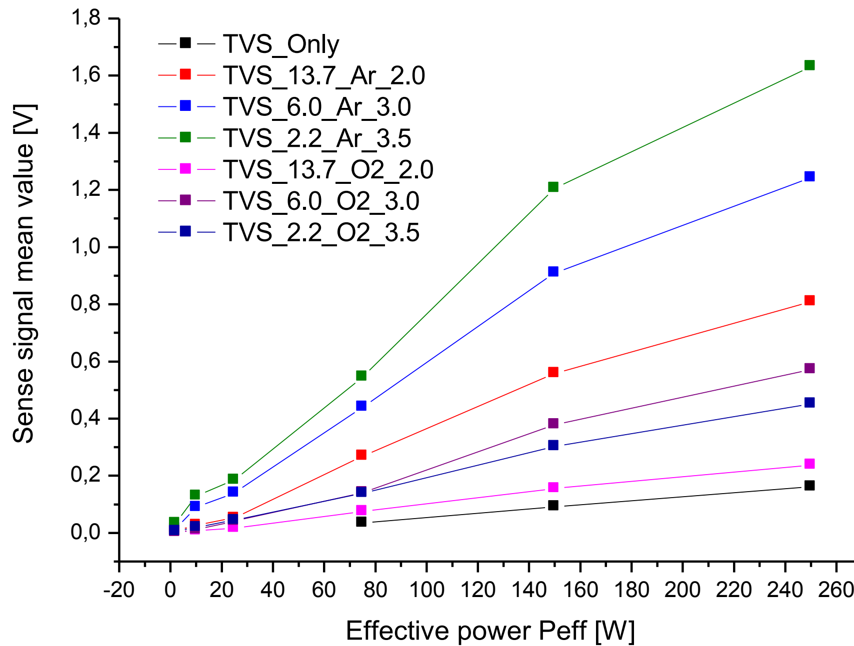

Fig. 33: Graph of dependence of plasma total light emission (Sense voltage) to studied supply power regimes. Gas mixtures are described by legend. Note: values of total light emission of 2W_{eff} and 10 W_{eff} are not obtained because in was under detection level.

From the dependences showed at figure Fig. 33 it can be concluded, that with increasing effective power supplied to the reactor the ionization density is increasing. This assumption good corresponds with results obtained from mass spectrometry, because ionization produce increased density of electrons, which can interacts with monomer species and affect the higher monomer fragmentation.

The influence of plasma total light emission (Sense voltage) response to the gas ratio added to the batch mix is represented by figure Fig. 34. Graph at figure Fig. 34 shows that in case of argon gas the optical intensity of total plasma light emission increases in whole gas to monomer ratio axe. In case of oxygen, the optical emission also increases up to about 80% oxygen in mixture. In cases, where mixtures with oxygen contents is higher than 80% the total plasma light emission is decreasing. This would be reasoned by decreasing content of particles with weaker ionization energy levels, which “assists” to oxygen ionization.

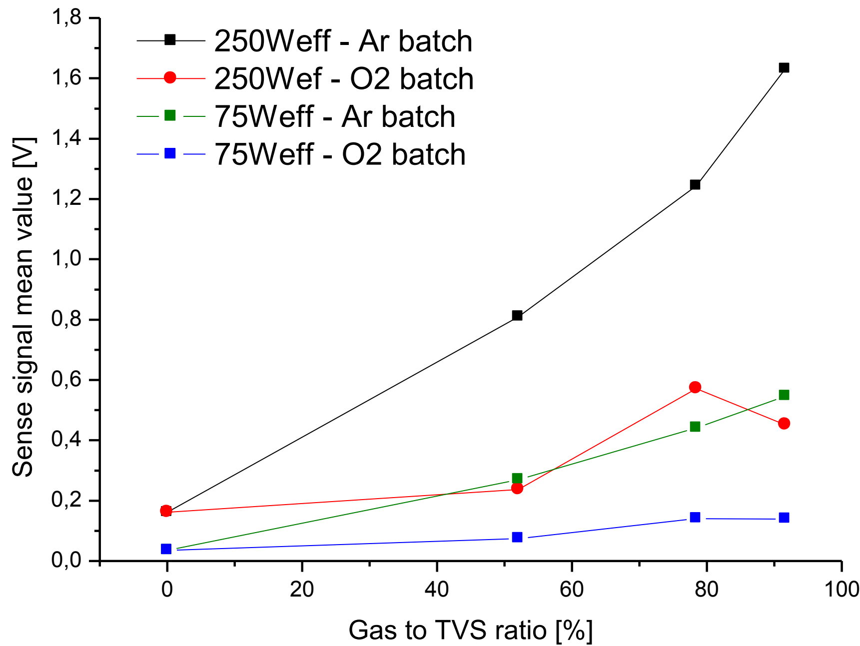

Fig. 34: Graph of dependence plasma total light emission (Sense voltage) to the argon, respectively oxygen gas to monomer ratio in mix

5.1.2 Mass spectroscopy of plasma species

Mass spectroscopy was used for monitoring of deposition plasma species and pr-deposition composition of reactive gas.

The acquired spectra was not normalized to any fragment for uses to show fragment to condition dependences, because it is no exact way how to consider what fragment intensity is constant in all mixes of gases and all power regimes. Also the vector normalization will distort the measurement, because with increasing power the presence of high molecular fragment are decreasing and reactor pressure is changing during deposition (refer to chapter 6.2.1). Mass spectrometry was used in its basic principle as the selective "pressure gauge" and concentration of fragments given by spectra was assumed as absolute. So the values may be influenced only by different pumping speed of different sizes of molecules, which can influence how much of them was intake to the MS.

5.1.2.1 Tetravinylsilane monomer MS spectra interpretation

For the following part of work is exactly high important to describe whole fragmentation process of tetravinylsilane molecule, which was take as the reference for following spectra and its general interpretation.

Study of fragmentation of tetravinylsilane molecule was made by Ing. Michal Bureš during his diploma thesis measurement [109]. Interpretation was taken to this work because the scope of study was not focused to detailed interpretation of processes acting during deposition.

At following figure Fig. 35 is detailed description of designed fragmentation process.

Fig. 35: Fragmentation process of tetravinylsilane molecule in electron ionization source [109] (author edited)

The molecule of tetravinylsilane has relative molecular weight 136.27. Molecular ion, which appears to non-ionized molecule of tetravinylsilane does not occurs in spectrum or only with very small intensity. More intensive and significant would be after hydrogen elimination fragment with $m/z = 135$. Losing the ending group CH_2 and after hydrogen overlap it arises fragment $m/z = 121$.

Fragment $m/z = 135$ by losing vinyl groups forms fragments $m/z = 109$, $m/z = 81$ and $m/z = 55$ or if the hydrogen overlap occurs the $m/z = 83$, $m/z = 57$ and $m/z = 31$ would be formed.

Fragment $m/z = 121$ similarly to the previous case by losing vynil and vynilidene groups forms fragments $m/z = 95$, $m/z = 67$ respectively $m/z = 43$. Loses from bigger fragments produces signals with $m/z = 25$, $m/z = 26$ and $m/z = 27$. Also smaller fragment may be in plasma formed such as hydrogen with $m/z = 2$.

5.1.2.2 Pre-deposition reactive gas composition

For monitoring of composition gas and for earning reference data the mass spectrometry of pre-deposition gas mixture (with 0W of effective power) was done. All of given spectra was measured at same configuration of pressure reducing slit and the pressure settings at the reactor (given by the capacitron gauge with resolution to 0.001 Pa). Spectra are incorporated to the following chapters 6.1.2.2 – 6.1.2.10 as reference for sample process gas spectra.

5.1.2.3 Mass spectrometry of TVS_only fragments and reference interpretation

Mass spectra of TVS_Only series acquired in range of effective power $0-250$ W are represented by following figure Fig. 36.

From the figure Fig. 36 may be seen, that with increasing effective power the concentration of fragments with higher values of m/z, which is in good agreement to the schema at figure Fig. 33. To increase predictive value of data from the major fragments was constructed dependence of them on effective power (Fig. 37).

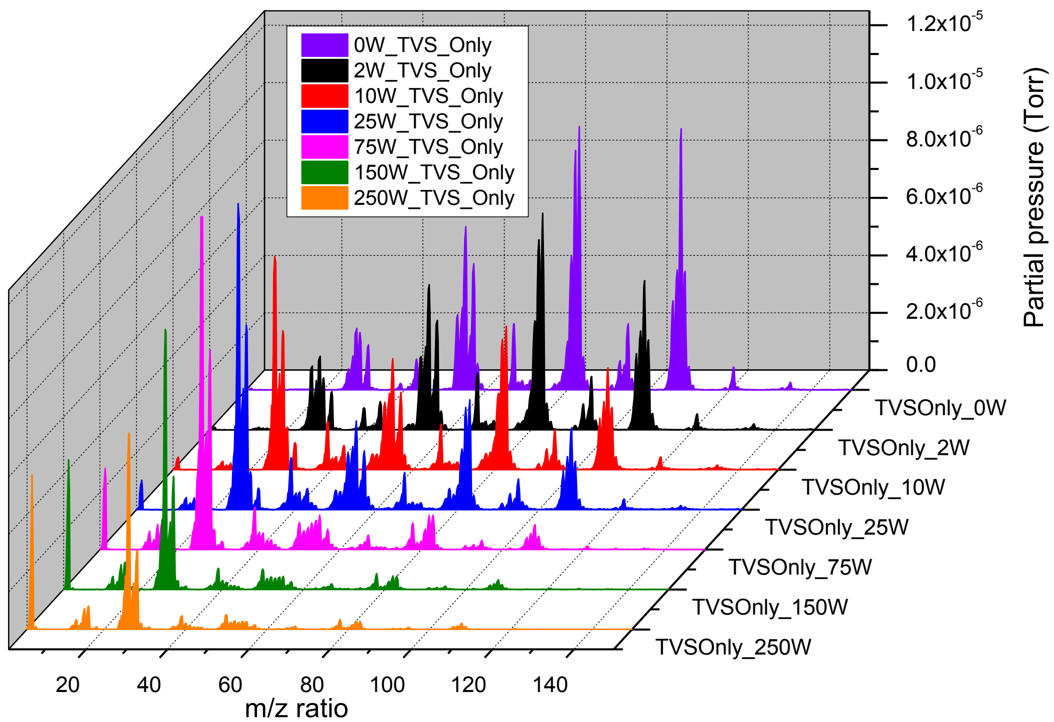

Fig. 36: Mass spectra of TVS_only series plasma species distinguished by effective power

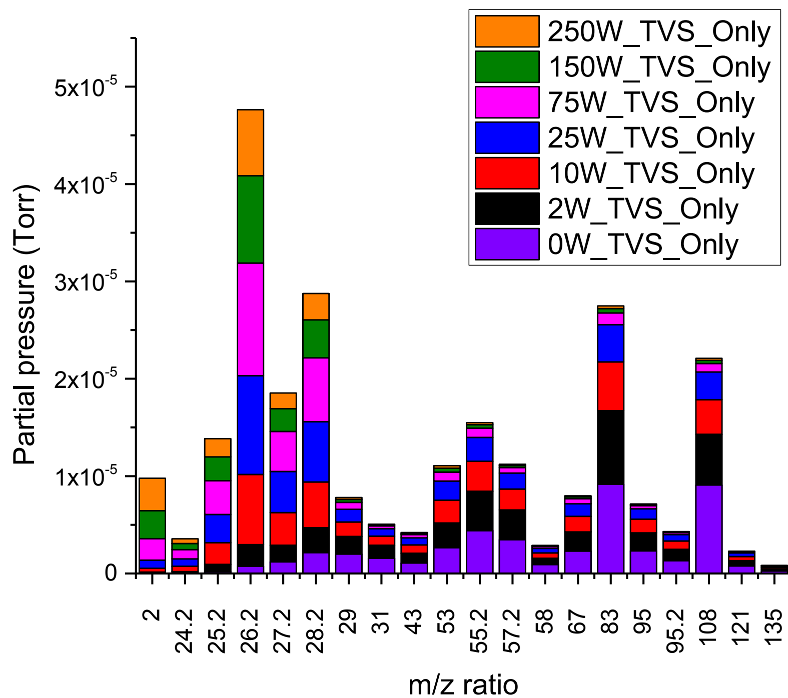

Fig. 37: Mass spectra of major species from TVS_only series plasma distinguished by effective power. Graph is stacked by Y axe.

Data presented by Fig. 37 is showing that the higher molecular fragments are due to plasma fragmented to smaller species. This trend increases with increasing power. Hydrogen content which is produced by recombination of atomic hydrogen formed by fragmentation is increasing with increasing power, which is in good agreement with trend of reducing content of higher molecular mass species. Smaller fragments content (products of previously mentioned fragmentation process) is increasing with increasing effective power.

5.1.2.4 Mass spectrometry of TVS_13.7_Ar_2.0 series

Mass spectra of TVS_13.7_Ar_2.0 series acquired in range of effective power $0 - 250$ W are represented by following figure Fig. 38. Because argon gas is almost absolutely inert gas is not assumed any change of chemical composition of plasma species due the chemical reaction. For the interpretation would be used same principle as in case of TVS_only series.

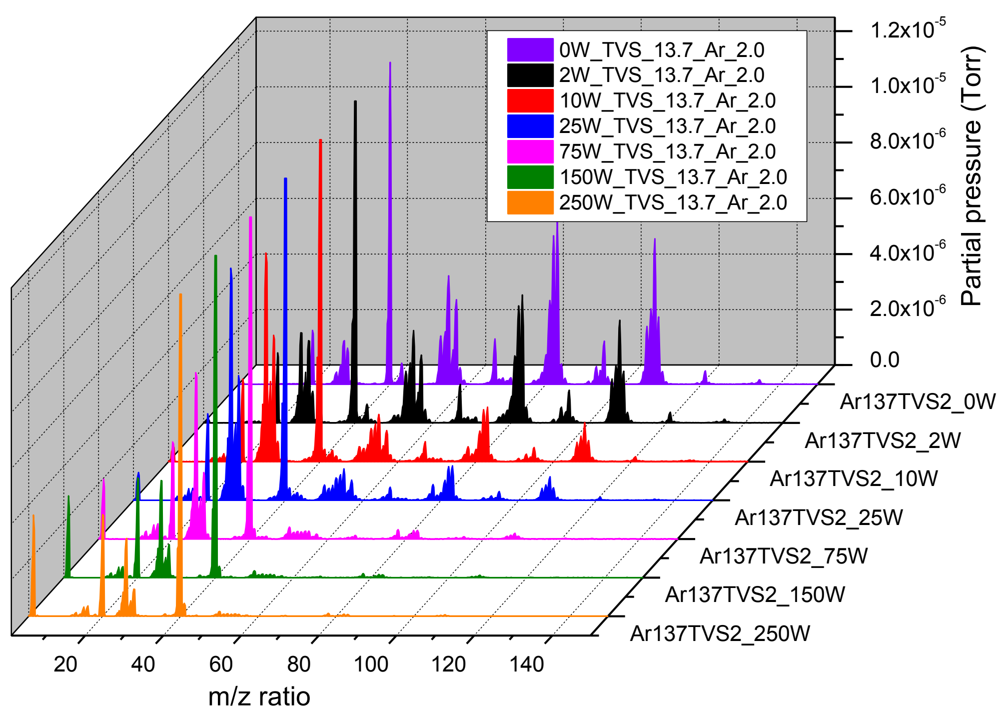

Fig. 38: Mass spectra of TVS_13.7_Ar_2.0 series plasma species distinguished by effective power

Figure Fig. 38 is showing that the assumption mentioned in TVS_only series discussion is valid also for series with argon gas in mixture. Fragments with higher m/z ratios are decreasing its content with increasing power supplied to the reactor. The main difference of spectra to the spectra of TVS_only series is overall lower intensity and then the incidence of Argon bands in spectra at $m/z = 40$, respectively $m/z = 20$. The influence of added argon gas mixture to the fragments composition is better showed at major fragments at Fig. 39.

At figure Fig. 39 (below) is shown dependence of major plasma fragments of monomer at different powers supplied to the reactor. Assumption mentioned at previous paragraph may be confirmed by graph at Fig. 38 because the $25-250$ W value range of RF power applied to the reactor almost absolutely excludes the occurrence of fragments with higher $m/z = 28$. Most significant fragments on area from $m/z = 24$ to $m/z = 28$ consider to the 10W, 25W and 75W powers. The partial pressures of fragments prepared by power higher than 75W has decreasing trend to the effective power incensement, which is most significant for fragments prepared by 250W. Hydrogen content confirmed by $m/z = 2$ peaks has high slope increase trend to the effective power value.

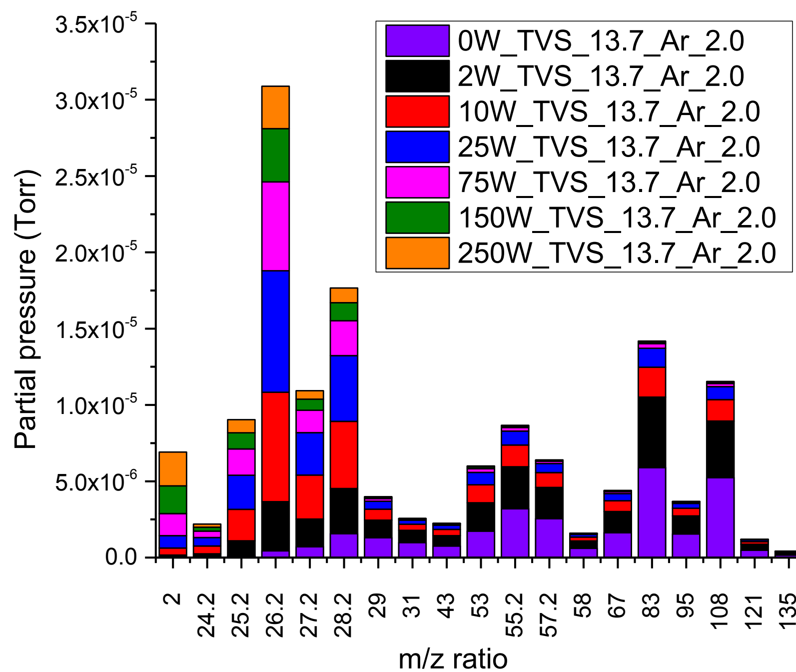

Fig. 39: Mass spectra of major species from TVS_13.7_ Ar_2.0 series plasma distinguished by effective power. Graph is stacked by Y axe.

5.1.2.5 Mass spectrometry of TVS_6.0_Ar_3.0 series

Mass spectra of TVS_6.0_Ar_3.0 series acquired in range of effective power $0-250$ W are represented by following figure Fig. 40, where it is shown dependence of fragment intensity to the effective power applied to the reactor.

Assumption of decreasing content of higher molecular mass species with increased power is also confirmed by this series at figure Fig. 40. At graph is shown evident decrease of presence of species with $m/z > 28$, which is the most evident for powers larger than 2W. Insignificant is content of plasma species $m/z > 28$ for all powers larger than 25W. Reduction of content of higher molecular species is going hand in hand with increasing amount of hydrogen $m/z = 2$. The most common species belonging to this series are species with $m/z = 26.2$, with would be assigned to the vinyl radical-ion $H\dot{C}{=}CH^{+}$. This particle is higher content in 10W of effective power scan and with increasing power is also decreasing its intensity.

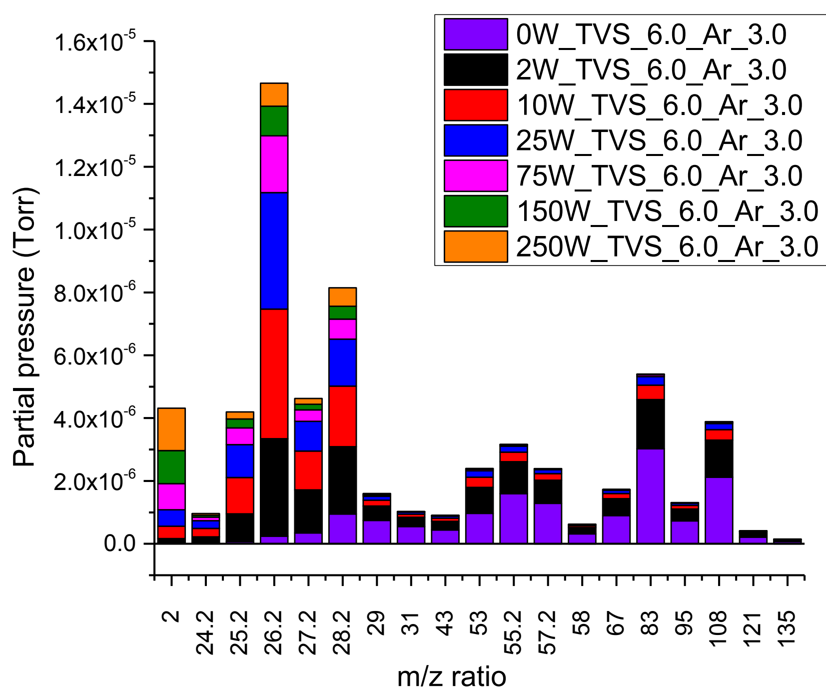

Fig. 40: Mass spectra of major species from TVS_6.0_Ar_3.0 series plasma distinguished by effective power. Graph is stacked by Y axe.

5.1.2.6 Mass spectrometry of TVS_2.2_Ar_3.5 series

Mass spectra of TVS_6.0_Ar_3.0 series acquired in range of effective power $0-250\ \mathrm{W}$ are represented by following figure Fig. 41, where it is shown dependence of fragment intensity to the effective power applied to the reactor.

From the following graph (Fig. 41) is shown that the next decrease of consistence of higher molecular mass fragments $(m/z > 28)$ decreases with increasing power. In this series with Argon content about 91.7% is content of higher molecular mass species perceptible only for fragments produced by 2W of effective power (slight bands also for 10W and 25W but almost insignificant). Interesting is also fact, that the $m/z = 26.2$ band is most significant for 2W sample and with increasing power has decreasing tendency. Hydrogen content represented by $m/z = 2$ is significantly increasing with applied effective power, which it may be connected to the higher fragmentation with assistance of Argon gas (electron produced by ionization).

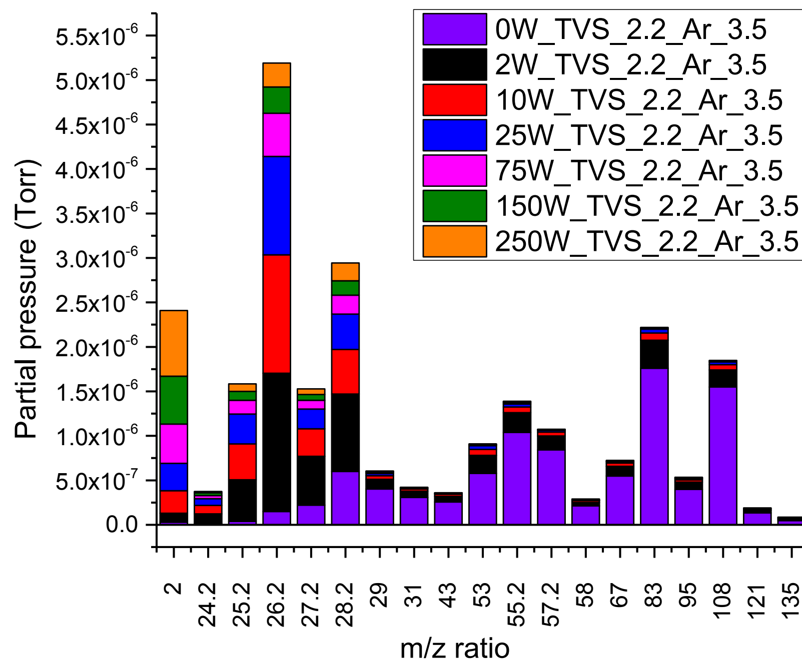

Fig. 41: Mass spectra of major species from TVS_2.2_Ar_3.5 series plasma distinguished by effective power. Graph is stacked by Y axe.

5.1.2.7 Mass spectrometry of TVS_13.7_O2_2.0 series

Mass spectra of TVS_13.7_O2_2.0 series acquired in range of effective power $0-250$ W are represented by following figure Fig. 42.

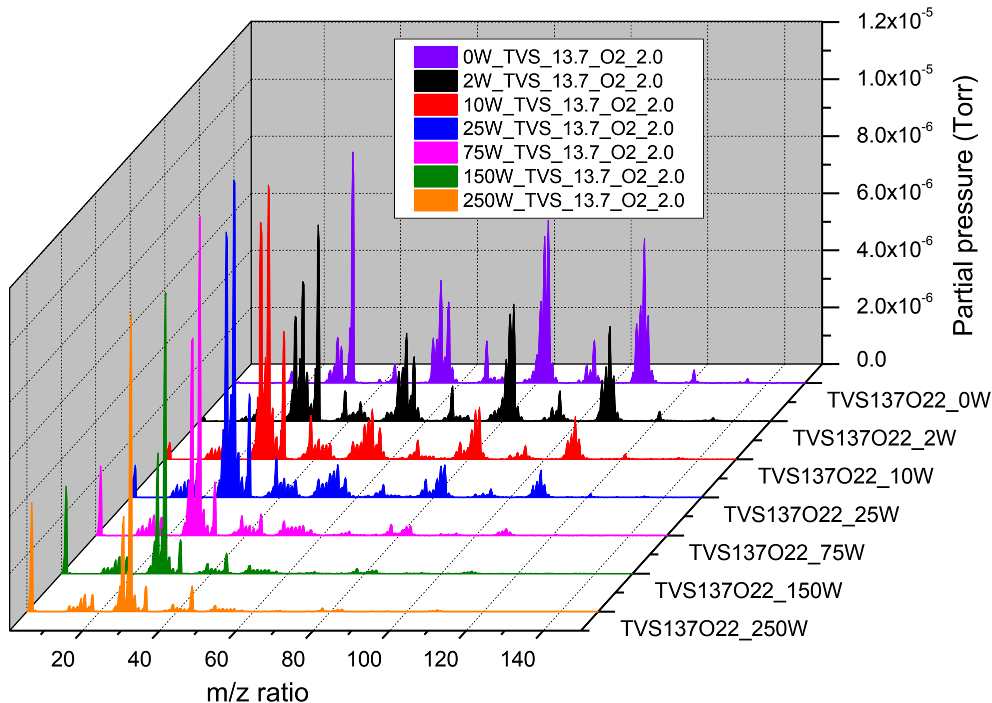

Fig. 42: Mass spectra of major species from TVS_13.7_O2_2.0 series plasma distinguished by effective power.

As is show at figure Fig. 42 spectra of tetravinylsilane to oxygen mixtures are different due the chemical reaction of fragment's with oxygen. Because exact determination of processes taking place in the TVS/O_2 plasma is really demanding and time consumptive only basic identification of significant bands will be commented.

From the spectra were identified main products contributing with oxygen chemical reactions. With lowest value from new identified fragments is $m/z=16$ atomic oxygen with has fundamental peak at $m/z=32$. Next new identified molecule is water with $m/z=18$, which content is little bit surprise, because in measurement of chamber and mass spectrometer background does not occurs (in significant values of partial pressure), so it can be assumed that part of its content is produced by chemical reaction of oxygen with released hydrogen atoms. Next newly identified molecule in plasma is CO_2 molecule, which is represented by significant $m/z=43.8$ peak. During fragmentation of CO2 (but also other molecules) the fragments of molecular carbon occurs at $m/z=16$. Near to CO_2 $m/z=43.8$ peak is assumed existence of $m/z=44.2$ peak, which may be connected to $SiO^{g\bullet}$. This assumption would not be sufficiently con-

firmed because the Si atomic peak would has his maxima at $m/z = 28$, where also exist fragment from TVS. Fragment with $m/z = 15$ contributes to CH_3 molecule.

From the graph at figure Fig. 42 is apparently that with increasing effective power supplied to the reactor decreases concentration of fragments with higher molecular mass. Better are trends for selected and characteristic peaks shown at following figure Fig. 43.

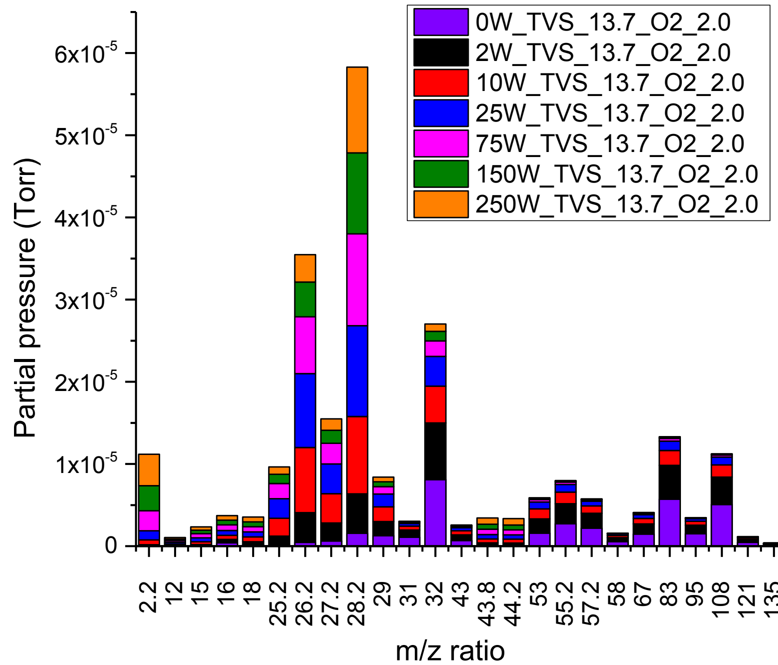

Fig. 43: Mass spectra of major species from TVS_13.7_O2_2.0 series plasma distinguished by effective power. Graph is stacked by Y axe.

At the figure Fig. 43 is shown that with increasing effective power is exactly decreasing concentration of fragments with $m/z > 28$, which should involves idea, that this trend is global and it is independent to gas mix TVS ratio. Highest content in this spectra has peak with $m/z = 28.2$, which is different in compare to Argon mix spectra, where is the highest content $m/z = 26.2$ peak. Interesting is also fact that intensity of peak value is for measurement with effective power larger than 10W effective almost power independent. The content of carbon dioxide peak $m/z = 43.8$ and content of water $(m/z = 18)$ is almost power independent too. The carbon peak is significant only for 2W series.

5.1.2.8 Mass spectrometry of TVS_6.0_ O2_3.0 series

Mass spectra of TVS_6.0_O2_3.0 series acquired in range of effective power $0-250$ W are represented by dependence of major fragments concentration to the effective power applied to the reactor graph at following figure Fig. 44.

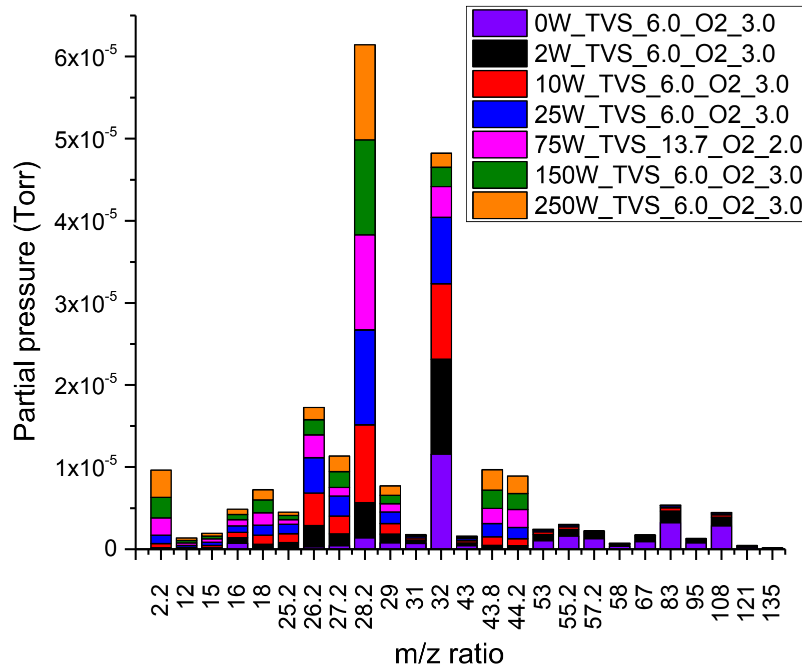

Fig. 44: Mass spectra of major species from TVS_6.0_O2_3.0 series plasma distinguished by effective power. Graph is stacked by Y axe.

At the figure Fig. 44 is shown that with increasing effective power is exactly decreasing concentration of fragments as was previously mentioned, but with significantly higher slope. Higher fragments with $m/z > 28$ (with exlusion of $m/z = 43-44$ area) are significant only for 2W series. The most significant peak in spectrum is peak with $m/z = 28.2$, which is the same as in previously mentioned mixture (TVS_13.7_O2_2.0). Considerable changes in compare to TVS_13.7_Ar_2.0 occurs in case of carbon dioxide peak $m/z = 43.8$ and assumpted $SiO^{g\bullet}$ peak $m/z = 44.2$, which are significantly higher intensity with increasing trend of their intensities by increasing effective power. Notable is also increased water content, which would be connected to same trend as in case of carbon dioxide and $SiO^{g\bullet}$. Hydrogen content is increasing with increasing power, but the absolute intensity is in compare to TVS_13.7_Ar_2.0 series decreased, which can be taken as confirmation of water in plasma forming.

5.1.2.9 Mass spectrometry of TVS_2.2_ O2_3.5 series

Mass spectra of TVS_2.2_O2_3.5 series acquired in range of effective power $0-250$ W are represented by dependence of major fragments concentration to the effective power applied to the reactor graph at following figure Fig. 45.

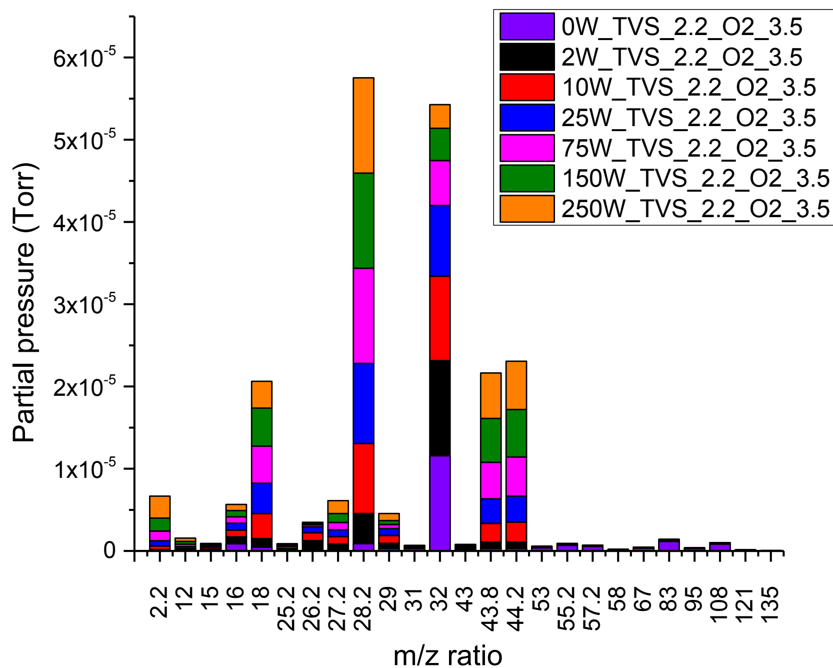

Fig. 45: Mass spectra of major species from TVS_13.7_O2_2.0 series plasma distinguished by effective power. Graph is stacked by Y axe.

At figure Fig. 45 the higher mass fragments with $m/z > 28$ (with exclusion of $m/z = 43-44$ area and oxygen $m/z = 36$) are insignificant for all power series. The most significant peak in spectrum is peak with $m/z = 28.2$, which is the same as in previously mentioned mixtures (TVS_6.0_O2_3.0 and TVS_13.7_O2_2.0). Considerable changes in compare to TVS_6.0_O2_3.0 occurs in case of carbon dioxide peak $m/z = 43.8$ and assumed $SiO^{g\bullet}$ peak $m/z = 44.2$, which are significantly higher intensity with increasing trend of their intensities by increasing effective power. Notable is also increased water content, which would be connected to same trend as in case of carbon dioxide and $SiO^{g\bullet}$. Hydrogen content is increasing with increasing power, but the absolute intensity is in compare to TVS_6.0_O2_3.0 series decreased, which is in good agreement to the assumed water forming plasma reaction.

5.1.2.10 Influence of oxygen content to major plasma species

Dependence of oxygen gas to TVS monomer ratio to the major fragments content for series prepared by 2W, 75W and 250W was studied. Dependences are described by graph at figures Fig. 46 to Fig. 48 below this paragraph.

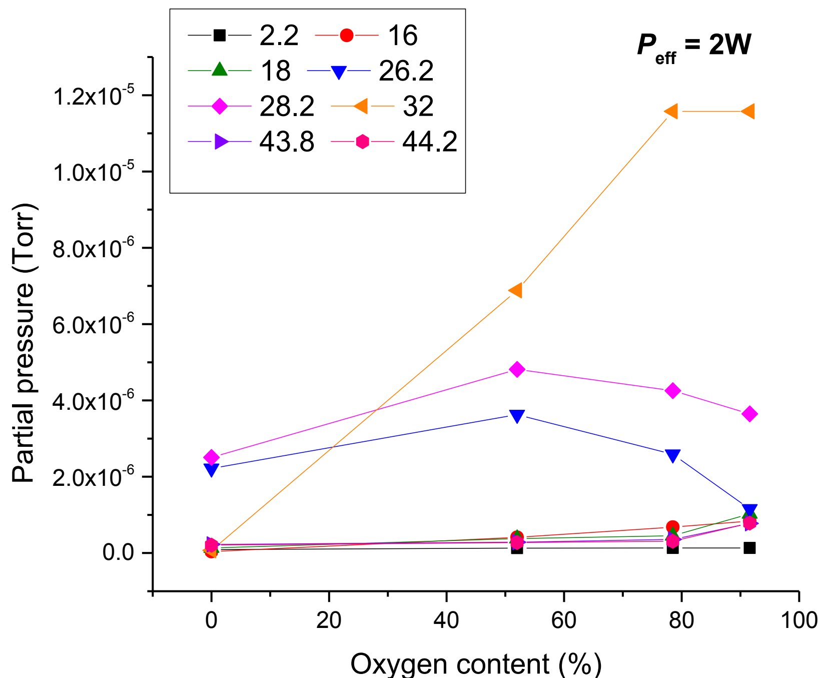

Fig. 46: Influence of oxygen content to the intensity of major plasma species in series prepared by 2W of effective power

Graph at figure Fig. 46 is showing influence of selected major species intensity obtained by mass spectrometry to oxygen content in reactive gas mix. Graph of oxygen species $m/z = 32$ is showing that the added oxygen is not so effectively consumed by chemical reactions in low powers plasmas. Trend should be confirmed by only very small oxygen ratio dependence of content of atomic oxygen $m/z = 16$ peak intensity. With increasing oxygen content in the mix are $m/z = 26.2$ and $m/z = 28.2$ peaks up to 52% in the mix slightly increasing, but after the 52% of oxygen is exceeded the intensities are decreasing. Higher slope of intensity loss has $m/z = 26.2$ peak. Hydrogen $m/z = 2.2$, Water $m/z = 18$, carbon dioxide $m/z = 43.8$ and assumed $SiO^{\delta\bullet}$ $m/z = 44.2$ peaks intensities are up to 80% of oxygen in the mix almost independent on oxygen to TVS ratio. For more 92% of the oxygen in the mix series, slight increasing trend of mentioned species occurs.

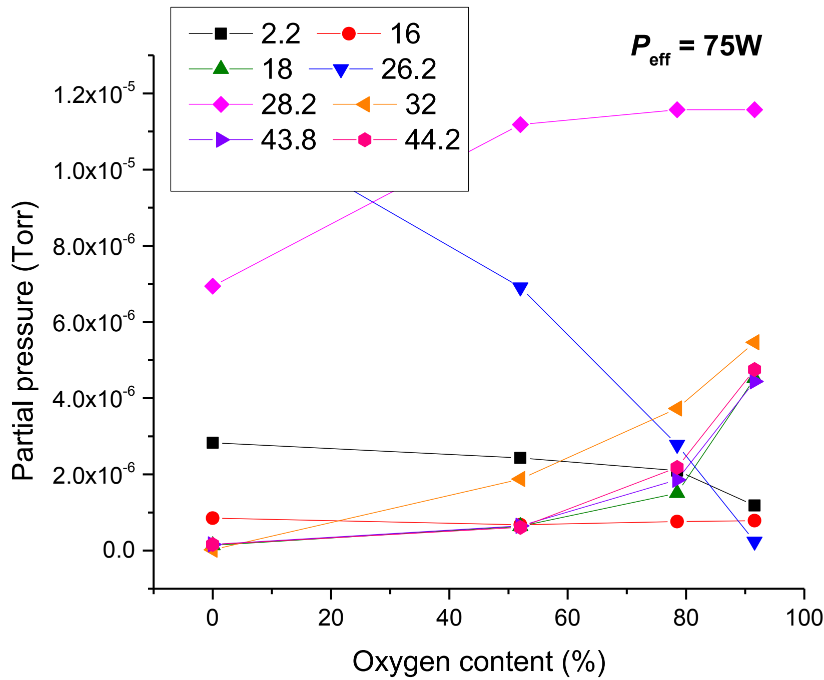

Fig. 47: Influence of oxygen content to the intensity of major plasma species in series prepared by 75W of effective power

Graph at figure Fig. 47 is showing influence of selected major species prepared by 75W of effective power intensity obtained by mass spectrometry to oxygen content in reactive gas mix. Graph of oxygen species $m/z=32$ is showing that the added oxygen is acting in plasma reaction much more than in 2W case, because of its weaker oxygen in mix content slope. With increasing oxygen content in the mix are the $m/z=26.2$ peaks strongly decreasing its intensities. Overleaf the $m/z=28.2$ are increasing its intensities with oxygen content. This would be explained as change by decreasing content of double bond fragment $m/z=26.2$ and also by increasing content of carbon dioxide with has at $m/z=28$ fragment $CO^{+\bullet}$. Carbon dioxide $m/z=43.8$, water $m/z=18$ and assumed $SiO^{\text{g}\bullet}$ $m/z=44.2$ are increasing with increasing oxygen in mix content. Hydrogen content is almost linearly decreasing with increasing oxygen content and its trend is just opposite to the water content.

At figure Fig. 48 is showing influence of selected major species prepared by 75W of effective power intensity obtained by mass spectrometry to oxygen content in reactive gas mix. Same trend of hydrogen vs. water content as in previously mentioned 75W series occurs. Same trend retains for Carbon dioxide $m/z=43.8$ and assumed $SiO^{\text{g}\bullet}$ $m/z=44.2$ peaks, but with much more higher intensities. Same situation of decresing double bond fragment $m/z=26.2$ with oxygen in mix content at the expense of fragment $m/z=28.2$ is retained.

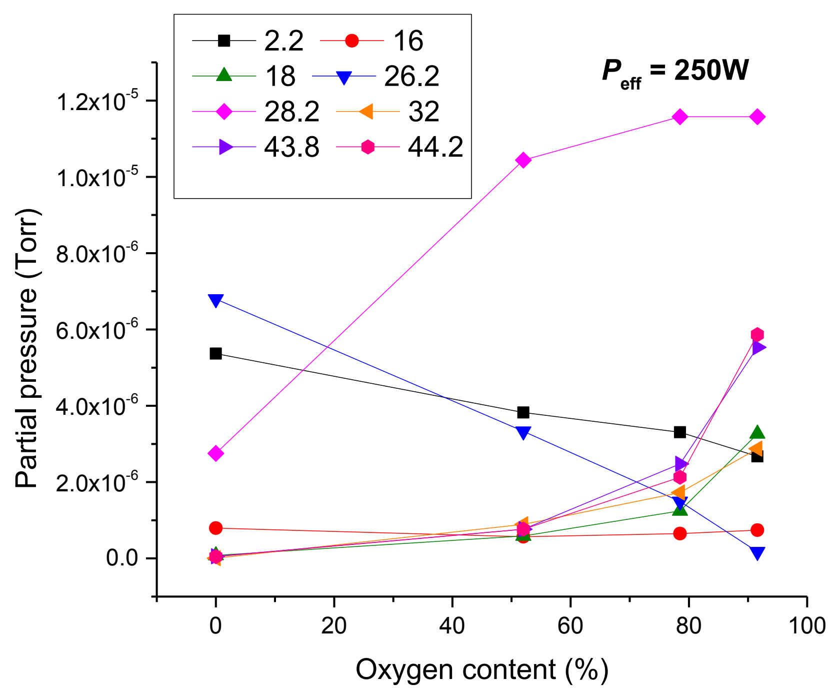

Fig. 48: Influence of oxygen content to the intensity of major plasma species in series prepared by 250W of effective power

5.2 Deposition conditions

5.2.1 Pressure and self-bias

During deposition, conditions in reactor are modified by reactions, which inside occurs. The most significant quantities subject to change are pressure and self-bias voltage. Plasma electrons fragmentate the monomer (or mixes), which causes higher relative pressure than pressure, which was at setup. But when also deposition occurs the fragments are consumed by process of plasma polymer grow and pressure is lower than setup pressure.

During the depositions, software A3_controller was used to log data of important parameters. Obtained data was processed by Origin software and analyzed. Typical graph obtained from deposition is shown as Fig. 49.

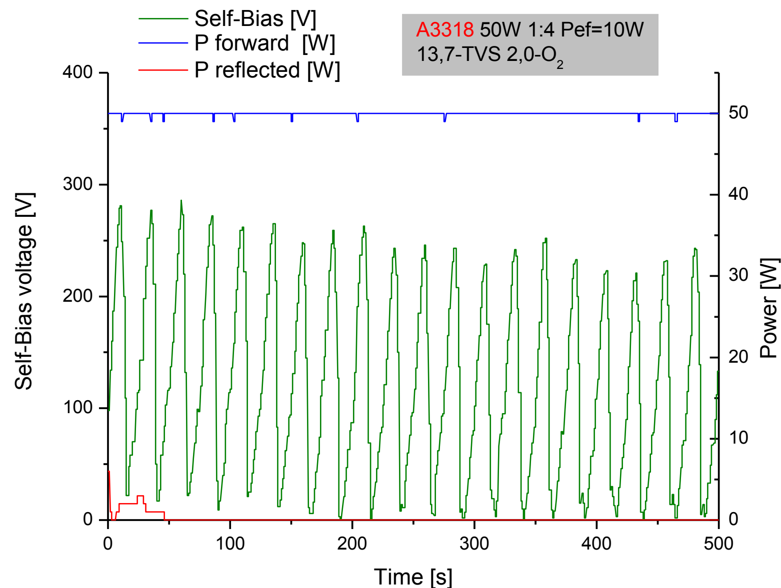

Fig. 49: Typical graph of obtained "power supply" data through deposition process. Graph shows forward and reflected power and self-bias

Earned data was statistically processed by the mean value and standard deviation. Standard deviation was used as the error bars in graphs showed in following paragraph. From the processed data graphs of reactor pressure (Fig. 50) dependence and inter-electrodes self-bias voltage (Fig. 51) on effective power was constructed.

At graph of reaction pressure mean value during deposition is showing that the deposition pressure of TVS_only series is almost constant up to 25 W of effective power. After the 25W of effective power value is exceeded, deposition pressure rapidly decreases up to 150W of effective power. Between $150 - 250$ W is pressure almost constant.

Argon series $(TVS_13.7_Ar_2.0, TVS_6.0_Ar_3.0, TVS_2.2_Ar_3.5)$ reaction pressure showed at figure Fig. 50 is for all series almost constant or slightly decreasing $(TVS_13.7_Ar_2.0)$ with increasing effective power.

Very different situation of reaction pressure is showed in case of oxygen series $(TVS_13.7_O_2_2.0, TVS_6.0_O_2_3.0, TVS_2.2_O_2_3.5)$, where the higher oxygen content series $(TVS_2.2_O_2_3.5)$ pressure is increasing with increasing effective power. This can be caused by formation of non-reactive compounds like carbon dioxide (CO_2) directly in deposition plasma. Mentioned assumption is in good agreement with information obtained from mass spectroscopy, where in case of oxygen series the carbon dioxide peak has high intensity. In case of lower content oxygen series $(TVS_6.0_O_2_3.0)$ is copping the trend of higher oxygen content series, with only slight deviation, in case of 10 W effective power, where slight decrease of pressure occurred. Very different from the $TVS_6.0_O_2_3.0, TVS_2.2_O_2_3.5$ series is $TVS_13.7_O_2_2.0$ series. The reaction pressure trend of this lowest oxygen content series is good copping decreasing trend of TVS_only series but with pressure constantly displaced to lower value.

Also interesting is fact, that in all series (and with take in account the dispersion represented by error bars) between $150-250$ W of effective power only insignificant pressure change occurs.

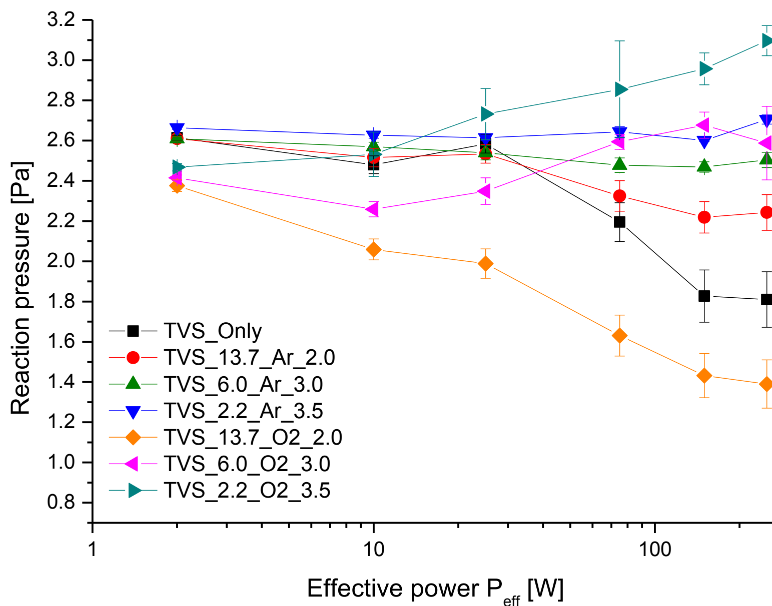

Fig. 50: Graph of deposition reaction pressure mean value during deposition. Error bars are connected to standard deviation.

At Fig. 51 the dependence of self-bias to effective power value is shown. The values of self-bias in all series are in very same trend, showing that with increasing effective power the self-bias voltage also increases. Series are different between themselves only in slope. Highest slope has TVS_only series followed by series with lowest dilution of TVS monomer by reactive gas (TVS_13.7_Ar_2.0, TVS_13.7_O2_2.0). Trend of decrease Self-bias voltage continues with other diluting ratios.

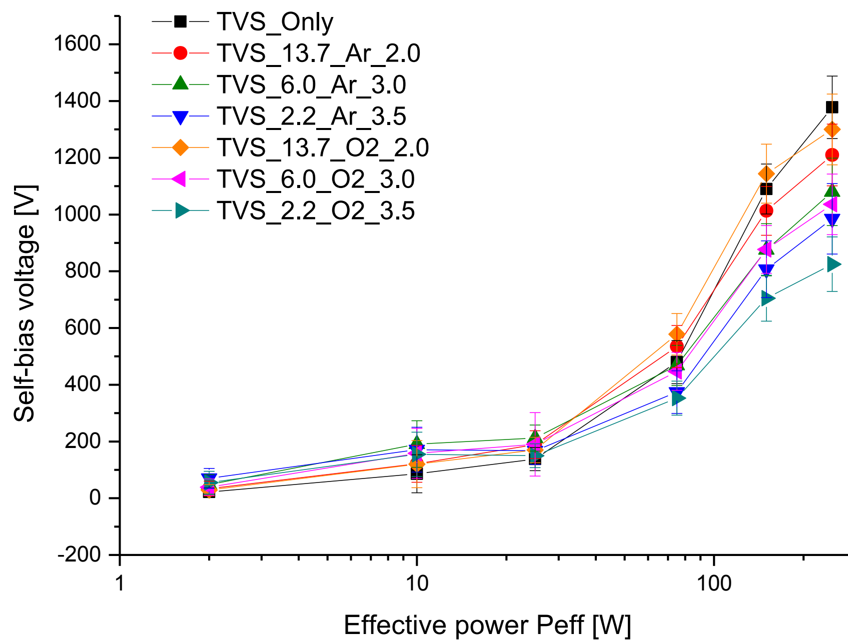

Fig. 51: Graph of deposition self-bias mean value during deposition. Error bars are connected to standard deviation.

From the data showed at figure Fig. 52 results, that the self-bias voltage value is for powers under 25W and slightly increasing or almost constant with increasing content of both used gases (oxygen and argon). For both gaseous mixtures types and power 75 W is situation different, because after increase of self-bias voltage in range pro 0% to about 50 % of gas content in mix, follow rapid decline. Very same situation is on oxygen mixture 150W. Both 250W and 150W argon mixture has decreasing value of self-bias voltage in whole range of gas ratios.

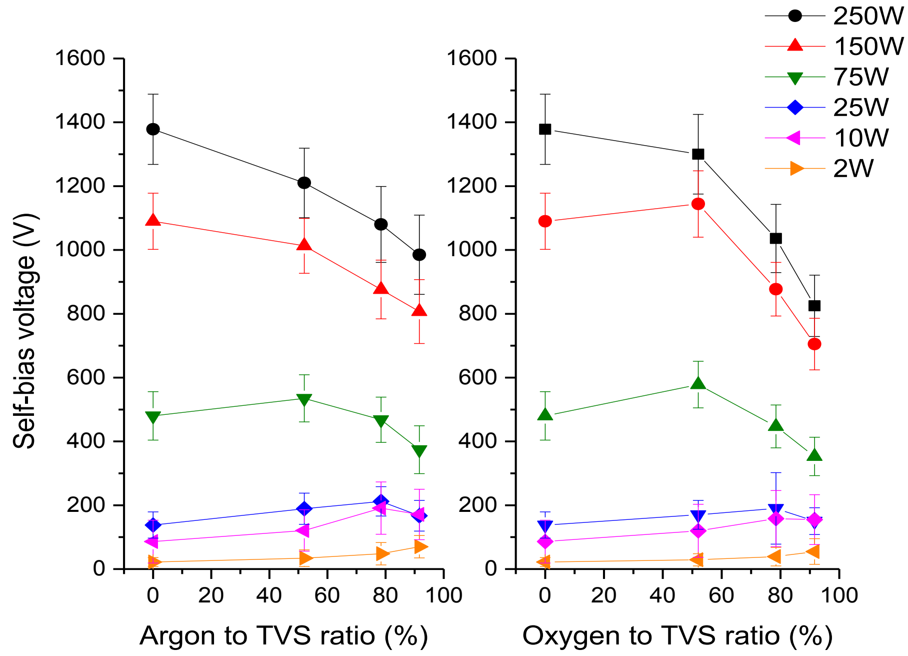

Fig. 52: Graph dependence of deposition self-bias mean value to Argon gas (left side) and oxygen gas (right side) ratio.

5.2.2 Deposition rates (ELL)

Deposition rates are one of most important parameters in thin-film processing technologies, because it is parameter which is used for setting of final thickness. In this work the deposition rates was obtained twice. Firstly it was obtained by probationary series depositions and secondly when the live series was made. Deposition speed was obtained by thickness obtained by ellipsometry and known deposition time. The deposition rate is defined by formula {19}.

$$v_{\text{dep}} = \frac{FT}{t_{\text{dep}}} \quad [nm \cdot s^{-1}] \qquad \{21\}$$

Following data used in this chapter is almost from live series. Data from probationary series was used primary only for setting deposition times for preparation samples of live series to defined thickness.

From the graph on Fig. 53 is noticeably, that the highest deposition rates in all regimes have TVS_only series. Relatively significant is fact that the deposition rate of TVS_only has linear increase if deposition rate up to 25W of effective power, then the deposition rate strongly linearly decreases. This can be explained by lower film grow speed for smaller fragments, which would be highly pumped out than the bigger one produced by lower effective powers. This decrease also may be also caused by higher and stronger ablation process, which is directly connected to higher self-bias voltage

respectively to the effective power (dependence of self-bias voltage to effective power was described by Fig. 55).

In case of series with about 50% content of added argon gas to mixture (TVS_13.7_Ar_2.0) the deposition rate slightly increases from 2W to 10W and from 10W to 150W is almost constant (slight decrease of deposition rate in 75W case may be caused by deviation and should be corrected by higher amount of measurements).

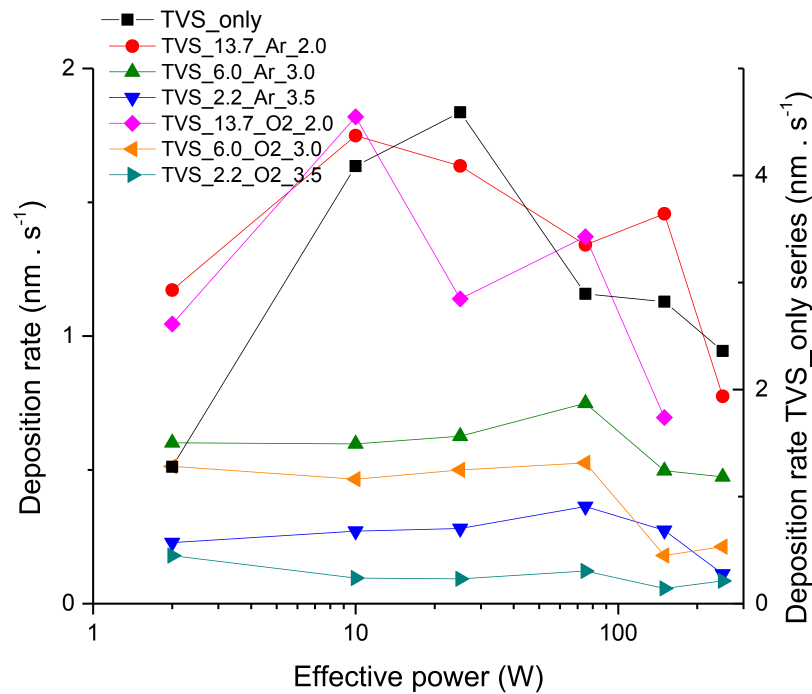

Fig. 53: Graph dependence of deposition rate to effective power value for selected reactive gas mixtures.

TVS_13.7_O_2_2.0 series deposition rate may be interesting by decrease of deposition rate at 75W of effective power, which should not be satisfactory explained without deeply study. With neglect of previously mentioned fact the series has alike trend like TVS_13.7_Ar_2.0 series.

All other series has almost constant and linear dependence of deposition rate to the effective power up to 75W. With exceed of 75W of effective power the deposition rates decreases. Trends for series TVS_6.0_O_2_3.0, TVS_6.0_Ar_3.0 are nearly the same, similar situation is in TVS_2.2_O_2_3.5, TVS_2.2_Ar_3.5 case series, which induces assumption, that the deposition rate trend is not strongly depending on type of gas but practically only on its content. This assumption is better showed by following graph at picture Fig. 54, which is showing the deposition rate dependence on the gas added to the mixture content.

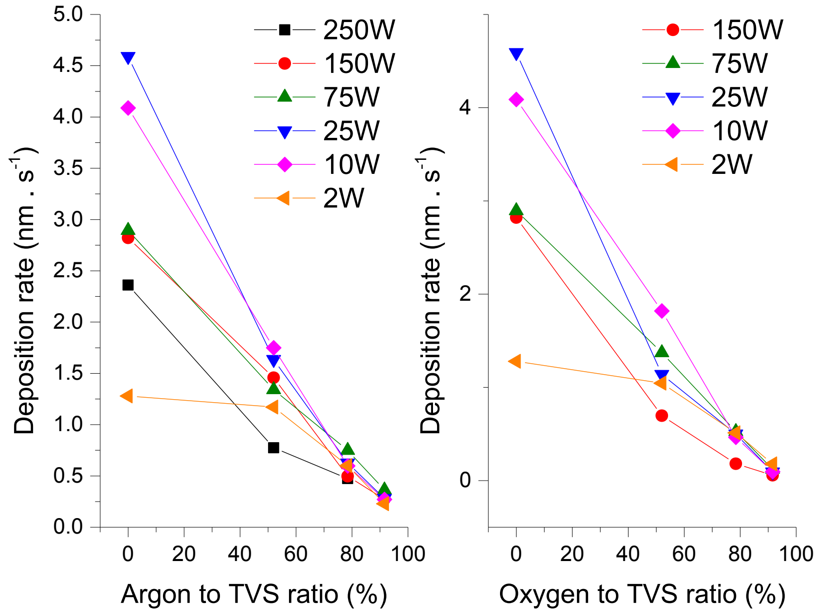

Fig. 54: Graph dependence of deposition rate to gas added to the mix ratio to TVS. (argon gas at left side and oxygen at right side)

Because the deposition rate should be strongly depending on self-bias voltage value, the deposition rate on mean self-bias voltage value graph was constructed. The graph is represented by Fig. 53.

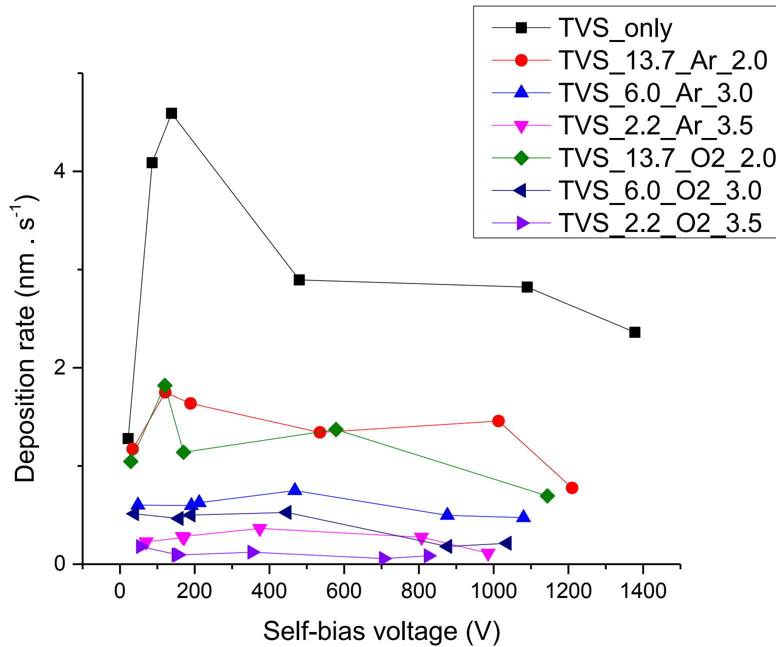

Fig. 55: Graph dependence of deposition rate to the self-bias voltage

5.3 Analysis of prepared thin films

5.3.1 Optical properties (ELL)

Optical properties of prepared thin films were studied by spectroscopic ellipsometry. Scope of this study was targeted to obtain information about refractive indexes (*n*) and extinction coefficients (*k*) of prepared samples and earn dependences of these optical constants to the deposition conditions (such as gas mixtures or effective power). Optical parameter was calculated by Tauc-Lorentz model.

5.3.1.1 Optical properties of TVS_only series

Characteristic optical properties of this series samples is represented by dispersion curves showed at following figure Fig. 56.

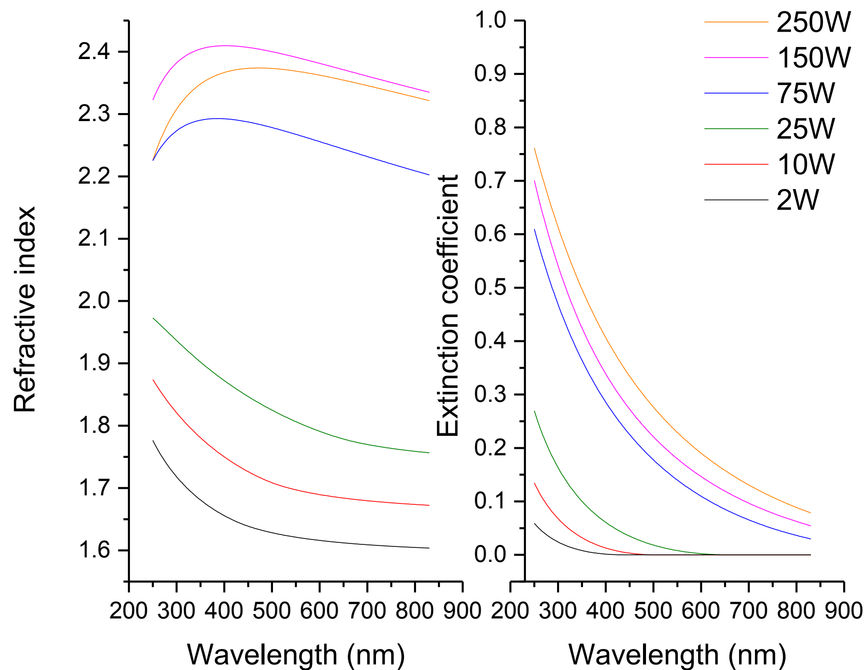

Fig. 56: Graph is showing dependence of TVS_Only series samples refractive indexes (left side) and extinction coefficients at the wavelength of incidence light.

From the graph at Fig. 56 results that the refraction indexes same as extinction coefficients are for TVS_Only series increasing with increasing effective power. The increasing values of characteristic indexes may be explained by increasing optical density of layer due to increasing density of a-SiC:H alloy. Little exclamation in this rule is at the refractive index of 250W effective power prepared sample, which is slightly below the 150W. This exception occurs also in nanoindentation test (chapter 6.3.4.1), where also 250W sample has lower mechanical properties, which may indicate the lower bond den-

sity (crosslinking) of 250W compared to 150W prepared samples. Extinction coefficients are scaled by power from minimal values of 2W of effective power, with minima in the UV region to the maximal values with are belonging to the sample prepared 250W and the minima is shifted to infra-red (IR) region.

5.3.1.2 Optical properties of TVS_13.7_Ar_2.0 series (52 % of argon in mixture)

Optical properties of samples belonging to the TVS_13.7_Ar_2.0 are represented by their dependence at wavelength (dispersion curves) graphs of following figure Fig. 57.

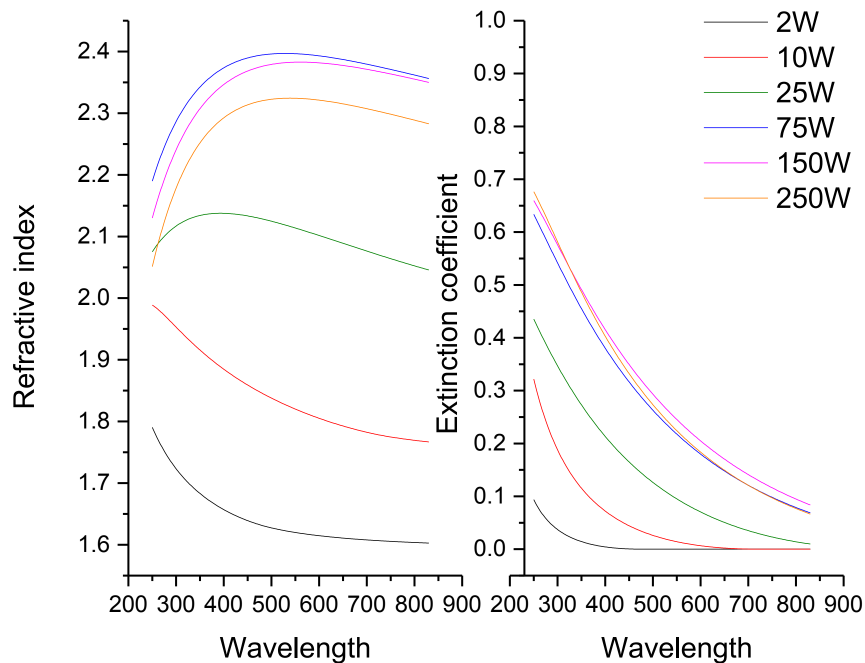

Fig. 57: Graph is showing dependence of TVS_13.7_Ar_2.0 series samples refractive indexes (left side) and extinction coefficients at the wavelength of incidence light.

At Fig. 57 is shown that the influence of argon content to the optical properties of TVS_13.7_Ar_2.0 series is most significant for 10W and 25W sample, which are shifted to the higher refractive indexes compared to TVS_only series. Same trend is shown at right side of the Fig. 57 in case of extinction coefficients, where also the 10W and 25W sample are shifted nearer to the extinction coefficients of samples prepared with powers higher than 75W and the minima are shifted nearer to the IR region. For the samples prepared by effective power range 75 – 250W is refractive index lowered in UV region, but with maxima at the almost same values to the TVS_only series. The highest value of refractive index in this series was obtained for the 75W sample. The 150W and 250W are following the dispersion curve of 75W sample but with lower maximal values. In case of extinction coefficient the 75 – 250W are almost the same trend and values. In compare to the TVS_only series minimal values have lower slope and they are shifted deeper to the IR region.

5.3.1.3 Optical properties of TVS_6.0_Ar_3.0 series (78,5% of argon in mixture)

Optical properties of samples belonging to the TVS_6.0_Ar_3.0 are represented by their wavelength dependence at graphs of following figure Fig. 58.

From figure Fig. 58 (lower) is noticeable that the refractive indexes of samples prepared with effective powers higher than 10W are near to themselves by its values. Significantly different situation occurs with samples with effective power 10W and 2W which is lower values.

Because from FTIR spectroscopy (chapter 6.3.2) is not noticeable any high significant change of chemical properties the change of refractive indexes and extinction coefficients dependence have to be caused by changed porosity or other parameter influencing optical density. Increased value of 2W series from this series in compared to the TVS_only and TVS_13.7_Ar_2.0 series induce idea, that the optical density and rigidity may be increased by ablation of summits of isles and produce layers with higher rigidity.

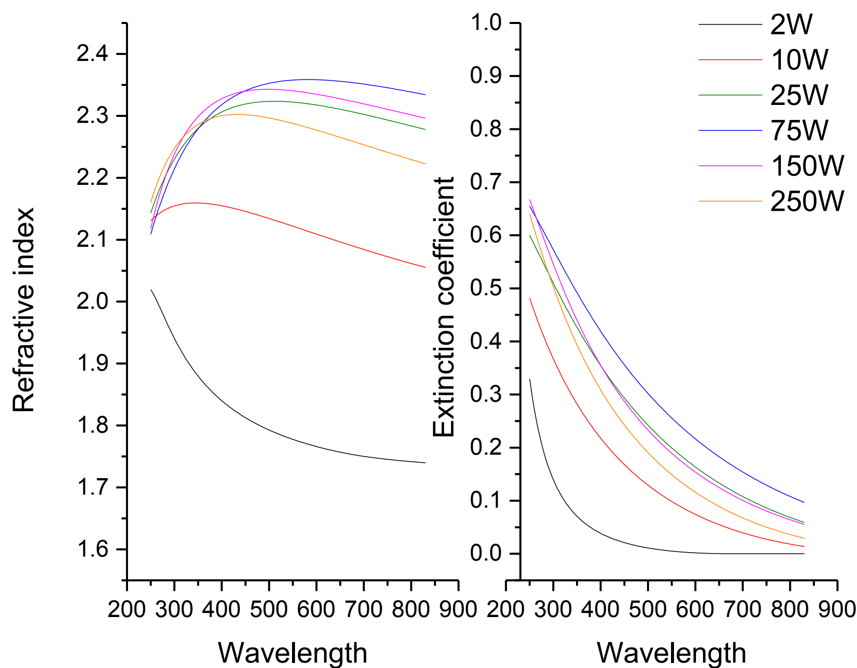

Fig. 58: Graph is showing dependence of TVS_6.0_Ar_3.0 series samples refractive indexes (left side) and extinction coefficients at the wavelength of incidence light.

5.3.1.4 Optical properties of TVS_2.2_Ar_3.5 series (91,6 % of argon in mixture)

Optical properties of samples belonging to the TVS_2.2_Ar_3.5 are represented by their wavelength dependence at graphs of following figure Fig. 59.

From figure Fig.59 is evident, that the characteristic optical properties are not in evident trends to the effective power value. From the data may be consulted that the lowest refractive index has 2W series and then the exact values of it wavelength dependence is higher than in the previous case (TVS_6.0_Ar_3.0) and also area with highest slope is moved to the higher wavelengths. Also may be commented that the 10W sample have almost the same optical properties as 250W of TVS_only series, which may induce idea, that the argon to added to the mix may move the optical properties of low power samples to the values belonging in TVS_only to higher effective powers. To exact confirmation of this idea the specialized measurements have to been done, which may be realized by further research work.

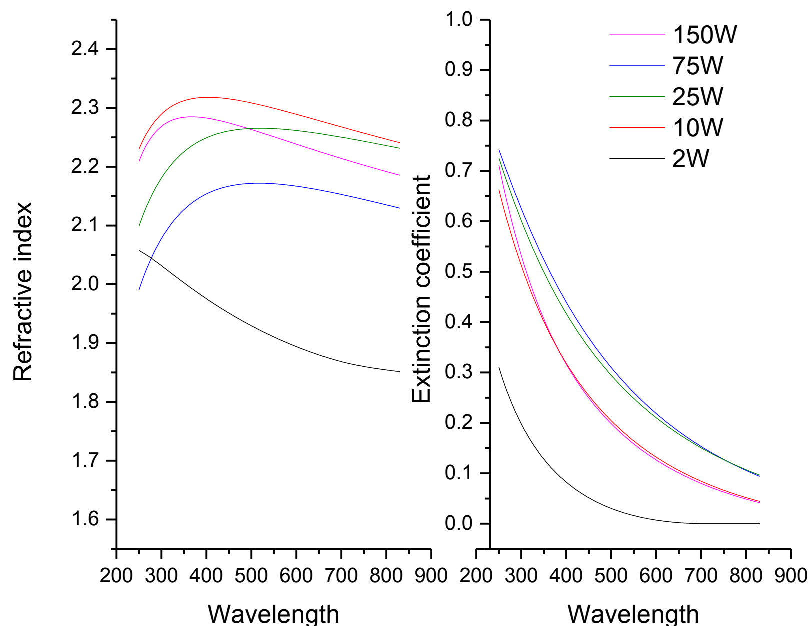

Fig. 59: Graph is showing dependence of TVS_2.2_Ar_3.5 series samples refractive indexes (left side) and extinction coefficients at the wavelength of incidence light.

5.3.1.5 Influence of effective power to optical properties Ar containing series

Because obtained data looks well trend-able, the graph of influence of effective power to the refractive index (Fig. 60) and extinction coefficients (Fig. 61) respectively were done. For the exact comparison the values belonging to wavelength 632 nm were used as the typical reference wavelength data [110].

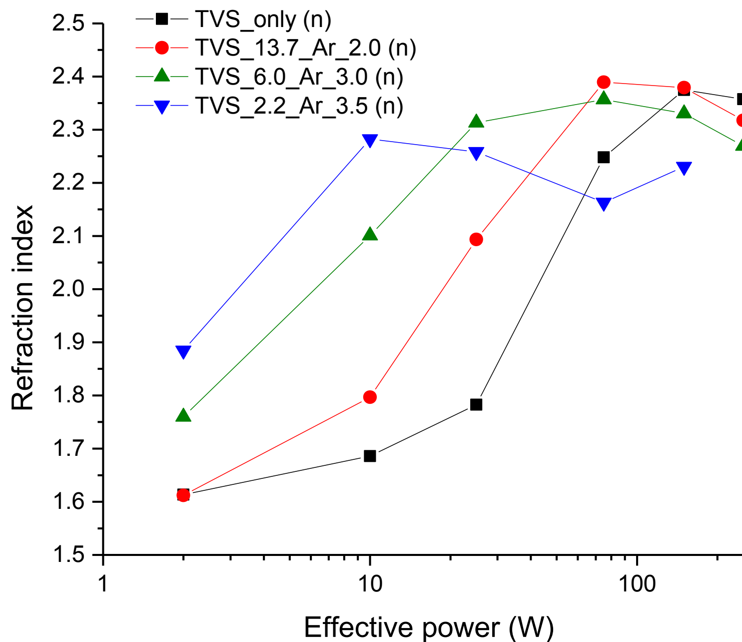

Fig. 60: Graph is showing dependence of samples refractive indexes at the effective power for reference wavelength 533 nm.

From the figure Fig. 60 can be seen trend increasing refractive index with increasing effective power for every series up to point were the trends ends and refractive index value is saturated on almost constant value. For these series is this value of refractive index near to $2.3 - 2.4$. From the picture can be also seen that the refractive index is increasing with increasing argon content in mixture, which is in good agreement to the previously mentioned assumption. Most evident is this trend in 10W of effective power prepared samples, because the 10W sample from TVS_2.2_Ar_3.5 series has higher value of refractive index than the 75W prepared sample from TVS_only series.

At figure Fig. 61 can be seen the dependence of extinction coefficients to the effective power values for argon containing series (without argon as reference). At the graph is shown that with increasing effective power in the range $2 - 75$ W the extinction coefficients for 633 nm are increased. After the effective power exceeds 75W, the TVS_2.2_Ar_3.5 and TVS_6.0_Ar_3.0 starts decreasing. The TVS_13.7_Ar_2.0 looks to be at 250W in maxima and may be slightly decreasing and TVS_only still increading.

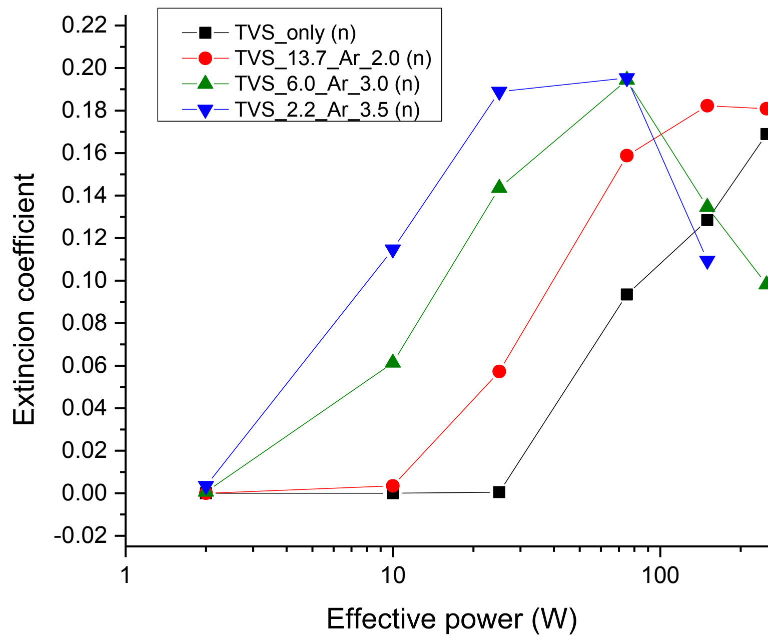

Fig. 61: Graph is showing dependence of samples refractive indexes at the effective power for reference wavelength 533 nm.

5.3.1.6 Influence of Ar content to optical properties Ar containing series

Because in previous chapter 5.3.1.5 was mentioned influence of argon content in the reactive mixture to the refractive index and extinction coefficient graphs of this dependences were constructed (Fig. 62, resp. Fig. 63).

From the graph at Fig. 62 could be seen that the highest influence of argon content to the refractive index acts on lower powers, especially for $2-25\text{W}$. For samples prepared with powers higher than 25W looks that the argon content influence is small. Samples prepared in these powers have almost the constant refractive index through the scale of used argon mixtures or it is slightly decreasing with increasing argon in mixture content.

In case of extinction coefficients (Fig. 63) may be commented, that for $2-25\text{W}$ of effective power, the extinction coefficient is raising its value in whole used range of argon content. For series prepared by 75W of effective power the extinction coefficient is raising up to about 82% of argon content where saturates a stays constant. Series prepared by 150W and 250W is raising its value up to about 50% of argon content and after decreases.

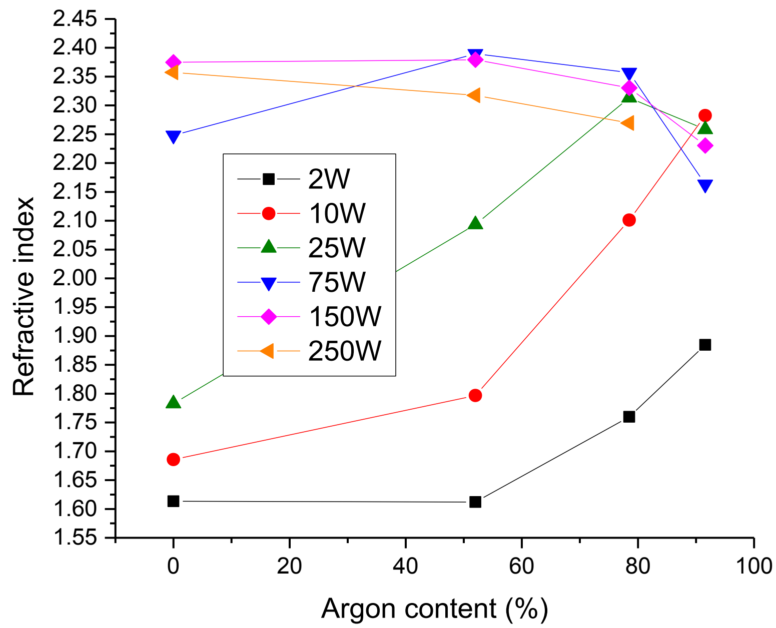

Fig. 62: Graph is showing dependence of samples refractive indexes for reference wavelength 533 nm at the argon content in reactive gas mixture.

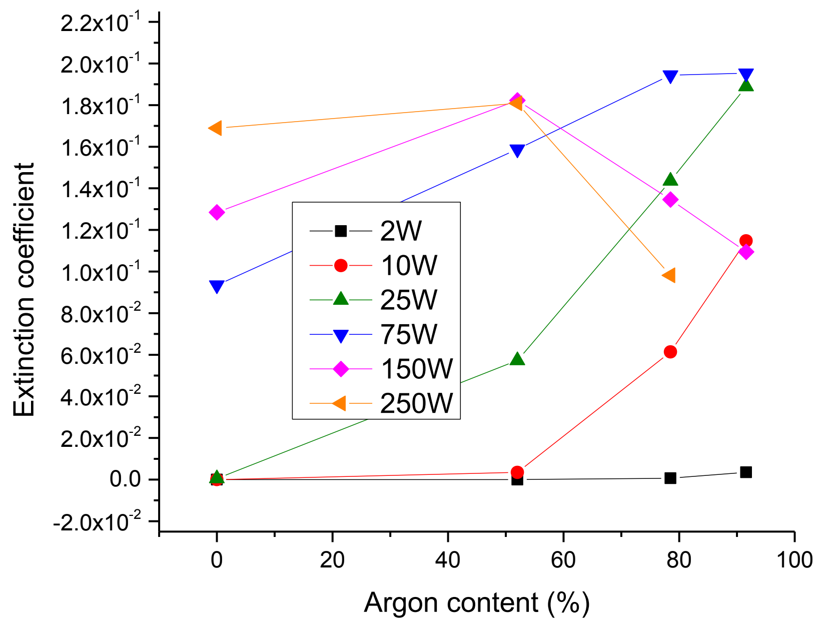

Fig. 63: Graph is showing dependence of samples refractive indexes for reference wavelength 533 nm at the argon content in reactive gas mixture.

5.3.1.7 Optical properties of TVS_13.7_O2_2.0 series (52 % of O_2 in mixture)

Optical properties of samples belonging to the TVS_13.7_O2_2.0 are represented by their wavelength dependence at graphs of following figure Fig. 64.

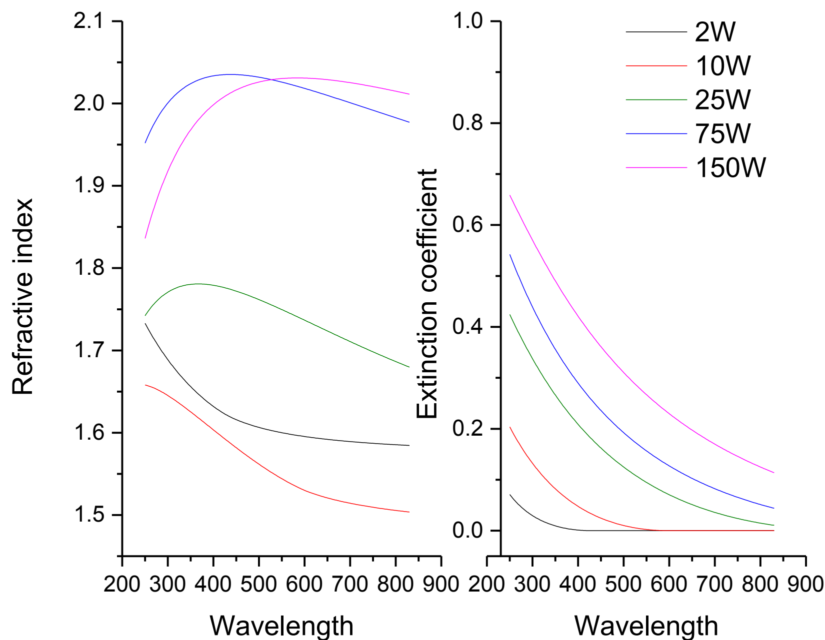

Fig. 64: Graph of dependence of TVS_13.7_O2_2.0 series samples refractive indexes (left side) and extinction coefficients (right side) on the wavelength of incidence light.

At figure Fig. 64 is shown, that the extinction coefficients are decreasing with increasing wavelength in almost same slope (but also from other begin value) and their exact value is increasing with increasing effective power. In case of refraction indexes the situation is different because the 2W and 10W samples are with decreasing in whole range of measured wavelengths and the $25-150\text{W}$ samples are after the starting increase with maxima about 400-450 nm decreasing. Series is also interesting by fact that added oxygen to the mixture of higher powers $75-150\text{W}$ slightly decreases the absolute values of extinction coefficients which mean that the layer is more transmissible than TVS only film and films with argon gas mix.

5.3.1.8 Optical properties of TVS_2.2_ O2_3.5 series (91,6 % of O_2 in mixture)

Optical properties of samples belonging to the TVS_2.2_O2_3.5 are represented by its wavelength dependence at graphs of figure Fig. 65.

At figure Fig.59 (below this paragraph) is shown that the refractive index of the samples prepared by effective powers in range $10-150$ W is almost the same. Only deviation occupies in case of 2W sample refractive index which is significantly higher and almost the same to the TVS_only series one. The $10-150$ W samples similarity may be supported by FTIR analysis, where only slight deviations between them occur and by data from X-ray photoelectron spectroscopy, where also no significant difference between samples from $25-150$ W occurs. Very low absolute values of extinction coefficients also induce that the samples prepared from series with added oxygen are higher transparent for VIS range of spectra.

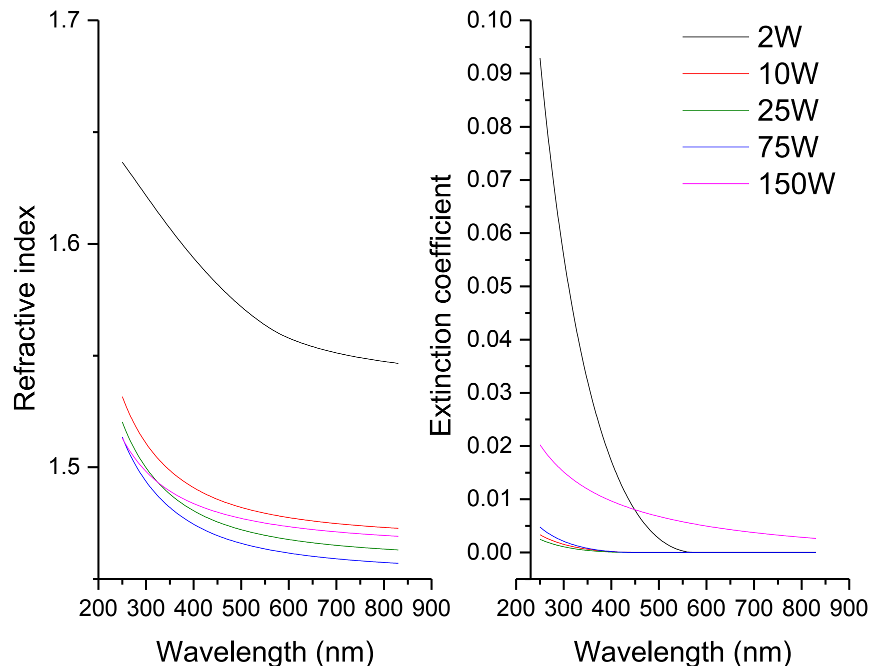

Fig. 65: Graph is showing dependence of TVS_2.2_O2_3.5 series samples refractive indexes (left side) and extinction coefficients at the wavelength of incidence light.

5.3.1.9 Influence of effective power to optical properties oxygen containing series

Because obtained data looks well trend-able, the graph of influence of effective power to the refractive index (Fig. 66) and extinction coefficients (Fig. 67) respectively were done. For the exact comparison the values belonging to wavelength 632 nm were used as the typical reference wavelength data [110].

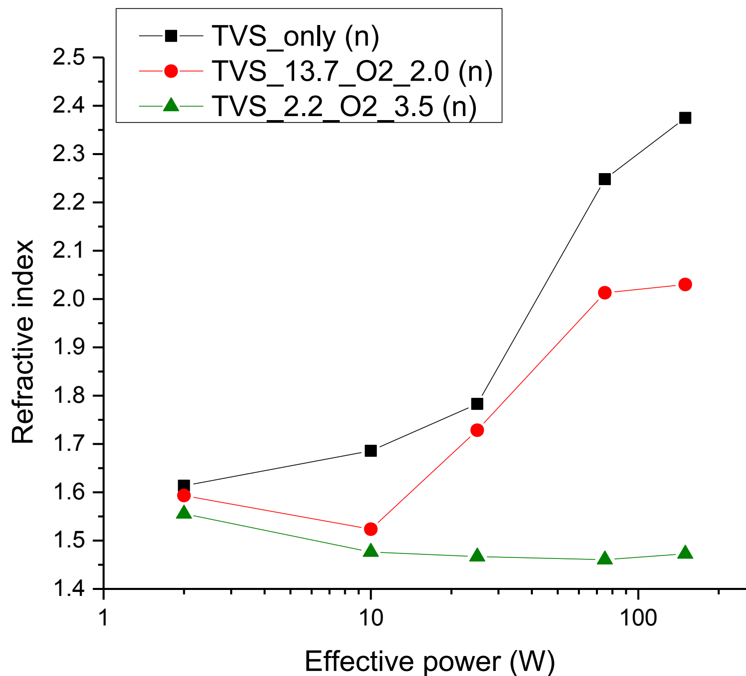

Fig. 66: Graph is showing dependence of samples refractive indexes at the effective power for reference wavelength 533 nm.

From the figure Fig. 66 can be seen trend increasing refractive index with increasing effective power for every series up to point were the trends ends and refractive index value is saturated on almost constant value or it is slightly decreasing. For these series is this value of refractive index near to $2.3-2.4$. For series with 52% content of oxygen in mixture and range of effective power $2-75$ W, were obtained results with lower values of refractive indexes in compare to TVS_only series with highest deviations in case of $150-250$ W samples. For series with 91.6% content of oxygen in mixture was obtained significantly lower values of refractive index with decreasing trend with increasing effective power.

At figure Fig. 67 can be seen the dependence of extinction coefficients to the effective power for oxygen containing series. For series containing 91.6% of oxygen in mixture, with exclusion of 250W series, was obtained almost independence on effective power, and also well optical transparency. Only for effective power 250W may be seen slight increase of extinction coefficient. Extinction coefficients dependence on effective pow-

er from TVS_13.7_O2_2.0 series were obtained as increasing with effective power , with almost the same slope to compared with TVS_only, but shifted to the lower value of effective power (10W, instead of 25W TVS_Only).

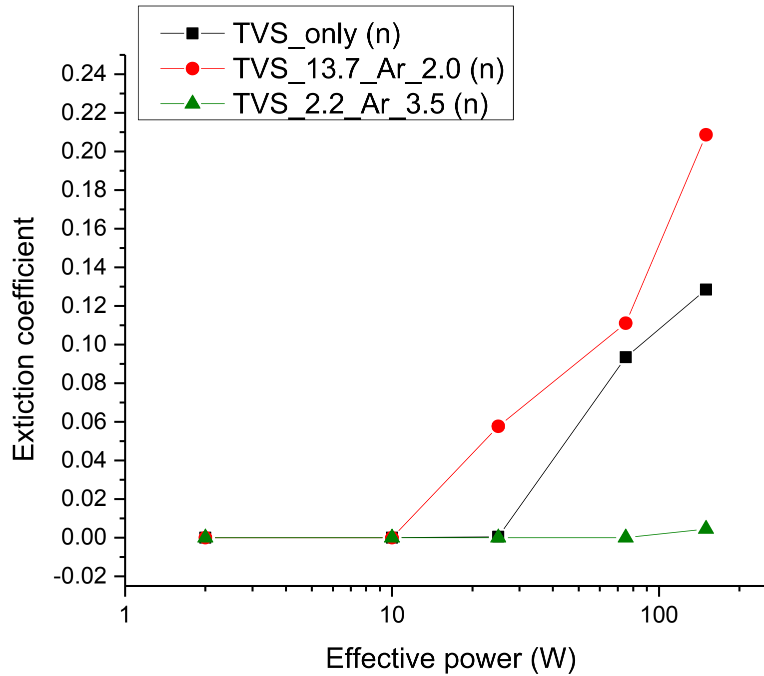

Fig. 67: Graph is showing dependence of samples extinction coefficients at the effective power for reference wavelength 533 nm.

5.3.1.10 Influence of oxygen content to optical properties oxygen containing series

Because in previous chapter 5.3.1.5 was mentioned influence of oxygen content in the reactive mixture to the refractive index and extinction coefficient graphs this dependences were constructed (Fig. 68, resp. Fig. 69) individually.

From the graph at Fig. 68 could be seen that the refractive index is for series prepared by $2-10$W of effective power slightly increasing up to 52% of oxygen content, followed by a decrease of value. For series prepared by $2-10$W of effective power may be commented that its value is decreasing in whole range of oxygen content. Notable is that the most significant decrease may be seen for the samples prepared by 150, 250W.

In case of dependence of samples refractive indexes (Fig. 69) to the oxygen may be seen, that the extinction coefficients for series prepared by $2-10$W is zero, and samples are for the selected wavelength fully transparent. With the increasing power the dependence on oxygen content in the mix is raising, and highest values are obtained from 150W series prepared by 52% of oxygen in mixture. In case of 91.6 % of oxygen containing series all samples are for the selected reference transparent.

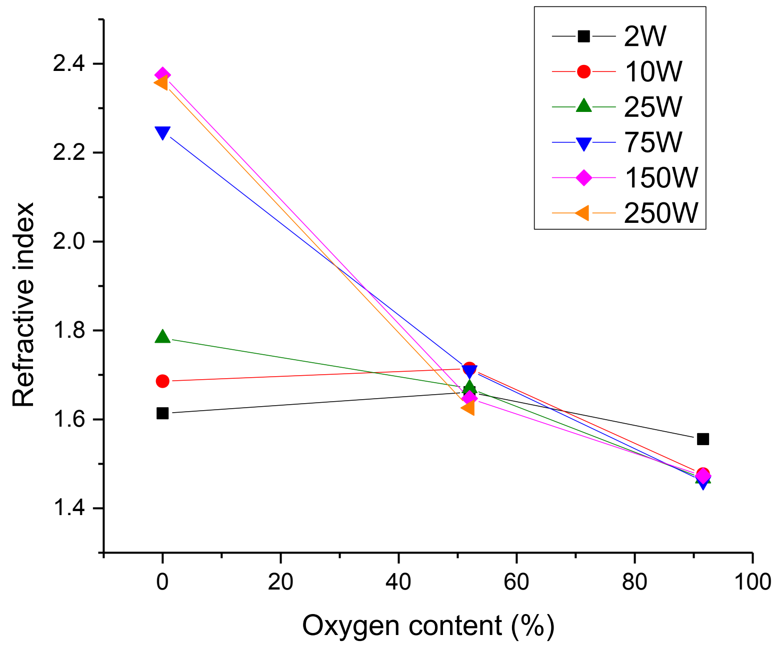

Fig. 68: Graph is showing dependence of samples refractive indexes for reference wavelength 533 nm at the argon content in reactive gas mixture.

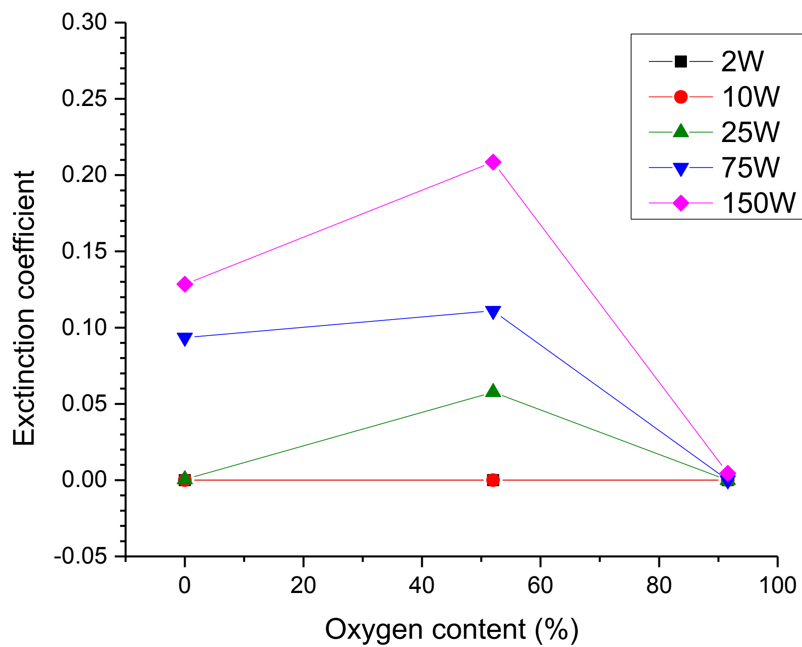

Fig. 69: Graph is showing dependence of samples refractive indexes for reference wavelength 533 nm at the argon content in reactive gas mixture.

5.3.2 Chemical structure (FTIR)

5.3.2.1 Typical absorption bands in TVS thin film

At figure Fig. 70 is shown detail of spectrum prepared from TVS_only batch and 10W of effective power, because the spectrum is one of the bands richest in the series.

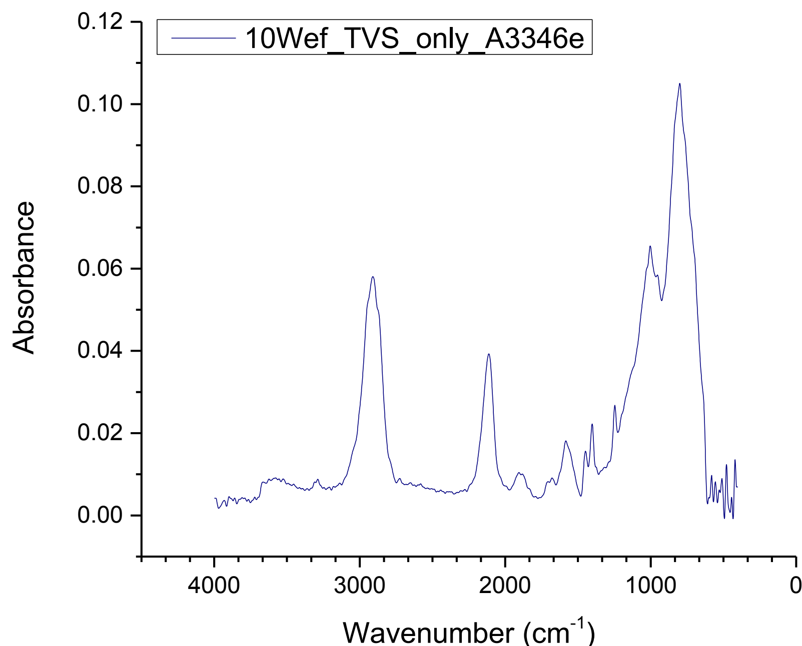

Fig. 70: Typical absorbance spectrum of film prepared from TVS monomer

Description of peaks interpretation is started at the highest wavenumbers (from the left side of x axe at Fig. 70). At the wavenumber range $3600-3200\,cm^{-1}$ is significant band of $-OH$ vibration, which would not be expected in spectra without oxygen, but between the measurement and deposition occurs several hours of post deposition oxygen and water degradation. Second significant band from left side at $3288\,cm^{-1}$ is harmonic vibration of $C=C$ in vinyl group. Following wide peak in range at $3100-2750\,cm^{-1}$ contributes with vibrations of $-CH_2, -CH_3$ groups. Next very significant band is $Si-H$ vibration with maximum at $2112\,cm^{-1}$. Peak, which also contributes with oxygen degradation (or oxygen in mixture) is peak belonging to $>C=O$ vibration with maxima at $1705\,cm^{-1}$. Subsequent significant peak is peak belonging to fundamental $>C=C<$ bond stretching in vinyl group. Following four bands contributes to $Si-CH=CH_2$ bands. Vibration with maxima at $1583\,cm^{-1}$ contributes with $>C=C<$ stretching, $1402\,cm^{-1}$ vibration contributes with $=CH_2$ def. , $1003\,cm^{-1}$ vibration contributes with $=CH$ wagging and $953\,cm^{-1}$ vibration contributes with $=CH_2$

wagging. Weaker intensity peak Wide peak in range $1100-1000\,cm^{-1}$ belongs to $Si-O-Si$, $Si-O-C$ bonds [112] [113] [114].

Mainly expected vibrational bands in the spectra was summarized into table Tab. 5 bellow this paragraph.

Tab. 5: Table of in TVS films expected characteristic vibrations wavenumbers interpretation [55] [112] [113] [114]

Vibrational wavenumber range	Expected bond	Note (describtion)
3600−3200	− OH	Typicaly from adsorbed water vapor or in oxygen series
3310−3280	>C=C<	Harmonic vibration of C = C bond with fundamental vibration on $1680\ cm^{-1}$ [106]
3100−2750	$-CH_3$, $-CH_2$	Alkane internal bonds and end bonds
2110	Si−H	Hidrogen to Si bond
1705	>C=O	Carbonyl group
1680	>C=C< str.	Doublebond in vinyl group fundamental wavenumber [113]
1580−1615	>C=C< str.	Double bond in $Si-CH=CH_2$ group
1450	$-CH_2$ sci.	Scissoring of $-CH_2$
1390−1410	$=CH_2$ def.	Deformation of $=CH_2$ bond in $Si-CH=CH_2$ group
1250−1200	$-CH_2$ wag.	Wagging of $Si-CH_2-R$ group
1020−1000	=CH wag.	Wagging of $=CH_2$ bond in $Si-CH=CH_2$ group
950−980	$=CH_2$ wag.	Wagging of $=CH_2$ bond in $Si-CH=CH_2$ group
1100−1000	Si−O−Si, Si−O−C str.	Multiband band of Si−O−Si, Si−O−C stretching
842−800	Si−H	Hidrogen to Si bond lower
800	Si−C	Carbon to Si bond

5.3.2.2 Spectra of TVS only series

Spectra of TVS_only series were measured just after deposition process ends. Spectra were obtained using real transmission module in range $400-4000\,cm^{-1}$ with resolution $2\,cm^{-1}$. Spectra were baselined and by offset normalized. Because the real transmission module significantly decreases signal incoming to the detector, detector with higher sensitivity was used and data was mathematicaly processed to obtain better signal to noise ratio (FFT filter, slope filter and mean filter).

Spectra of TVS_only series prepared in different effective power regimes are represented by following figure Fig. 71.

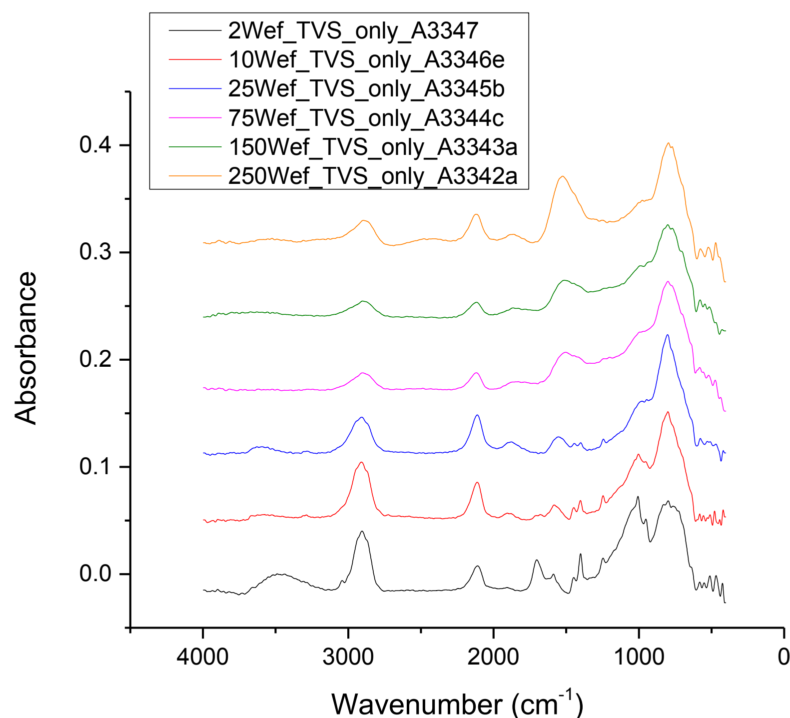

Fig. 71: Absorbance spectra of films prepared from TVS monomer at different effective power regimes

From the spectra showed at Fig. 71 it can be assumed, that the most prone to oxygen (water respectively) attack and degradation are samples prepared with effective powers bellow 25W, which has in spectra at the wavenumber range $3600-3200\ cm^{-1}$ is significant band of $-OH$ vibration, but the mixture did not contained any oxygen or water vapor. Same situation occurs in area near $1705\ cm^{-1}$ for $>C=O$ bond and $Si-O-C$ bonds at $1100-1000\ cm^{-1}$. This would be explained by lower crosslinking density caused by lower self-bias voltage. From the spectra can be also presumed that with the increasing effective power the content of hydrogen is decreasing, which is most obvious in case of decreasing intensity of $Si-H$ bond and decreasing intensity of alkanes bonds $\left(-CH_2,-CH_3\right)$ with increasing effective power and at the other side icrease of $>C=C<\left(\sim 1680\ cm^{-1}\right)$ and $=CH_2\left(\sim 1410\ cm^{-1}\right)$bonds intensities. Intensity of $1003\ cm^{-1}$ vibration contributes with $=CH$ wagging and $953\ cm^{-1}$ vibration contributes with $=CH_2$ wagging looks with exception of 2W series almost constant. Vibration of bonds, which strongly contributes with vinyl groups are identifiable only in samples prepared by effective power below 25W. Most significant are in sample prepared by 2W of effective power.

5.3.2.3 Spectra of TVS_13.7_Ar_2.0 (52% of argon gas in mixture)

Spectra of TVS_13.7_Ar_2.0 series were measured just after deposition process ends. Spectra were obtained using real transmission module in range $400-4000\ \mathrm{cm}^{-1}$ with resolution $2\ \mathrm{cm}^{-1}$. Spectra were baselined and by offset normalized. Because the real transmission module significantly decreases signal incoming to the detector, detector with higher sensitivity was used and data was mathematicaly processed to obtain better signal to noise ratio (FFT filter, slope filter and mean filter).

Spectra of TVS_13.7_Ar_2.0 series prepared in different effective power regimes are represented by following figure Fig. 72.

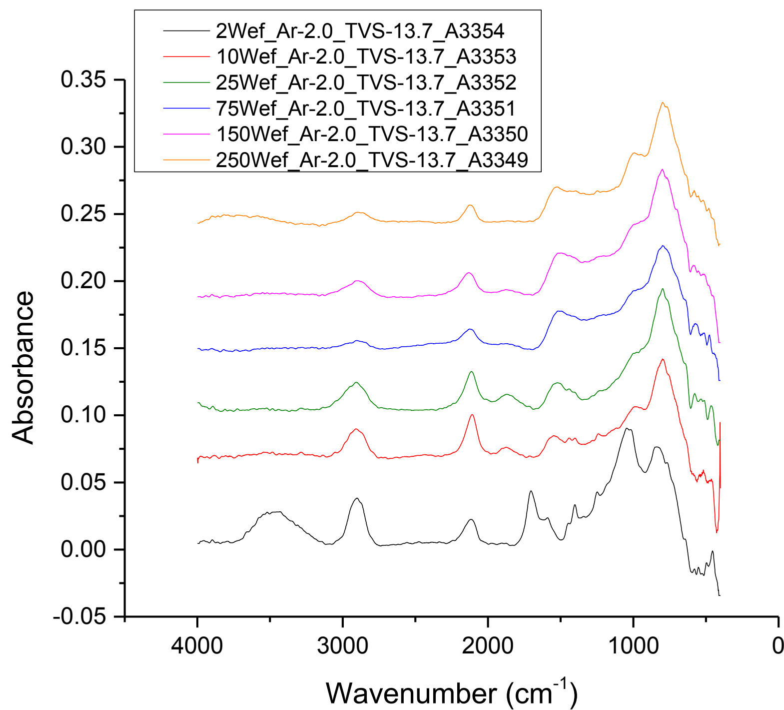

Fig. 72: Absorbance spectra of films prepared from TVS and argon mixture with argon content 52% at different effective power regimes

From the spectra showed at Fig. 72 it is apparently, that the most prone to oxygen (water respectively) attack and degradation are samples prepared with effective powers bellow 10W, which has in spectra at the wavenumber range $3600-3200\ \mathrm{cm}^{-1}$ is significant band of $-\mathrm{OH}$ vibration, but the mixture did not contained any oxygen or water vapor same as in TVS_only series. Situation, which occurs in area near $1705\ \mathrm{cm}^{-1}$ for $>\mathrm{C}=\mathrm{O}$ bond and $\mathrm{Si}-\mathrm{O}-\mathrm{C}$ bonds at $1100-1000\ \mathrm{cm}^{-1}$ is also noticeable oxygen degradation. This would be explained by lower crosslinking density caused by lower self-bias voltage.

Spectra and trends between them is almost in the same trends as like in TVS_only series. As like in TVS_only series it can be also presumed that with the increasing effec-

tive power the content of single bonds in alkanes is decreasing, which is most obvious in case of decreasing intensity of alkanes bonds $\left(-CH_2, -CH_3\right)$ with increasing effective power and at the other side increase of $>C=C<\left(\sim 1680\,\mathrm{cm}^{-1}\right)$ and $=CH_2\left(\sim 1410\,\mathrm{cm}^{-1}\right)$bonds intensities. Intensity of $1003\,\mathrm{cm}^{-1}$ vibration contributes with $=CH$ wagging and $953\,\mathrm{cm}^{-1}$ vibration contributes with $=CH_2$ wagging looks with exception of 2W series almost constant. Vibration of bonds, which strongly contributes with vinyl groups are identifiable only in samples prepared by effective power below 25W. These bands are most significant in case of sample prepared by 2W of effective power.

5.3.2.4 Spectra of TVS_6.0_Ar_3.0 (78.5 % of argon gas in mixture)

Spectra of TVS_6.0_Ar_3.0 series were measured just after deposition process ends. Spectra were obtained using real transmission module in range $400-4000\,\mathrm{cm}^{-1}$ with resolution $2\,\mathrm{cm}^{-1}$. Spectra were baselined and by offset normalized. Because the real transmission module significantly decreases signal incoming to the detector, detector with higher sensitivity was used and data was mathematically processed to obtain better signal to noise ratio (FFT filter, slope filter and mean filter).

Spectra of TVS_6.0_Ar_3.0 series prepared in different effective power regimes are represented by following figure Fig. 73.

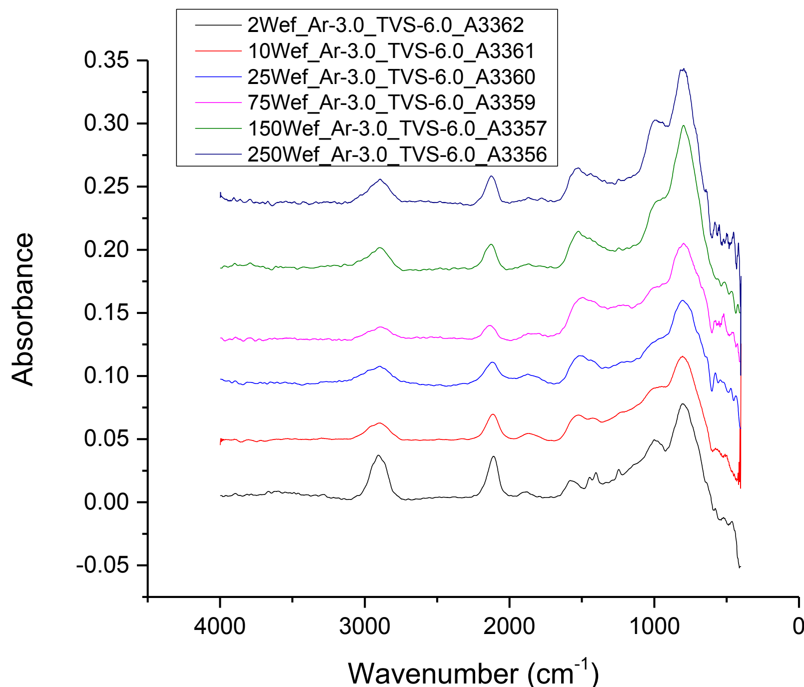

Fig. 73: Absorbance spectra of films prepared from TVS and argon mixture with argon content 78.5% at different effective power regimes

Spectra obtained from TVS_6.0_Ar_3.0 series are very interesting in fact that the vinyl vibration bands are absolutely clear only in measurement sample produced by 2W of effective power. Also interesting is that the intensities of $250-10\ \mathrm{W}$ bands are very similar just with exclusion of small intensity difference of 75W sample, which has slightly higher intensity double bonds $\mathrm{Si-C=C}\ (\sim 1580\ \mathrm{cm^{-1}})$ and $=\mathrm{CH_2}\ (\sim 1410\ \mathrm{cm^{-1}})$ at the expense of $\mathrm{Si-H}$ bonds intensities. Other almost insignificant increase of $\mathrm{Si-C}$, $\mathrm{Si-O-C}$ bands in case of 150W and 250W sample, but which may be caused by minor difference in thickness. Small difference can be also found in slight higher intensity of $\mathrm{Si-C=C}\ (\sim 1580\ \mathrm{cm^{-1}})$ band to $=\mathrm{CH_2}\ (\sim 1410\ \mathrm{cm^{-1}})$ band in 150W and 250W samples spectra.

5.3.2.5 Spectra of TVS_2.2_Ar_3.5 (91.6 % of argon gas in mixture)

Same as in previously mentioned situations the spectra was acquired by real transmission module in range $400-4000\ \mathrm{cm^{-1}}$ with resolution $2\ \mathrm{cm^{-1}}$ just before deposition (or in technologically unrecoverable delay). Spectra were baselined, by offset normalized, obtained data was mathematically processed to obtain better signal to noise ratio (FFT filter, slope filter and mean filter).

Spectra of TVS_2.2_Ar_3.5 series prepared in different effective power regimes are represented by following figure Fig. 74.

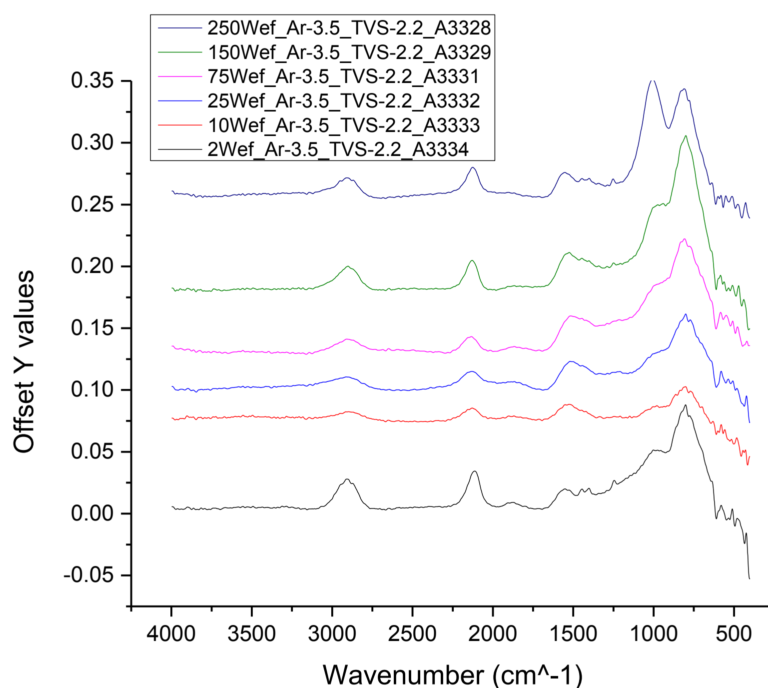

Fig. 74: Absorbance spectrum of films prepared from TVS and argon mixture with argon content 91,6 % at different effective power regimes

Spectrum of TVS film prepared by effective power 2W is different from the other spectra in the series, but it is very similar to the 2W spectra of TVS_6.0_Ar_3.0 series, just with little bit slighter intensities of vinyl vibrations. Rest of spectrums shares the same trend of increasing $=\mathrm{CH}\left(\sim 1003\,\mathrm{cm}^{-1}\right)$ wagging, respectively $Si-O-C$ bond with effective power. Deviation of 25W spectra from other spectra should be affected by its different thickness.

5.3.2.6 Comparison of 2W spectra by the argon content

The influence of gas added to the reactive mix is showed at example of 2W samples obtained from TVS_only, TVS_2.2_Ar_3.5, TVS_6.0_Ar_3.0, TVS_13.7_Ar_2.0 series at figure Fig. 75.

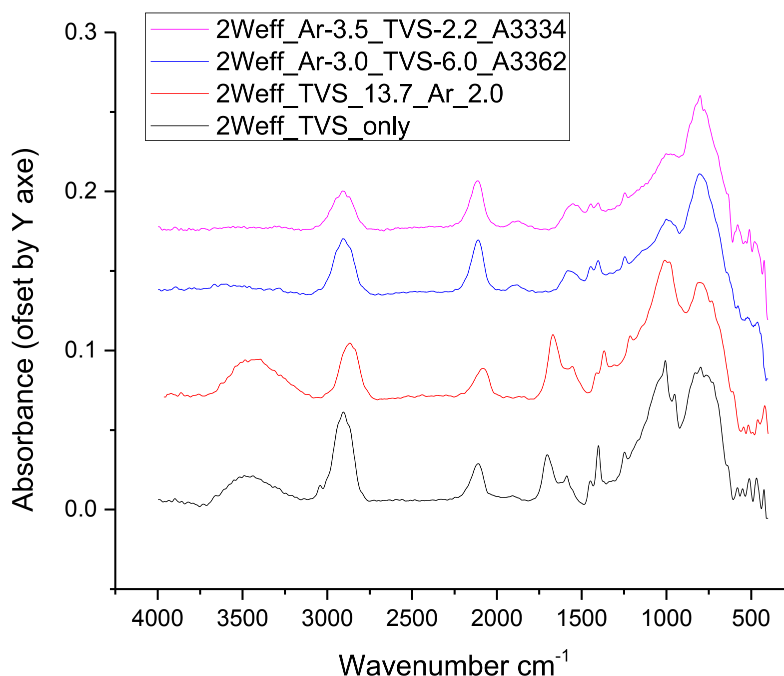

Fig. 75: Absorbance spectra of films prepared from TVS to argon mixtures and 2W of effective power

At the figure Fig. 65 the spectra are showing that the vinyl group bands intensities are decreasing with increasing content of argon in the mix. Also is remarkable that the series with higher content of argon should be more crosslinked, because they are not so oxygen degraded as the series of TVS_only or TVS_13.7_Ar_2.0, which is observable as significant band of $-\mathrm{OH}$ vibration in range $3600-3200\,\mathrm{cm}^{-1}$ and absence of carbonyl group vibration on $1705\,\mathrm{cm}^{-1}$. Significant difference is also in case of $=\mathrm{CH}\left(\sim 1003\,\mathrm{cm}^{-1}\right)$ wagging, respectively $\mathrm{Si}-\mathrm{O}-\mathrm{C}$ bond, which is significantly in-

tensified for TVS_only or TVS_13.7_Ar_2.0, which is in good agreement with the intensities of vinyl groups.

5.3.2.7 Comparison of 75W spectra by the argon content

Comparison of medium power processed spectra is represented by following figure Fig. 76.

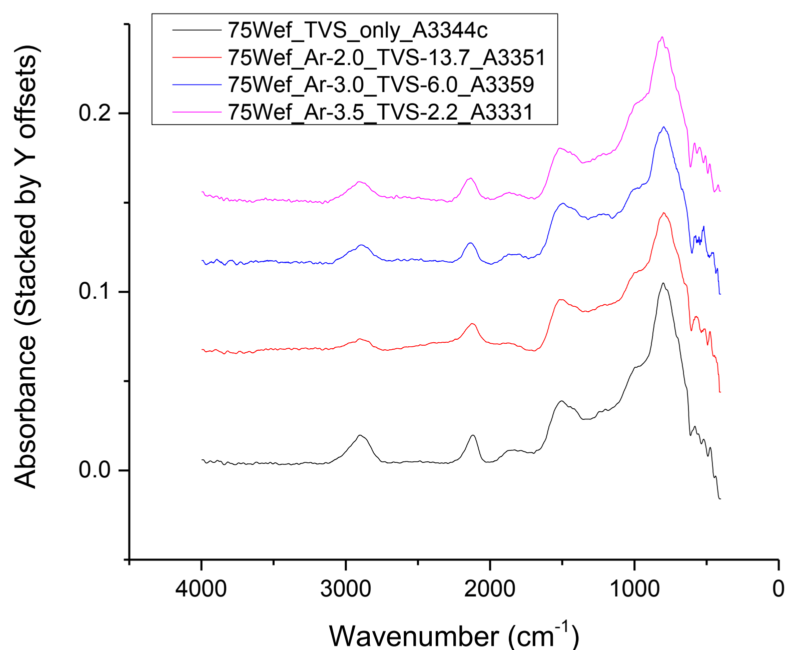

Fig. 76: Absorbance spectra of films prepared from TVS to argon mixtures and 75W of effective power

From spectra on figure Fig. 66 results, that the type of bonds and its intensities is not so depending on argon added to mixture for effective powers higher than 25W and minimal to the 150W. Spectra showed in Fig. 76 are almost similar, without significant bond character change or content. Insignificant differences especially in wavenumbers $3100-2750\ cm^{-1}$ contributing with vibrations of $-CH_2, -CH_3$ is mainly caused by not absolutely same thickness of measurement.

This assumption may be supported by spectra obtained by 150W effective powers showed at Fig. 77, because the spectra are almost the same for all argon gas to TVS monomer mixing ratios. Potential insignificant deviation should be produced by not quite the same thickness.

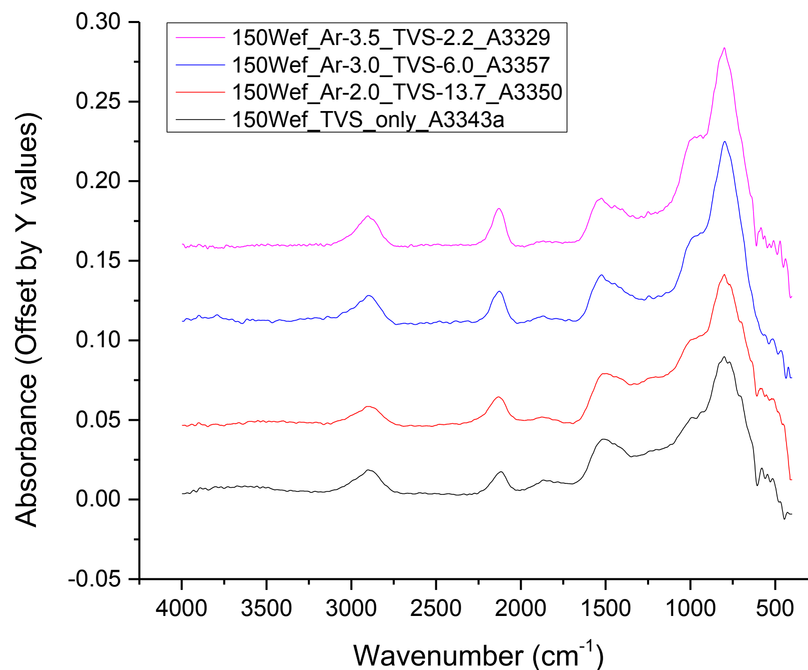

Fig. 77: Absorbance spectra of films prepared from TVS to argon mixtures and 150W of effective power

From spectra at Fig. 77 results that only minor or insignificant changes occurs with changing monomer TVS to argon ratio for 150W effective power series.

5.3.2.8 Spectra of TVS_6.0_O2_3.0 (78.5 % of oxygen gas in mixture)

Spectra of TVS_6.0_O2_3.0 series was obtained just after deposition process ends, using real transmission module in measurement range $400-4000\,cm^{-1}$ and resolution $2\,cm^{-1}$. Spectra were baselined and by offset normalized. To obtain higher signal to noise ratio data was mathematically processed (FFT filter, floating slope filter and floating mean filter).

Spectra of TVS_6.0_O2_3.0 series prepared in different effective power regimes are represented by following figure Fig. 78.

At figure Fig. 78 are spectra showing that the oxygen contained bonds bands are significantly increased intensity than in series without oxygen. The $-OH$ vibration in range $3600-3200\,cm^{-1}$ and is most intensive for low effective powers $2-10W$. With increasing power the $-OH$ vibrations intensities are decreasing. Also near $1705\,cm^{-1}$ $>C=O$ bond is decreasing intensity with increasing power. Trend of decreasing intensities with increasing effective power used for samples preparation acts also in the case of alkanes bonds $(-CH_2, -CH_3)$ at $3000-2750\,cm^{-1}$ and with the $Si-H$ vibration at $2110-2115\,cm^{-1}$, which will induce assumption that with increasing power is decreasing presence of hydrogen and increased existence of double bonds, or other bond va-

lences of carbon atoms. This should be corrected by further investigation using high-resolution XPS or other methods with are more sensitive to valences. Not so intensive, but remarkable is presence of CO_2 valence vibration at $2330\ cm^{-1}$, which can be produced by encapsulated CO_2 molecules.

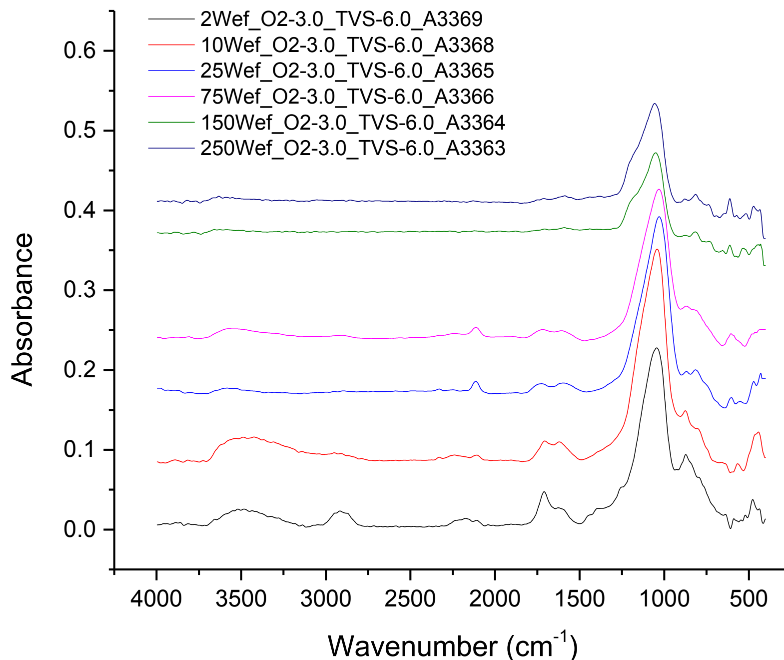

Fig. 78: Absorbance spectra of films prepared from TVS to oxygen mixture with oxygen content 78.5% and ranges of effective power

5.3.2.9 Spectra of TVS_2.2_O2_3.5 (91.6 % of oxygen gas in mixture)

Spectra of TVS_6.0_O2_3.0 series was obtained just after deposition process ends, using real transmission module in measurement range $400-4000\ cm^{-1}$ and resolution $2\ cm^{-1}$. Spectra were baselined and by offset normalized. To obtain higher signal to noise ratio data was mathematically processed (FFT filter, floating slope filter and floating mean filter).

Spectra of TVS_6.0_O2_3.0 series prepared in different effective power regimes are represented by following figure Fig. 79.

Spectra showed at figure Fig. 79 are with exclusion of 2W series almost similar. Spectra prepared by effective powers larger than 2W are so similar to the SiO2 spectra, than the NIST database spectrum of SiO_2 [115] attached is almost indistinguishable from the samples only with small but difference on vibration at $2330\ cm^{-1}$. This vibration is with high probability appropriate CO_2 valence vibration. The atmosphere CO_2

contamination is almost excreted by measurement in vacuum. This evolve assumption, that the CO_2 should be in the film encapsulated and film should be porous.

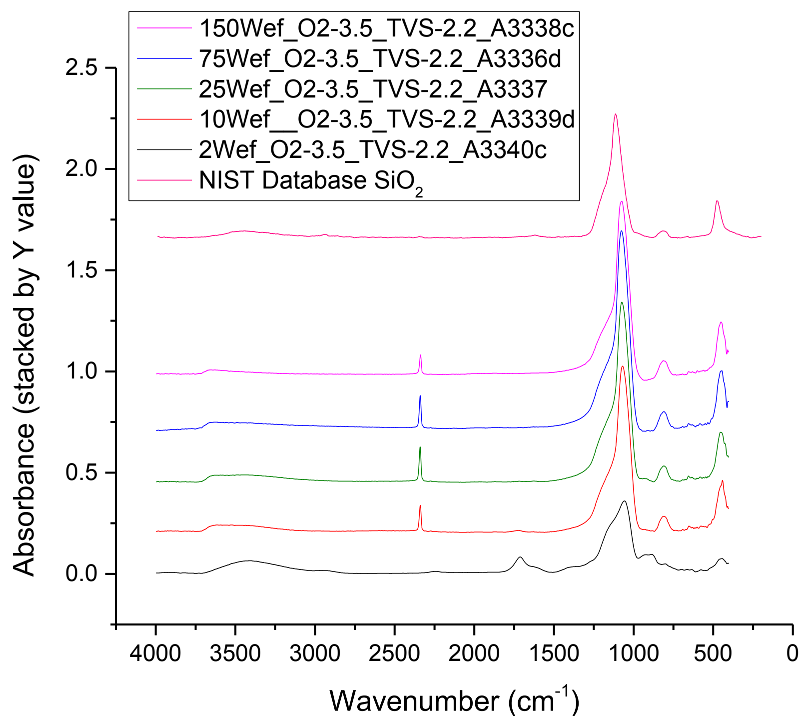

Fig. 79: Absorbance spectra of films prepared from TVS to oxygen mixture with oxygen content 91.6% and range of effective power 2-150W. In graph is at first position attached also graph

5.3.3 Elemental surface composition (XPS)

Elemental surface composition was given for sample series TVS_only, TVS_2.2_Ar_3.5 and TVS_2.2_O2_3.5 by X-ray photoelectron spectroscopy (XPS). From obtained data the graphs of Carbon, Oxygen and Silicon content on effective power dependence were constructed.

At figure Fig. 80 the elemental composition of samples in TVS_only and TVS_2.2_Ar_3.5 is shown.

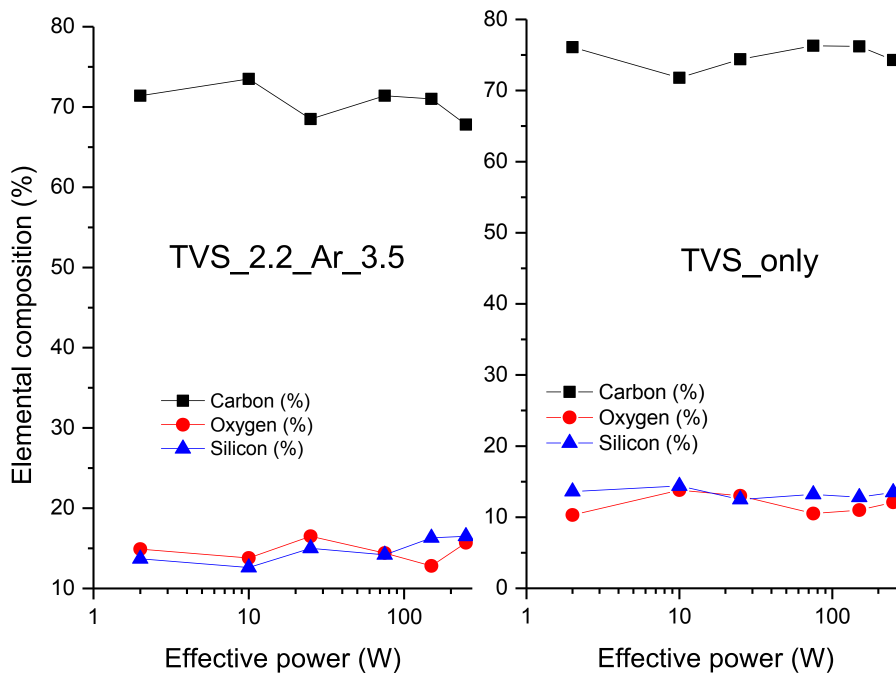

Fig. 80: Elemental chemical composition of samples prepared from TVS only and prepared from mixture of 91,6% of Argon to TVS mixture dependence on effective power.

From the graph at figure Fig. 80 is evident that the elemental composition of samples in their series is almost constant to the effective power. Also is evident then only slightly lower content of carbon and slightly higher content of oxygen and silicon have TVS_2.2_Ar_3.5 series with compare it to the TVS_only values.

At following figure Fig. 81 is shown data obtained from measurement of surface composition of samples from TVS_2.2_O2_3.5 series. From the graph is evident trend of decreasing carbon content with increasing effective power up to 25W. With the trend of decreasing carbon content goes hand in hand trend of increasing oxygen and silicon content. Higher slope of increase content has oxygen, which is also more contained in films prepared with effective powers over 25W. When power exceeds 25W of effective power, the elemental surface composition stayed almost constant up to the 250W of effective power.

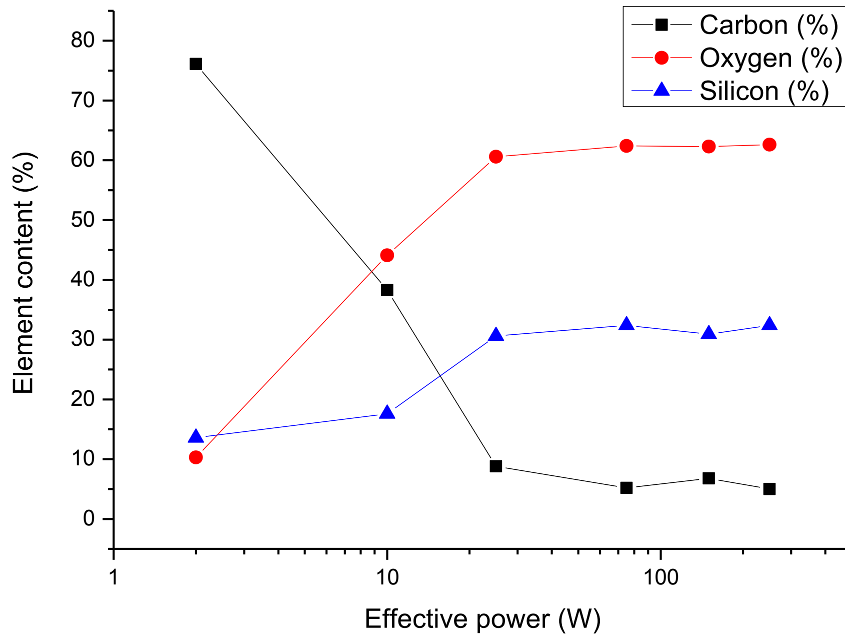

Fig. 81: Elemental chemical composition of TVS_2.2_O2_3.5 series samples

5.3.4 Mechanical properties (Nanoindentation)

Nanoindentation test on samples was made by method of cyclic nanoindentation. Resulted data was averaged and average data were used for construction of following graphs of mechanical properties (Young's modulus and Hardness) dependence on effective power.

5.3.4.1 TVS_only series mechanical properties

Prepared TVS_only thin films were measured by nanoindentation test with slight time delay from preparation to measurement applied to decrease influence of non-relaxed deformations in film, which would distort measurement. Mechanical properties of TVS_only series films are represented by figure Fig. 82 bellow this paragraph.

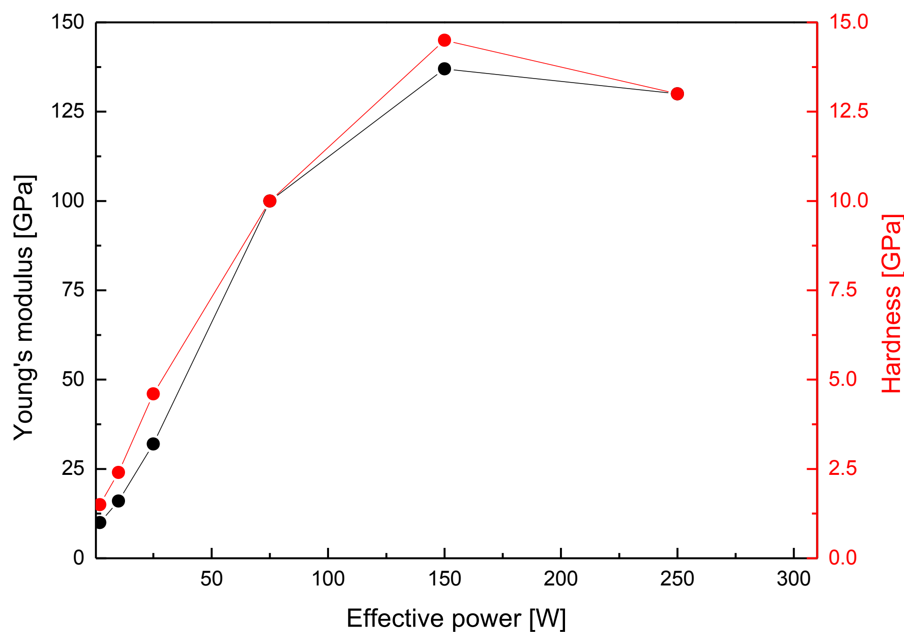

Fig. 82: Resultant graph containing Young's modulus of elasticity and Hardness for prepared samples from TVS_only series as the material property to production used Effective power dependence.

Hardness and Young's modulus of elasticity is on graph at figure Fig. 82 up to 150W almost linearly increasing with increasing effective power. Maximum hardness and Young's modulus was obtained for 150W with values of hardness $H = 14,5\ \text{GPa}$ and Young's modulus $E = 137\ \text{GPa}$, which is values at the bottom border of properties of DLC materials [91] , [116]. Than effective power exceeds 150W decrease of mechanical properties occurs.

5.3.4.2 TVS_2.2_Ar_3.5 series mechanical properties (91.6% of argon content)

Prepared TVS_2.2_Ar_3.5 thin films were measured by nanoindentation test with slight time delay from preparation to measurement applied to decrease influence of non-relaxed deformations in film, which would distort measurement. To avoid the distortion of measurement by degradation of sample cyclic nanoindentation were used and data was obtained from depth profile.

Mechanical properties of TVS_2.2_Ar_3.5 series films are represented by following figure Fig. 83.

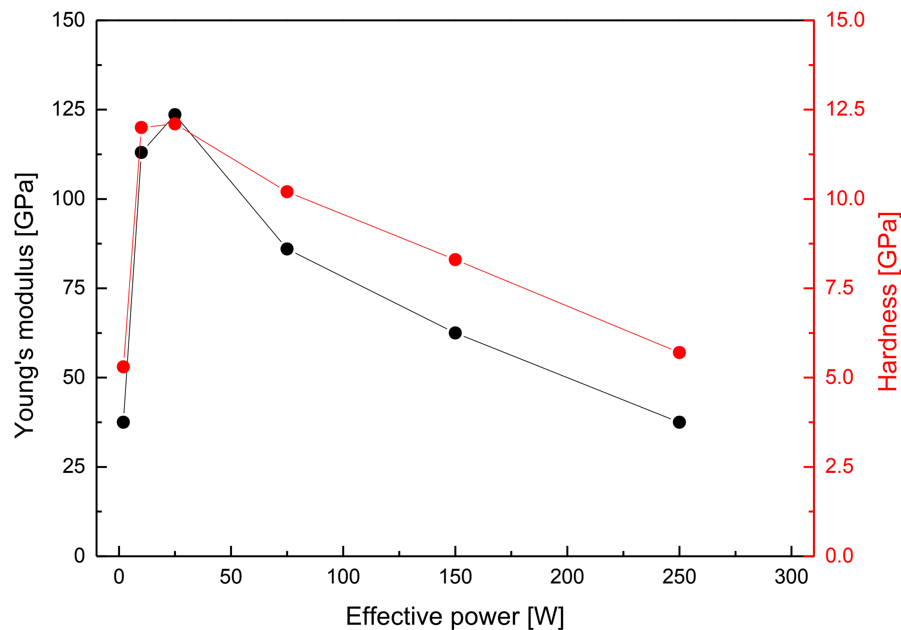

Fig. 83: Resultant graph containing Young's modulus of elasticity and Hardness for prepared samples from TVS_2.2_Ar_3.5 series as the material property to production used Effective power dependence.

After the really significant rise of mechanical properties from 2W sample (worst values) to maximum values obtained by 10W and 25W series graduated decreasing of material properties occurs. Obtained maximal mechanical properties are from 25W sample and they are lower but close to the values obtained from the TVS only series. Interesting is fact that the maximum values obtained in case of TVS_only series with effective power about 125W may be obtained by TVS_2.2_Ar_3.5 series with 25W only.

5.3.4.3 TVS_2.2_O2_3.5 series mechanical properties (91.6% of oxygen content)

Prepared TVS_2.2_O2_3.5 thin films were measured by nanoindentation test with slight time delay from preparation to measurement applied to decrease influence of non-relaxed deformations in film, which would distort measurement. To avoid the distortion of measurement by degradation of sample cyclic nanoindentation were used and data was obtained from depth profile.

Mechanical properties of TVS_2.2_O2_3.5 series films are represented by following figure Fig. 84.

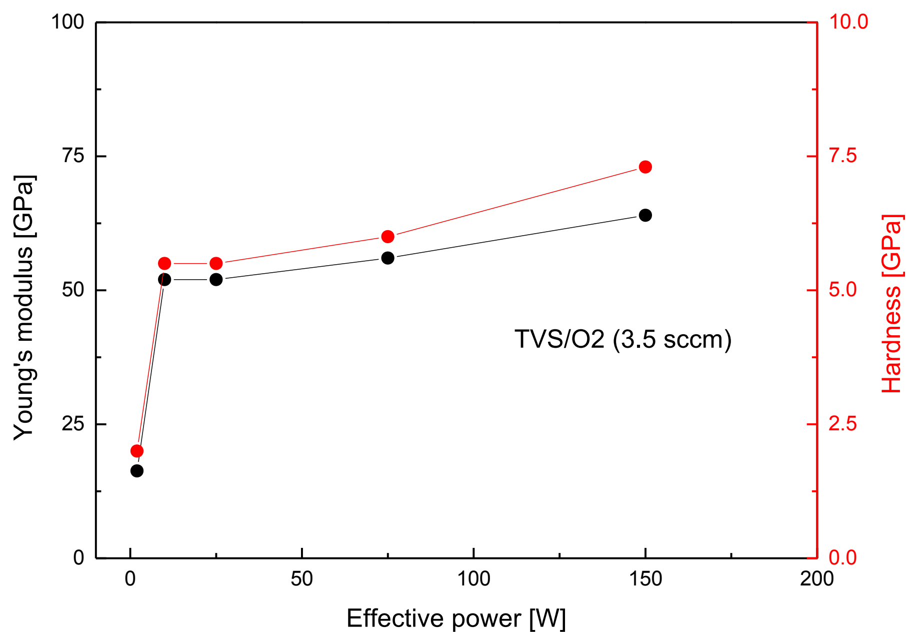

Fig. 84: Resultant graph containing Young's modulus of elasticity and Hardness for prepared samples from TVS_2.2_O2_3.5 series as the material property to production used Effective power dependence.

From the graph at figure Fig. 84 is apparently that after strong increase of both studied mechanical properties between $2-10\,\mathrm{W}$, slight increase of mechanical properties occurs. Maximal properties are given by sample prepared by 150W of effective power. This sample hardness $H = 7{,}3\,\mathrm{GPa}$ and Young's modulus $E = 64\,\mathrm{GPa}$ are almost the same to the calibration SiO_2 sample, which is in good agreement with the chemical composition earned by FTIR spectroscopy (chapture 6.3.2.9)

6 CONCLUSION

This diploma thesis was focused to preparation (deposition) of plasma polymer thin film samples from tetravinylsilane monomer and its mixtures with argon and oxygen gas. The influence of deposition conditions (effective power, pressure, self-bias, gas to tvs ratios etc.) on physical and chemical properties of deposited material was investigated. Structure and chemical properties of plasma polymer films were investigated by infrared spectroscopy and X-ray photoelectron spectroscopy Mechanical properties were evaluated by nanoindentation measurements. Optical properties and film thicknesses were measured by spectroscopic ellipsometry. Also mass spectroscopy was used for glow discharge characterization.

Stable deposition conditions for preparation of plasma polymer thin films from TVS and its mixtures with argon and oxygen gas were successfully determined by plasma optical stability measurement. For the sample preparation set of diferent gas mixtures containing 52 %, 78,5 % and 91,7 % of argon or oxygen gas were used. As the reference also samples prepared from tetravinylsilane monomer were prepared.

To obtain information about processes, which occurs in plasma discharge of tetravinylsilane monomer and its mixtures with different effective RF power was used mass spectroscopy of process gas during deposition. The influence of effective RF power to fragmentation of all gas mix series was obtained. In case of oxygen to tetravinylsilane mixes the chemical reaction occurring directly in plasma discharge was investigated (mainly water and carbon dioxide formation).

The dispersion curves of plasma polymers were investigated for tetravinylsilane series, all series of argon mixtures and for 52 % and 91,6 % mixtures of oxygen gas. From the obtained data results very different oxygen and argon to tetravinylsilane mixture ratio to optical properties influence. The samples deposited from TVS only dispersion curves dependence for the refractive index moved to higher values with enhanced power same as in previous works realized to this theme [107] [109] [111]. Same trend was obtained for extinction coefficient, where with increasing power the extinction coefficient minima were shifted to nearer to IR region. Trend of influence of Ar gas contain in mixture to the optical properties was obtained. With increasing argon content the trend of increasing optical parameters was investigated. Samples prepared from Ar gas series with lower powers has optical parameters very same to the optical parameters of higher powers prepared samples from TVS mixtures only.

The infrared spectra of deposited samples were compared and discussed depending on the used RF power for tetravinylsilane series, all series of argon mixtures and for 52% and 91,6% mixtures of oxygen gas. Absorption bands connected with vinyl groups decreased with increasing effective power in all series. In tetravinylsilane series was assumed that the higher power series prepared with higher values of self-bias voltage may be more cross-linked, than the series prepared at lower effective power, especially because their higher oxygen degradation resistance. It was not confirmed significant influence of argon gas to chemical properties given by FTIR analysis. In oxygen series the very significant influence of oxygen content to chemical composition of deposited thin films were obtained. With increasing oxygen concentration, increases bands with contribution with oxygen such as carbonyl group, Si-O-Si or Si-O-C. In case of 91,6% oxygen series the result material is almost same to the silicon oxide.

Elemental composition of surface of TVS series, 91,6% oxygen series, 91,6% argon series deposited thin films was studied by x-ray photoelectron spectroscopy. In case of Argon series in contribution TVS series no significant change of surface elemental composition was obtained. In case of oxygen series the surface of material was very different to the previous one and for powers higher than 10W also the idea of the silicon oxide similarity of samples was confirmed.

Nanoindentation was used for obtain Young's modus and Hardness of samples from the of TVS series, 91,6% oxygen series, 91,6% argon series deposited on silicon wafer substrates. From the measurement of TVS series the interesting mechanical properties of thin films prepared with effective power 150W was obtained, because they are near to properties of DLC. Measurement of argon series shows that the mechanical properties of deposited films are decreasing with increasing power, but the highest value of mechanical properties was obtained from sample prepared by 25W of effective power, with is near to the 150W sample from TVS series mechanical properties. In oxygen series the trend of increasing mechanical properties to the increasing effective power was obtained. In case of 250W sample from this series the mechanical properties are almost the same to the calibration sample of silicon oxide, which would confirm previously mentioned silicon oxide similarity of samples from this series.

Conclusions of this thesis would be used for further investigation and for real application in many kinds of industries.

REFERENCES

[1]. **Biederman, Hynek.** *Plasma Polymer Films.* Singapore : World Scientific, 2004. ISBN 978-186-0945-380.

[2]. *Corrosion protection by PECVD-SiOx as a top coating on TiN-coated steel.* **He, J.L., et al., et al.** 1-2, Surface and Coatings Technology, Vol. 63, pp. 15-23. DOI 10.1016/S0257-8972(05)80003-9.

[3]. *Fatigue resistance of PECVD coated steel alloy.* **BARAGETTI, S and TORDINI, F.** 9-11, International Journal of Fatigue, Vol. 29, pp. 1832-1838. DOI 10.1016/j.ijfatigue.2007.02.008.

[4]. *Influence of film structure and composition on diffusion barrier performance of SiOx thin films deposited by PECVD.* **Gruniger, A., et al., et al.** 14-15, 2006, Surface and Coatings Technology, Vol. 200, pp. 4564-4571. DOI 10.1016/j.surfcoat.2005.03.044.

[5]. *Barrier coating for polymer light-emitting diodes using carbon nitride thin films deposited at low temperature by PECVD technique.* **Nardes, A.M., et al., et al.** 5, Materials Science and Engineering: C, Vol. 24, pp. 607-610. DOI 10.1016/j.msec.2004.08.043.

[6]. *Hard and relaxed a-SiNxHy films prepared by PECVD: Structure analysis and formation mechanism.* **Xu, Xiangdong, et al., et al.** Applied Surface Science, Vol. 264, pp. 823-831. DOI 10.1016/j.apsusc.2012.10.149.

[7]. *Mechanical and optical properties of hard SiCN coatings prepared by PECVD.* **Jedrzejowski, P., et al., et al.** Thin Solid Films, Vols. 447-448, pp. 201-207. DOI 10.1016/S0040-6090(03)01057-5.

[8]. *Preparation and tribological characterization of amorphous carbon nitride coatings in a RF PECVDâ€“DC PVD hybrid coating process.* **Wang, Pengfei, et al., et al.** 17, Applied Surface Science, Vol. 258, pp. 6576-6582. DOI 10.1016/j.apsusc.2012.03.082.

[9]. *Investigation of deposition temperature effect on properties of PECVD SiOCH low-k films.* **Wong, T.K.S., et al., et al.** Thin Solid Films, Vols. 462-463, pp. 156-160. DOI 10.1016/j.tsf.2004.05.048.

[10]. **Wasa, Kiyotaka, Adachi, Hideaki and Kitabatake, Makoto.** *Thin film materials technology: sputtering of compound materials.* Norwich : William Andrew Publishing, c2004. p. 518 s. ISBN 08-155-1483-2.

[11]. **Ohring, Milton.** *Materials Science of Thin Films.* 2nd ed. Burlington : Elsevier, 2001. ISBN 978-008-0491-783.

[12]. **Seshan, Krishna.** *Handbook of thin film deposition: techniques, processes, and technologies.* 3rd ed. Waltham : William Andrew, 2012. pp. xviii, 392 p. ISBN 14-377-7873-9.

[13]. **Guo, Zhen and Tan, Li.** *Fundamentals and applications of nanomaterials.* Boston : Artech House, c2009. pp. xvii, 249 p. ISBN 15-969-3262-7.

[14]. **Wolf, CRC. Ed. by Bernhard.** *Handbook of ion sources.* Boca Raton [u.a.] : CRC Press, 1995. ISBN 978-084-9325-021.

[15]. **Brown, edited by Ian G.** *The physics and technology of ion sources.* 2nd rev. and extended ed. Weinheim : Wiley-VCH, 2004. ISBN 978-352-7604-548.

[16]. **Eason, edited by Robert.** *Pulsed Laser Deposition of Thin Films Applications-Led Growth of Functional Materials.* [Onlline-Ausg.]. Hoboken : John Wiley, 2006. ISBN 978-047-0052-112.

[17]. **Jong-Hee Park, T.** *Chemical vapor deposition.* Materials Park, Ohio : ASM International, 2001. ISBN 978-161-5032-242.

[18]. **Jones, Anthony C. and Hitchman, Michael L.** *Chemical vapour deposition: precursors, processes and applications.* Cambridge, UK : Royal Society of Chemistry, 2009. pp. xv, 582 p. ISBN 08-540-4465-5.

[19]. **Fridman, Alexander.** *Plasma chemistry.* 1st ed. New York : Cambridge University Press, 2008. pp. xlii, 978 s. ISBN 978-0-521-84735-3.

[20]. **Bittencourt, J.** *Fundamentals of plasma physics.* 3rd ed. New York : Springer, 2004. pp. xxiii, 678 p. ISBN 03-872-0975-1.

[21]. **Michael A. Lieberman, Michael A.Allan J.** *Principles of Plasma Discharges and Materials Processing.* 2. Hoboken : John Wiley, 2005. ISBN 978-047-1724-247.

[22]. **Krebs, Frederik C.** *Stability and Degradation of Organic and Polymer Solar Cells.* Hoboken, United States : Wiley, 2012. ISBN 1118312236.

[23]. **Bowick, Christopher and Ajluni, with John Blyler and Cheryl.** *RF circuit design.* 2nd ed. Amsterdam : Newnes/Elsevier, 2008. ISBN 978-008-0553-429.

[24]. **Franssila, Sami.** *Introduction to microfabrication.* 2nd ed. Chichester, West Sussex [England] : John Wiley, 2010. pp. xiv, 518 s. ISBN 978-0-470-749-83-8.

[25]. **Dobkin, Daniel Mark and Zuraw, Michael K.** *Principles of chemical vapor deposition.* Dordrecht ; Boston : Kluwer Academic Publishers, 2003. pp. xi, 273 p. ISBN 14-020-1248-9.

[26]. **Inagaki, N.** *Plasma surface modification and plasma polymerization.* Lancaster : Technomic Publishing Company, 1996. p. 265 s. ISBN 15-667-6337-1.

[27]. *Synthesis of transparent and hard SiOC(â˘'H) thin films on polycarbonate substrates by PECVD method.* **Noborisaka, Mayui, et al., et al.** 8-9, 2012, Surface and Coatings Technology, Vol. 206, pp. 2581-2584. DOI /10.1016/j.surfcoat.2011.11.017.

[28]. *Mid-frequency PECVD of a-SiCN: H films and their structural, mechanical and electrical properties.* **Peter, S., et al., et al.** 1, 2013, Vacuum, Vol. 90, pp. 155-159. DOI 10.1016/j.vacuum.2012.04.001.

[29]. *Trimethylsilane-based pretreatments in a Mg-rich primer corrosion prevention system.* **Schulz, Douglas L., et al., et al.** 2, 2008, Progress in Organic Coatings, Vol. 63, pp. 149-154. DOI 10.1016/j.porgcoat.2008.04.017.

[30]. *Organosilicon/silicon oxide gas barrier structure encapsulated flexible plastic substrate by using plasma-enhanced chemical vapor deposition.* **Wu, Cheng-Yang, et**

al., et al. 22, 2012, Surface and Coatings Technology, Vol. 206, pp. 4685-4691. DOI 10.1016/j.surfcoat.2012.05.080.

[31]. *Deposition of tetramethylsilane on the glass by plasma-enhanced chemical vapor deposition and atmospheric pressure plasma treatment.* **Chen, Ko-Shao, et al., et al.** -, 2012, Surface and Coatings Technology, pp. -. DOI 10.1016/j.surfcoat.2012.09.032.

[32]. *Mechanical properties of a-C/ Si-containing a-C:H multilayered coatings grown by LF-PECVD.* **Chouquet, C., et al., et al.** 5-7, 2008, Surface and Coatings Technology, Vol. 203, pp. 745-749. DOI 10.1016/j.surfcoat.2008.08.008.

[33]. *Growth mechanisms of SiO2 thin films prepared by plasma enhanced chemical vapour deposition.* **Yanguas-Gil, A., et al., et al.** 1-4, 2005, Surface and Coatings Technology, Vol. 200, pp. 881-885. DOI 10.1016/j.surfcoat.2005.01.070.

[34]. *Use of a PECVDâ€"PVD process for the deposition of copper containing organosilicon thin films on steel.* **Daniel, A., et al., et al.** 3, 2009, Applied Surface Science, Vol. 256, pp. S82-S85. DOI 10.1016/j.apsusc.2009.04.195.

[35]. *Effects of surface treatments using PECVD-grown hexamethyldisiloxane on the performance of organic thin-film transistor.* **Moon, Mi Ran, et al., et al.** 14, 2009, Thin Solid Films, Vol. 517, pp. 4161-4164. DOI 10.1016/j.tsf.2009.02.048.

[36]. *Measurement of CH4-concentration in HMDSO-containing process plasmas by quantum cascade laser absorption spectroscopy.* **Wolter, Matthias, Hundt, Morten and Kersten, Holger.** 4, 2010, Vacuum, Vol. 85, pp. 482-485. DOI 10.1016/j.vacuum.2010.01.016.

[37]. *Deposition of silicon oxide films by non-equilibrium, atmospheric-pressure plasma jet.* **Zeng, Jie-liang, Lin, Jiang and Zhang, Xi-wen.** -, 2012, Surface and Coatings Technology, pp. -. DOI 10.1016/j.surfcoat.2012.05.055.

[38]. *Deposition of thin-films on EPDM substrate with a plasma-polymerized coating.* **Alba-Elías, Fernando, Ordieres-Meré, JoaquÃn and Gonzalez-Marcos, Ana.** 2-3, 2011, Surface and Coatings Technology, Vol. 206, pp. 234-242. DOI 10.1016/j.surfcoat.2011.06.054.

[39]. *Characteristics of multilayered plasma-polymer thin films using toluene and TEOS by PECVD.* **Cho, Sang-Jin and Boo, Jin-Hyo.** -, 2012, Microelectronic Engineering, Vol. 89, pp. 19-22. DOI 10.1016/j.mee.2011.04.004.

[40]. *Adhesion study of tetra methyl cyclo tetra siloxanes (TMCTS) and tri methyl silane (3MS)-based low-k films.* **Widodo, J., et al., et al.** 1, 2005, Microelectronic Engineering, Vol. 81, pp. 35-43. DOI 10.1016/j.mee.2004.11.017.

[41]. *Thickness dependent glass transition temperature of PECVD low-k dielectric thin films: effect of deposition methods.* **Zhou, H., et al., et al.** 3, 2002, Microelectronics Journal, Vol. 33, pp. 221-227. ISSN 00262692.

[42]. *Amorphous silicon solar cells deposited with non-constant silane concentration.* **Muthmann, S. and Gordijn, A.** 2, 2011, Solar Energy Materials and Solar Cells, Vol. 95, pp. 573-578. DOI 10.1016/j.solmat.2010.09.019.

[43]. *Thin crystalline silicon solar cells based on epitaxial films grown at 165Â°C by RF-PECVD.* **Cariou, Romain, Labrune, Martin and Roca i Cabarrocas, Pere.** 8, 2011, Solar Energy Materials and Solar Cells, Vol. 95, pp. 2260-2263. DOI 10.1016/j.solmat.2011.03.038.

[44]. *Optical and structural proprieties of nc-Si: H prepared by argon diluted silane PECVD.* **Amrani, Rachid, et al., et al.** 17, 2012, Journal of Non-Crystalline Solids, Vol. 358, pp. 1978-1982. DOI 10.1016/j.jnoncrysol.2012.01.022.

[45]. *Temperature dependence of mechanical properties of DLC/Si protective coatings prepared by PECVD.* **Bursikova, V., et al., et al.** 1-2, 2002, Materials Science and Engineering: A, Vol. 324, pp. 251-254. DOI 10.1016/S0921-5093(01)01320-X.

[46]. *Dual FCVA/€"PECVD deposition for DLC films.* **Meunier, C., et al., et al.** 1-2, 2005, Thin Solid Films, Vol. 482, pp. 197-200. DOI 10.1016/j.tsf.2004.11.173.

[47]. *A comparative analysis of a-C: H films deposited from five hydrocarbons by thermal desorption spectroscopy.* **Peter, S., Gunther, M. and Richter, F.** 6, 2012, Vacuum, Vol. 86, pp. 667-671. DOI 10.1016/j.vacuum.2011.07.037.

[48]. *Influence of hydrogen on the mechanical properties and microstructure of DLC films synthesized by r.f.-PECVD.* **Hsu, Jiong-Shiun, Tzeng, Shinn-Shyong and Wu, Ying-Jie.** 3, 2008, Vacuum, Vol. 83, pp. 622-624. DOI 10.1016/j.vacuum.2008.04.070.

[49]. *Correlation between SiOx content and properties of DLC: SiOx films prepared by PECVD.* **ZAJIKOVA, L.** -, 2003, Surface and Coatings Technology, Vols. 174-175, pp. 281-285. DOI 10.1016/S0257-8972(03)00681-9.

[50]. **Yoo, Chue San.** *Semiconductor manufacturing technology.* London : World Scientific, c2008. pp. xii, 470 p. ISBN 98-125-6823-9.

[51]. **Valeri P. Tolstoy, Valeri P.Irina V.** *Handbook of Infrared Spectroscopy of Ultrathin Films.* New Jersey : John Wiley, 2003. ISBN 978-047-1461-838.

[52]. **Drake, Gordon W.** *Springer handbook of atomic, molecular, and optical physics.* New York : Springer, 2006. pp. lviii, 1504 p. ISBN 03-872-6308-X.

[53]. *Behaviour of amorphous silicon carbide in Au/a-SiC/Si heterostructures prepared by PECVD technology using two different RF modes.* **Perny, Milan, et al., et al.** -, 2013, Applied Surface Science, Vol. 269, pp. 143-147. DOI 10.1016/j.apsusc.2012.09.086.

[54]. *Investigation of nanocrystallization of a-Si1âˆ'xGex: H thin films diluted with argon in the PECVD system.* **Xu, Rui, et al., et al.** -, 2013, Journal of Non-Crystalline Solids, Vol. 365, pp. 37-41. DOI 10.1016/j.jnoncrysol.2013.01.026.

[55]. *A study on structural and electrical properties of low dielectric constant SiOC(â€"H) thin films deposited via PECVD.* **Navamathavan, R., et al., et al.** 5, 2012, Journal of Physics and Chemistry of Solids, Vol. 73, pp. 641-645. DOI 10.1016/j.jpcs.2012.01.002.

[56]. *Influence of deposition pressure on p-type a-Si: H window layer doped by trimethylboron for a-Si.* **Zhao, Lei, et al., et al.** -, 2012, Materials Science in Semiconductor Processing, pp. -. DOI 10.1016/j.mssp.2012.08.013.

[57]. *Mass and bond density measurements for PECVD a-SiCx: H thin films using Fourier transform-infrared spectroscopy.* **King, S.W., et al., et al.** 21, 2011, Journal of Non-Crystalline Solids, Vol. 357, pp. 3602-3615. DOI 10.1016/j.jnoncrysol.2011.07.004.

[58]. **Fujiwara, Hiroyuki.** *Spectroscopic ellipsometry principles and applications.* Chichester, England : John Wiley, 2007. ISBN 978-047-0060-186.

[59]. **Tompkins, Harland G and Irene, Eugene A.** *Handbook of ellipsometry.* Heidelberg, Germany : Springer, c2005. pp. xvi, 870 p. ISBN 35-402-2293-6.

[60]. *A comparison of structures and properties of SiNx and SiOx films prepared by PECVD.* **Xu, Xiangdong, et al., et al.** 1, 2012, Journal of Non-Crystalline Solids, Vol. 358, pp. 99-106. DOI 10.1016/j.jnoncrysol.2011.08.029.

[61]. *Optical characterisation of SiOxCyHz thin films non-uniform in thickness using spectroscopic ellipsometry, spectroscopic reflectometry and spectroscopic imaging reflectometry.* **Ohlidal, Ivan, et al., et al.** 9, 2011, Thin Solid Films, Vol. 519, pp. 2874-2876. DOI 10.1016/j.tsf.2010.12.069.

[62]. *Nanostructuring Siâ€"C alloys by plasma enhanced chemical vapor deposition: An ellipsometry and Raman spectroscopy investigation.* **Giangregorio, M.M., et al., et al.** 9, 2011, Thin Solid Films, Vol. 519, pp. 2787-2790. DOI 10.1016/j.tsf.2010.11.074.

[63]. *Microstructure characterization of microcrystalline silicon thin films deposited by very high frequency plasma-enhanced chemical vapor deposition by spectroscopic ellipsometry.* **Zhang, He, et al., et al.** 2, 2011, Thin Solid Films, Vol. 520, pp. 861-865. DOI 10.1016/j.tsf.2011.04.166.

[64]. *Optical characterizations of complete TFTâ€"LCD display devices by phase modulated spectroscopic ellipsometry.* **Gaillet, MÃ©lanie, Yan, Li and Teboul, Eric.** 2-4, 2007, Thin Solid Films, Vol. 516, pp. 170-174. DOI 10.1016/j.tsf.2007.05.053.

[65]. *Influence of PECVD parameters on the properties of diamond-like carbon films.* **Caschera, D., et al., et al.** 12, 2011, Thin Solid Films, Vol. 519, pp. 4087-4091. DOI 10.1016/j.tsf.2011.01.197.

[66]. *Influence of film structure and composition on diffusion barrier performance of SiOx thin films deposited by PECVD.* **GrÃ¼niger, A., et al., et al.** 14-15, 2006, Surface and Coatings Technology, Vol. 200, pp. 4564-4571. DOI 10.1016/j.surfcoat.2005.03.044.

[67]. *Characteristics of low-k SiOC(â€"H) films deposited at various substrate temperature by PECVD using DMDMS/O2 precursor.* **Kim, Chang Young, et al., et al.** 2-4, 2007, Thin Solid Films, Vol. 516, pp. 340-344. DOI 10.1016/j.tsf.2007.06.097.

[68]. *Surface and thin film analysis: principles, instrumentation, applications.* Weinheim : Wiley-VCH, 2002. p. 336 s. ISBN 35-273-0458-4.

[69]. **Rau, U, Abou-Ras, Daniel and Kirchartz, Thomas.** *Advanced characterization techniques for thin film solar cells.* Weinheim, Germany : Wiley-VCH, c2011. pp. xxxvi, 547 p. ISBN 35-274-1003-1.

[70]. **Kolbesen, Bernd O.** *Analytical and diagnostic techniques for semiconductor materials, devices and processes: joint proceedings of the symposia on ALTECH 99, satellite symposium to ESSDERC 99, Leuven, Belgium [and] the Electrochemical Society Symposium on Diagnostic Techniques for Semiconductor Materials and Devices.* Pennington, N.J. : Electrochemical Society, c1999. pp. ix, 552 p. ISBN 08-194-3497-3.

[71]. **Verma, H.R.** *Atomic and nuclear analytical methods XRF, Mössbauer, XPS, NAA and ion-beam spectroscopic techniques.* Berlin : Springer, 2007. ISBN 978-354-0302-797.

[72]. *Structural and Physical Characteristics of PECVD Nanocrystalline Silicon Carbide Thin Films.* **Huran, J., et al., et al.** -, 2012, Physics Procedia, Vol. 32, pp. 303-307. DOI 10.1016/j.phpro.2012.03.560.

[73]. *Morphology, optical and electrical properties of Cuâ€"Ni nanoparticles in a-C: H prepared by co-deposition of RF-sputtering and RF-PECVD.* **Ghodselahi, T., et al., et al.** 2, 2011, Applied Surface Science, Vol. 258, pp. 727-731. DOI 10.1016/j.apsusc.2011.07.145.

[74]. *High rate deposition of hard a-C: H films using microwave excited plasma enhanced CVD.* **Gunther, M., et al., et al.** -, 2011, Surface and Coatings Technology, Vol. 205, pp. S94-S98. DOI 10.1016/j.surfcoat.2010.12.047.

[75]. *High rate deposition of amorphous hydrogenated carbon films by hollow cathode arc PECVD.* **Zimmermann, Burkhard, et al., et al.** -, 2012, Surface and Coatings Technology, Vol. 212, pp. 67-71. DOI 10.1016/j.surfcoat.2012.09.020.

[76]. *Influence of the source gas ratio on the hydrogen and deuterium content of a-C: H and a-C.* **Ozeki, K., et al., et al.** 2013, Applied Surface Science, Vol. 265, pp. 750-757. DOI 10.1016/j.apsusc.2012.11.100.

[77]. **Edmond de Hoffmann, Vincent Stroobant.** *Mass spectrometry principles and applications.* 3rd ed. Chichester, England : J. Wiley, 2007. ISBN 978-047-0512-135.

[78]. **Kraj, Agnieszka, Desiderio, Dominic M. and Nibbering, Nico M.** *Mass Spectrometry Instrumentation, Interpretation, and Applications.* Hoboken : John Wiley, 2008. ISBN 978-047-0395-806.

[79]. *Preparation of silica membranes inside macroporous alumina tubes by PECVD for hydrogen selectivity.* **Rouessac, V., Ferreira, P. and Durand, J.** 1-3, 2003, Separation and Purification Technology, Vol. 32, pp. 37-43. DOI 10.1016/S1383-5866(03)00039-X.

[80]. *Ion contributions to gasâ€"surface interactions in inductively-coupled fluorocarbon plasmas.* **Cuddy, Michael F., Blechle, Joshua M. and Fisher, Ellen R.** -, 2012, International Journal of Mass Spectrometry, Vols. 330-332, pp. 46-57. DOI 10.1016/j.ijms.2012.09.006.

[81]. *Plasma Composition by Mass Spectrometry in a Ar-SiH4-H2 LEPECVD Process During nc-Si Deposition.* **Moiseev, T., Chrastina, D. and Isella, G.** 1, 2011,

Plasma Chemistry and Plasma Processing, Vol. 31, pp. 157-174. DOI 10.1007/s11090-010-9277-9.

[82]. **Haugstad, Greg.** *Atomic force microscopy: understanding basic modes and advanced applications.* Hoboken, N.J. : John Wiley, c2012. pp. xxii, 464 p. ISBN 978-047-0638-828.

[83]. **Khursheed, Anjam.** *Scanning electron microscope optics and spectrometers.* Hackensack, N.J. : World Scientific Pub. Co., 2011. pp. xiii, 402 p. ISBN 9789812836670.

[84]. **Echlin, by Patrick.** *Handbook of sample preparation for scanning electron microscopy and x-ray microanalysis.* Online-Ausg. New York : Springer, 2009. ISBN 978-038-7857-312.

[85]. *Scanning microscopy for nanotechnology: techniques and applications.* New York : Springer, 2007. pp. xiv, 522 s. ISBN 03-873-3325-8.

[86]. *Investigation of RF power effect on the deposition and properties of PECVD TiSi2 thin film.* **Fouad, Osama A, Yamazato, Masaaki and Nagano, Masamitsu.** 1-4, 2002, Applied Surface Science, Vol. 195, pp. 130-136. DOI 10.1016/S0169-4332(02)00544-5.

[87]. *Characteristics of multilayered plasma-polymer thin films using toluene and TEOS by PECVD.* **Cho, Sang-Jin and Boo, Jin-Hyo.** -, 2012, Microelectronic Engineering, Vol. 94, pp. 19-22. DOI 10.1016/j.mee.2011.04.004.

[88]. *Amorphous silicon carbide thin films (a-SiC: H) deposited by plasma-enhanced chemical vapor deposition as protective coatings for harsh environment applications.* **Daves, W., et al., et al.** 18, 2011, Thin Solid Films, Vol. 519, pp. 5892-5898. DOI 10.1016/j.tsf.2011.02.089.

[89]. *Si-rich a-SiC: H thin films.* **Kunle, Matthias, et al., et al.** 1, 2010, Thin Solid Films, Vol. 519, pp. 151-157. DOI 10.1016/j.tsf.2010.07.085.

[90]. *Investigation of the mechanical properties of thin films by nanoindentation, considering the effects of thickness and different coatingâ€“substrate combinations.* **Chen, Shaohua, Liu, Lei and Wang, Tzuchiang.** 1, 2005, Surface and Coatings Technology, Vol. 191, pp. 25-32. DOI 10.1016/j.surfcoat.2004.03.037.

[91]. *Nanoindentation measurements on modified diamond-like carbon thin films.* **Dwivedi, Neeraj, Kumar, Sushil and Malik, Hitendra K.** 23, 2011, Applied Surface Science, Vol. 257, pp. 9953-9959. DOI 10.1016/j.apsusc.2011.06.114.

[92]. *Effect of deposition conditions on mechanical properties of low-temperature PECVD silicon nitride films.* **Huang, H., et al., et al.** -, 2006, Materials Science and Engineering: A, Vols. 435-436, pp. 453-459. DOI 10.1016/j.msea.2006.07.015.

[93]. *Nanoindentation creep of plasma-enhanced chemical vapor deposited silicon oxide thin films.* **Cao, Zhiqiang and Zhang, Xin.** 3, 2007, Scripta Materialia, Vol. 56, pp. 249-252. DOI 10.1016/j.scriptamat.2006.09.022.

[94]. *Depth profile of mechanical properties of plasma-polymerized tetravinylsilane films evaluated by cyclic nanoindentation.* **Trivedi, R., Hoferek, L. and Cech, V.** -,

2011, Surface and Coatings Technology, Vol. 205, pp. S470-S474. DOI 10.1016/j.surfcoat.2011.01.062.

[95]. **Butt, Hans-Jürgen, Graf, Kh and Kappl, Michael.** *Physics and chemistry of interfaces.* Weinheim : Wiley-VCH, 2003. pp. xii, 361 p. ISBN 35-274-0413-9.

[96]. *Wetting and superhydrophobic properties of PECVD grown hydrocarbon and fluorinated-hydrocarbon coatings.* **Sarkar, D.K., Farzaneh, M. and Paynter, R.W.** 11, 2010, Applied Surface Science, Vol. 256, pp. 3698-3701. DOI 10.1016/j.apsusc.2009.12.049.

[97]. *Hydrogen containing DLC coatings on UHMW-PE deposited by r.f.-PECVD.* **Reisel, Guido and Dorner-Reisel, Annett.** 4-7, 2007, Diamond and Related Materials, Vol. 16, pp. 1370-1373. DOI 10.1016/j.diamond.2006.11.095.

[98]. *Morphology, photocleaning and water wetting properties of cotton fabrics, modified with titanium dioxide coatings synthesized with plasma enhanced chemical vapor deposition technique.* **Sobczyk-Guzenda, Anna, et al., et al.** -, 2013, Surface and Coatings Technology, Vol. 217, pp. 51-57. DOI 10.1016/j.surfcoat.2012.11.071.

[99]. *Development of low-k precursors for next generation IC manufacturing.* **Doniat, Francois, et al., et al.** -, 2012, Microelectronic Engineering, Vol. 92, pp. 34-37. DOI 10.1016/j.mee.2011.05.040.

[100]. *Development of micromorph tandem solar cells on foil deposited by VHF-PECVD.* **Liu, Y., Rath, J.K. and Schropp, R.E.I.** 22-23, 2007, Surface and Coatings Technology, Vol. 201, pp. 9330-9333. DOI 10.1016/j.surfcoat.2007.04.095.

[101]. *Investigations of plasma polymerized SiOx barrier films for polymer food packaging.* **Plog, Simone, et al., et al.** -, 2011, Surface and Coatings Technology, Vol. 205, pp. S165-S170. DOI 10.1016/j.surfcoat.2011.01.034.

[102]. *A novel technique to enhance surface properties of DLC films deposited on the inner wall of cylindrical PET barrel by DC-RF hybrid discharge.* **Tian, Xiubo, et al., et al.** 5, 2011, Surface and Coatings Technology, Vol. 206, pp. 1016-1019. DOI 10.1016/j.surfcoat.2011.03.099.

[103]. *Organosilicon/silicon oxide gas barrier structure encapsulated flexible plastic substrate by using plasma-enhanced chemical vapor deposition.* **Wu, Cheng-Yang, et al., et al.** 22, 2012, Surface and Coatings Technology, Vol. 206, pp. 4685-4691. DOI 10.1016/j.surfcoat.2012.05.080.

[104]. *Structural, mechanical, tribological, and corrosion properties of a-SiC: H coatings prepared by PECVD.* **Guruvenket, S., et al., et al.** 21-22, 2010, Surface and Coatings Technology, Vol. 204, pp. 3358-3365. DOI 10.1016/j.surfcoat.2010.03.031.

[105]. *Single layer and multilayered films of plasma polymers analyzed by nanoindentation and spectroscopic ellipsometry.* **Cech, V., et al., et al.** 21, 2009, Thin Solid Films, Vol. 517, pp. 6034-6037. DOI 10.1016/j.tsf.2009.05.025.

[106]. *Functional multilayer coatings of tetravinylsilane.* **Studynka, J., Cechalova, B. and Cech, V.** 22-23, 2008, Surface and Coatings Technology, Vol. 202, pp. 5505-5507. DOI 10.1016/j.surfcoat.2008.06.027.

[107]. *Plasma polymer multilayers of organosilicones and their optical properties controlled by RF power.* **Kontarova, S., Perina, V. and Cech, V.** -, 2011, Surface and Coatings Technology, Vol. 205, pp. S451-S454. DOI 10.1016/j.surfcoat.2011.01.064.

[108]. **Sigma-Aldrich Co. LLC.** Tetravinylsilane. *Sigma aldrich catalogue: Tetravinylsilane.* [Online] 2013. http://www.sigmaaldrich.com/catalog/product/aldrich/318256?lang=en®ion=CZ.

[109]. **Bureš, Michal.** *Studium plazmových produktů pomocí hmotnostní spektrometrie: Study of plasma species by mass spectroscopy.* Brno : Vysoké učení technické, Fakulta chemická, 2008. pp. 1 elektronický optický disk [CD-ROM / DVD]. Bachelor thesis. Brno university of technology.

[110]. **Kontárová, Soňa.** *Nanolayered Composites: Nanovrstevnaté kompozity.* Brno : Vysoké učení technické, Fakulta chemická, 2011. p. 157 s. doctoral thesis. Brno Unversity of Technology.

[111]. **Žák, Luboš.** *Plasma enhanced chemical vapor deposition.* Brno : Vysoké učení technické v Brně, Fakulta chemická, 2011. p. 68 l. Diploma thesis. Brno University of Technology.

[112]. *Effect of RF-plasma deposition parameters on the composition and properties of organic layers deposited on glass fibers.* **Balkova, R., Jancar, J. and Cech, V.** 14, Composites Science and Technology, Vol. 69, pp. 2485-2490. DOI 10.1016/j.compscitech.2009.06.024.

[113]. **Lin-Vien, Daimay.** *The Handbook of infrared and raman characteristic frequencies of organic molecules.* Boston : Academic Press, c1991. pp. xvi, 503 p. ISBN 01-245-1160-0.

[114]. *Physico-chemical properties of plasma-polymerized tetravinylsilane.* **Cech, V., et al., et al.** 9-11, Surface and Coatings Technology, Vol. 201, pp. 5512-5517. DOI 10.1016/j.surfcoat.2006.07.086.

[115]. **National instutute of standarts and technology, Material measurement laboratory.** Dioxosilane. *NIST database.* [Online] 2009. http://webbook.nist.gov/cgi/cbook.cgi?ID=C7631869&Units=SI&Type=IR-SPEC&Index=2#IR-SPEC.

[116]. *A study of microstructure and nanomechanical properties of silicon incorporated DLC films deposited on silicon substrates.* **Zhao, J.F, et al., et al.** 3-7, 2001, Diamond and Related Materials, Vol. 10, pp. 1070-1075. DOI 10.1016/S0925-9635(00)00544-6.

[117]. **Kurt J. Lesker Company.** Pump Classifications Technical Notes. *Pump Classifications Technical Notes.* [Online] 2013. http://www.lesker.com/newweb/Vacuum_Pumps/vacuumpumps_technicalnotes_1.cfm.

LIST OF USED ABBREVIATIONS

Abbreviation		Description
AC	-	Alternating current
AFM	-	Atomic force microscopy
amu	-	Atomic mass units
APCVD	-	Atmospheric pressure chemical vapor deposition
ATR	-	Attuned total reflectance
CF	-	Conflat
CVD	-	Chemical vapor deposition
DC	-	Direct current
DLC	-	Diamond like carbon
DRIFTS	-	Diffuse reflectance infrared fourier transform spectroscopy
ECR	-	Electron cyclotron resonance
ELL	-	Elipsometry
ERDA	-	Elastic recoil detection analysis
ESCA	-	Electron spectroscopy for chemical analysis
FIR	-	Far infrared
FTIR	-	Fourier transform infrared spectroscopy
ICPCVD	-	Inductively coupled plasma
IR	-	Infra red
KF	-	Klein flansche
LECVD	-	Laser enhanced chemical vapor deposition
LPCVD	-	Low pressure chemical vapor deposition
MALDI	-	Matrix assisted laser deposition ionization
MIR	-	Multiple internal reflection
MOCVD	-	Methal-organic chemical vapor deposition
MS	-	Mass spectroscopy
MW	-	Microwave
NI	-	Nanoindentation

OFHC	-	Oxygen free high conductivity
OMVPE	-	Organometallic vapor phase epitaxy
PC	-	Personal computer
PE	-	Polyethylene
PECVD	-	Plasma enhanced chemical vapor deposition
PLC	-	Programable logic control
pp	-	Plasma polymerized
PVD	-	Physical vapor deposition
RBS	-	Rutherford backscattering spectrometry
RF	-	Radio frequency
RGA	-	Residual gas analysis
SCEM	-	Single channel electron multiplier
SEM	-	Scanning electron mictroscopy
SFM	-	Scanning force microscopy
SPG	-	Sample process gas
SPM	-	Scanning probe microscope
TEOS	-	Tetramethyldisiloxane
TMS	-	Tetramethylsilane
TOF	-	Time of flight
TVS	-	Tetravinylsilane
UHV	-	Ultra high vacuum
UV	-	Ultra violet
VIS	-	Visible
XPS	-	X ray photoelectron spectroscopy

LIST OF ANNEXES

APPENDIX A - A3 vacuum schema A1